

Studies on Development of ABA Receptor Antagonists

メタデータ	言語: en 出版者: Shizuoka University 公開日: 2015-04-24 キーワード (Ja): キーワード (En): 作成者: Takeuchi, Jun メールアドレス: 所属:
URL	https://doi.org/10.14945/00008273

Studies on Development of ABA Receptor Antagonists

Jun TAKEUCHI

Graduate School of Science and Technology, Educational Division

Department of Bioscience

Shizuoka University

June 2014

Studies on Development of ABA Receptor Antagonists

ABA 受容体アンタゴニストの創出研究

竹内 純

静岡大学

大学院自然科学系教育部

バイオサイエンス専攻

2014年6月

Contents

1. Introduction	4
1-1. Plant hormone receptors	4
1-2. Chemical structure of abscisic acid	8
1-3. Physiological action	9
1-4. Biosynthesis, transportation and catabolism	10
1-4-1. Biosynthesis	10
1-4-2. Transportation	12
1-4-3. Catabolism	14
1-5. Identification of ABA receptors	16
1-6. The function of PYL and ABA signal transduction	17
1-7. Objective	19
1-7-1. The structural basis for PYL-PP2C interaction	20
1-7-2. Structure–Activity Relationships	25
2. Results	29
2-1. Design and synthesis	29
2-2. Physiological effects of <i>AS_n</i> on plants	33
2-3. Biochemical characterization of <i>AS_n</i>	42
2-4. Thermodynamic and structural analysis of PYL- <i>AS₆</i> complexes	45
2-5. The functional selectivity of <i>AS_n</i>	50
2-6. Molecular determination for the functional selectivity of <i>AS₂</i>	51
3. Discussion	55
4. Experimental	57
Summary	73
Acknowledgements	76
References	78
List of Publications	92

Abbreviations

AAO	abscisic aldehyde oxidase
ABA	abscisic acid
ABA-GE	1- <i>O</i> -Glucosyl ester of abscisic acid
ABC	ATP binding cassette
AFB	auxin signaling F-box
AIT1	ABA-importing transporter 1
ARF	auxin responses factor
Aux/IAA	auxin/indole-3-acetic acid
BRI1	brassinosteroid insensitive1
BRL	BRI1-like
CHLH	H subunit of Mg-chelatase
COI1	coronatine-insensitive 1
DAD2	decreased apical dominance 2
ETR1	ethylene resistant 1
ERS	ethylene response sensor
EIN4	ethylene insensitive 4
FCA	flowering time control protein A
GA	gibberellin
GCR2	G protein-coupled receptor like receptor 2
DELLA	the protein that contain as N-terminal DELLA domain
GID	gibberellin-insensitive dwarf
GPCR	G protein-coupled receptor
GTG	GPCR-type G proteins
HOABA	hydroxyl-ABA
HPLC	high performance liquid chromatography
HRMS	high resolution mass spectrometry
IC ₅₀	concentration giving half-maximal inhibition
ID	island domain
JA	jasmonic acid
JA-Ile	jasmonate-isoleucine conjugate

JAZ	jasmonate ZIM-domain
K_i	inhibition constant
K_m	Michaelis constant (enzyme kinetics)
LEA	late-embryogenesis abundant
MAX2	more axillary growth 2
MEP	2-C-methyl-D-erythritol 4-phosphate
NECD	nine- <i>cis</i> -epoxycartenoid dioxygenase
NMR	nuclear magnetic resonance
NPR	nonexpresser of pathogenesis-related
NSY	neoxanthin synthase
ODS	octadecylsilyl
PA	phaseic acid
PDC	programmed cell death
PP2C	type 2C protein phosphatases
PyrA	Pyrabactin
RCAR	regulatory component of ABA receptor
PYR1	PYRABACTIN RESISTANCE 1
PYL1–13	PYR1-like protein 1–13
SA	salicylic acid
SCF	Skp1-Cullin-F-box
SDR	short-chain alcohol dehydrogenase/reductase
SERK	somatic embryogenesis receptor kinase
SL	strigolactone
SLY	sleepy
SnRK2	sucrose non-fermenting 1-related protein kinase 2
TIR1	transport inhibitor response 1
VDE	violaxanthin de-epoxidase
ZEP	zeaxanthin epoxidase

1. Introduction

1-1. Plant hormone receptors

Plant hormones, also known as phytohormones, are biologically active substances produced within plants that can function at very low concentrations. Phytohormones regulate plant growth and development, and affect the plant's ability to respond to its environment. The five major classes of plant hormones: auxin, gibberellin (GA), ethylene, cytokinin and abscisic acid (ABA) were identified during the first half of the twentieth century¹. Recently, several additional small molecules have been recognized as plant hormones, including brassinosteroid, jasmonic acid, salicylic acid (SA) and strigolactone (SL). With the applications of genetic and molecular biological approaches, mainly in *Arabidopsis thaliana*, many aspects of hormone studies have progressed rapidly². In particular, the biosynthetic pathways of all the plant hormones, except SL, have been elucidated. Conversely, our understanding of their catabolic pathways and transportation systems remains fragmented.

An ethylene receptor, ethylene resistant 1 (ETR1), which was identified from an ethylene insensitive mutant of *Arabidopsis* in 1988³, was the first of the plant hormone receptors to be discovered. ETR1 belongs to the two-component input regulators, which consist of a transmitter histidine kinase and a response regulator⁴. This protein exists as a disulfide-linked homodimer and requires a copper ion to bind ethylene^{5,6}. In *Arabidopsis*, there are four homologs of ETR1 (ETR2, ERS1, ERS2 and EIN4) and they are all able to bind ethylene at the endoplasmic reticulum.

The brassinosteroid receptor, brassinosteroid insensitive 1 (BRI1), was identified in 1997 from *Arabidopsis* dwarf mutants that do not respond to exogenous brassinosteroids⁷. BRI1 is a plasma membrane-associated leucine-rich repeat (LRR) receptor-like kinase. It is composed of an extracellular domain of 25 LRRs and a cytoplasmic kinase domain, connected by a single membrane-spanning helix. In addition, a 70-residue island domain (ID) is inserted between the 21st and 22nd LRR domains. Brassinosteroids bind a hydrophobic groove between the ID and the inner surface of the 21st LRR^{8,9}, which triggers the formation of a docking platform for the binding of co-receptors, somatic embryogenesis receptor kinases (SERKs), which activate their kinase domains via transphosphorylation¹⁰. Three homologs of BRI1 (BRL1, BRL2 and BRL3) exist in *Arabidopsis*, and they are all expressed in vascular

cells^{11,12}.

Seven other hormone receptors were identified in the *Arabidopsis* genome¹³. In 2001, a cytokinin receptor, cytokinin response 1 (CRE1), was identified from *Arabidopsis* by genetically screening for cytokinin insensitivity¹⁴. Subsequently, two close homologs, AHK2¹⁵ and AHK3¹⁶, were identified. These receptors belong to the membrane-bound two-component input regulators, as well as the ethylene receptors. Cytokinins bind to their extracellular input domains and allow the activation of the intracellular histidine kinase domain via autophosphorylation. This results in a phospho-relay that eventually activates cytokinin responses.

The first GA receptor was isolated and characterized from the GA-insensitive dwarf 1 mutant (*gid1*) of rice in 2005¹⁷. Later, three orthologous genes (*GID1a*, *GID1b* and *GID1c*) were identified in *Arabidopsis*. The *gid1a/gid1b/gid1c* triple mutant showed a GA-insensitive phenotype, suggesting that GA responses require GID1 proteins in both rice and *Arabidopsis*^{18,19}. The GID1 proteins have a primary structure similar to that of the hormone-sensitive lipases and exist in the nucleus. GA binds to GID1 and probably induces a conformational change in a mobile lid moiety. This lid is likely to be open in the apoenzyme state but closes to create an interaction surface that enables binding to the DELLA proteins, which are transcriptional repressors of GA signaling^{18,20}. GID-bound DELLA interacts with the F-box protein, sleepy 1 (SLY) / GID2^{21,22}. This interaction ultimately leads to the ubiquitination and degradation of DELLA, which induces GA responses.

In the same year, a nuclear auxin receptor was identified by a pull-down assay using an F-box protein, transport inhibitor response 1 (TIR1), and an auxin/indole-3-acetic acid (Aux/IAA) transcriptional repressor^{23,24}. Auxin binds to a TIR1 surface groove and enhances the TIR1–Aux/IAA interaction by filling a cavity between the two proteins; that is, auxin acts as a molecular glue²⁵. Upon interacting with Aux/IAA, the ubiquitin ligase complex, SCF^{TIR1}, promotes the ubiquitin-dependent proteolysis of Aux/IAA repressors. Degradation of Aux/IAs permits the auxin response factor (ARF)-dependent auxin responses²⁶. The *TIR1* genes consist of seven related F-box protein genes²⁷, and three of them, *AFB1*, *AFB2* and *AFB3*, are involved in auxin perception in *Arabidopsis*²³.

A jasmonate receptor was first isolated from the *Arabidopsis coronatine-insensitive 1*

(*coi1*) mutant in 1994²⁸. *COI1* encodes an F-box protein that is closely related to the auxin receptors. This suggested that jasmonate signaling requires the SCF^{COI1}-dependent degradation of repressor proteins. However, more than a decade after the identification of COI1, the substrates of SCF^{COI1} had not been discovered. In 2007, a novel family of jasmonate-regulated nuclear targets of SCF^{COI1}, jasmonate ZIM-domain (JAZ) proteins, was identified^{29,30}. The bioactive hormone, jasmonate-isoleucine conjugate (JA-Ile), induces the binding of COI1 to JAZ repressors and leads to JAZ degradation by the ubiquitin-proteasome pathway, which relieves transcriptional repression of jasmonate-responsive genes. The crystal structure of the COI1-JA-Ile complex with the JAZ1 peptide indicated that JA-Ile promotes COI1-JAZ interactions by a molecular glue mechanism, as well as the auxin system³¹.

As described below, two types of ABA receptors, GTG1/GTG2 and PYR/PYL/RCAR, were identified in 2009.

In 2012, non-expresser of pathogenesis-related (NPR) genes NPR3 and NPR4, which are paralogs of NPR1, were identified as SA receptors³². These proteins bind SA with different affinities and function as adaptors of the Cullin 3 ubiquitin ligase, mediating NPR1 degradation in an SA-regulated manner. SA promotes the NPR1–NPR3 interaction, whereas SA disrupts the interaction between NPR1 and NPR4. According to a recent study, SA may bind NPR4 to attenuate its accessibility to NPR1, allowing the accumulation of NPR1, which induces basal resistance in the absence of a pathogen challenge. After being challenged by pathogens, SA levels are increased both locally and systemically³³. In infected cells, the higher SA level induces the NPR1–NPR3 interaction, leading to programmed cell death through NPR1 degradation. In neighboring cells, the lower SA level limits the NPR1–NPR3 interaction, enabling NPR1 accumulation to restrict the spread of programmed cell death and induce systemic acquired resistance.

In the same year, 2012, an SL receptor, decreased apical dominance 2 (DAD2), was identified from petunia³⁴. *DAD2* is an ortholog of the rice and *Arabidopsis D14* genes that are involved in branching. The crystal structure of DAD2/D14 confirms that this protein is a member of the α/β hydrolase fold family, as well as a homolog of the GA receptor GID1. However, unlike the GID1 receptor, DAD2/D14 retains a hydrolysis activity that is required for SL signal transduction. SL promotes the interaction between

D14 and an F-box protein of the SCF complex (D3 in rice, MAX2 in *Arabidopsis* and PhMAX2 in petunia). More recently, the substrate of SCF^{D3}, DWARF53 (D53), which acts as a repressor of SL signaling, was identified in rice^{35,36}. According to a proposed model, SL binding induces a conformational switch in D14 to SCF^{D3} and D53 binding, which induces D53 degradation by the proteasome-ubiquitin pathway.

As described above, all plant hormone receptors have now been identified. However, until recently, our knowledge of the molecular mechanisms of plant hormone perception was fragmentary compared with those of animals³⁷. One reason may be that plant researchers have studied various plant species; therefore, some of the observations could not be interpreted conceptually. In addition, the biochemical purification of plant hormone receptors is probably more difficult than that of animal receptors because plant cells both produce and respond to many hormones, unlike animal systems where organs and glands are separate. This may also be the reason for the delayed identification of plant hormone receptors. Deciphering the *Arabidopsis* genome sequence provided a major breakthrough in the understanding of plant hormones' perception and signal transduction. Recently, a library of *Arabidopsis* mutants has been organized and anyone can easily study these mutants. However, a negative effect of the decipherment of the *Arabidopsis* genome has been the lack of studies on the action mechanisms of plant hormones in other plant species, including crops. This is probably one of the reasons why the application of plant hormones in agricultural fields is still limited.

In this study, we focused on ABA and developed a receptor antagonist that inhibits ABA signal transduction by blocking the activation of receptor proteins. This small molecule can regulate ABA responses temporarily and arbitrarily, so it will be a useful tool for studying the molecular mechanisms of ABA signaling in multiple plant species, including non-model organisms and crops. Furthermore, ABA receptor antagonists will enable us to manipulate ABA responses in plants, thus they may have potential agricultural value as tools to control ABA functions, such as seed germination³⁸, which may contribute to enhanced crop productivity through the induction of simultaneous germination³⁹.

1-2. Chemical structure of abscisic acid

ABA (**1**) was first isolated from cotton as a promoter of leaf abscission, and originally named abscisin II, in 1963⁴⁰. In 1964, a different group isolated a compound inducing dormancy using the *Avena* coleoptile growth assay from sycamore leaves and called it dormin⁴¹. Based on the crystal structural analysis, dormin was identified as abscisin II⁴², and then a unified name, abscisic acid, was adopted in 1967. The planar structure of ABA was determined by Ohkuma in 1965⁴³. The molecular structure of ABA has many features that are important for biological activity in plants. ABA has an asymmetric carbon at the C1' position, and there are two enantiomers. Although the naturally occurring form is *S*-(+)-ABA, the enantiomer *R*-(-)-ABA and their racemic compounds can be obtained by chemical synthesis. Thus, the relationship between absolute configuration and activity has been examined for a long time⁴⁴. *R*-ABA has a weaker bioactivity than *S*-ABA in many assays, such as stomatal closure. Whereas, *R*-ABA has a comparable activity to that of *S*-ABA in some elongation inhibition tests, such as in rice seedlings. This has been explained by the near symmetry of the ABA molecule (Fig. 1)⁴⁵. The comparison of *R*-ABA with *S*-ABA in the conformation with an axial side-chain reveals no differences in the spatial positions of the C7' and C9' functional methyl and oxygen groups. Recently this hypothesis was confirmed by the crystal structure of the PYL(-)-ABA complex^{46,47}. The ring conformation is a significant factor in determining the three-dimensional shape of ABA. In other words, the spatial positions of the substituents depend on the conformation of the six-membered ring of ABA. The conformation of ABA can theoretically have at least two thermodynamically stable conformers; one is a half-chair with the axial side-chain, and the other is a half-chair with the equatorial side chain⁴⁸. The crystal structure of ABA revealed that its conformation is the axial side-chain form, and the nuclear overhauser effect (NOE) experiments suggested that the conformation of the ABA side-chain adopts the axial position in solution^{49,50}. However, the ratio of axial side-chain form to equatorial side-chain form is 97.8 to 2.2 at 185 K, meaning that the free-energy difference between the two conformers is 1.4 kcal mol⁻¹ at this temperature⁵¹. The activation barrier to interconversion between the two conformers is calculated to be 11.2 kcal mol⁻¹, suggesting that the conformation of ABA ring is very flexible at room temperature.

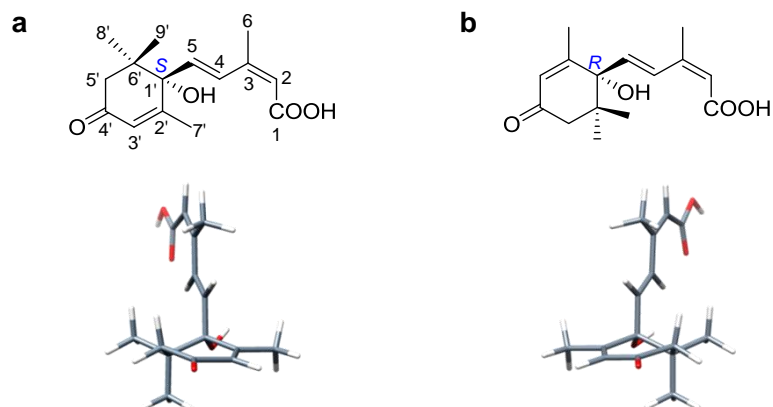


Figure 1 | Structures of S-(+)- abscisic acid (ABA) (a) and R(-)-ABA (b).

1-3. Physiological action

The plant hormone ABA regulates various physiological processes and adaptive responses to environmental stresses. Because plants are not mobile like animals, it is a matter of course that plant hormones are causally related to environmental adaptation. Among them, ABA in particular plays an important role in the induction of drought stress tolerance and the maintenance of seed dormancy. Considering that ABA also induces desiccation tolerance in vegetative tissues of basal plants, such as *Physcomitrella patens*⁵², the acquisition of sensation and response mechanisms for ABA by their ancestors would be critical for disbursement on, and adaptation to, land, where water potentials vary continuously.

In the seed maturation process, ABA is essential for the occurrence of seed dormancy. Dormancy in immature sunflower seeds is inhibited by treatment with a carotenoid synthesis inhibitor, fluridone⁵³. The ABA-deficient and -insensitive *Arabidopsis* variants undergo precocious seed germination^{54,55}. In contrast, the ABA hypersensitive mutant of *Arabidopsis*, *eral*, has an increased dormancy period⁵⁶. ABA is also involved in seed germination, shoot elongation, root growth and senescence⁵⁷. Seed germination is regulated by the balance of endogenous levels of ABA and GA. Maintenance of dormancy is necessary to synthesize ABA⁵⁸, whereas release from dormancy is affected by increasing rates of ABA catabolism and GA synthesis, and decreasing levels of GA-inactivating enzymes^{59,60}.

The important function of ABA during vegetative growth is the induction of

responses to environmental stresses, such as desiccation, low temperature and salinity⁶¹⁻⁶³. Under drought conditions, the endogenous ABA level dramatically increases in plants, and it regulates the transpiration rate by inducing stomatal closure and inhibiting stomatal opening^{64,65}. Moreover, ABA induces an accumulation of compatible solutes, such as sorbitol, proline, glycine-betaine, and small hydrophilic proteins that confer stress tolerance by decreasing the osmotic potential in plant cells⁵⁷. ABA also induces the late-embryogenesis abundant (LEA) protein, which is probably involved in the retention of moisture, protection of biological membranes and ionic homeostasis⁶⁶. Thus, ABA can be considered a water stress-related phytohormone that contributes to the dehydration and desiccation tolerance of cells.

1-4. Biosynthesis, transportation and catabolism

ABA actions and homeostasis are appropriately controlled to produce adaptive responses to environmental changes through biosynthesis, transportation and catabolism in plants.

1-4-1. Biosynthesis

ABA is a sesquiterpenoid ($C_{15}H_{20}O_4$), and the ultimate biosynthetic precursor is isopentenyl diphosphate (IDP). So far, two pathways have been proposed for ABA biosynthesis. In the sesquiterpenoid pathway (direct pathway), ABA is derived from farnesyl diphosphate (FDP)⁶⁷, a common precursor for sesquiterpenoids, which appears to be plausible for the biosynthetic pathway to ABA following IDP. However, in the carotenoid pathway (indirect pathway), ABA is produced from the cleavage of carotenoids⁶⁸. This pathway was proposed by the structural similarities between ABA and xanthoxin, which is a carotenoid degradation product. Since then, many experiments have been performed to distinguish the sesquiterpenoid and carotenoid pathways. The carotenoid pathway was confirmed in the 1990s by a variety of biochemical studies, ¹⁸O₂-labeling experiments and the characterization of ABA-deficient mutants. Thus, now it is thought that ABA is biosynthesized by the carotenoid pathway in higher plants. However, the reason why ABA is synthesized from carotenoids is not well understood.

The carotenoid pathway is shown in Fig. 2^{69,70}. Zeaxanthin is converted to violaxanthin via the intermediate antheraxanthin by zeaxanthin epoxidase (ZEP). After isomerization of *trans*-violaxanthin and *trans*-neoxanthin to their 9-*cis* isomers, they are cleaved by 9-*cis*-epoxycarotenoid dioxygenase (NCED) to release the 15C compound xanthoxin from plastids. This oxidative fission process is the rate-limiting step of ABA biosynthesis. Neoxanthin synthesis is conducted by ABA4, which is a plastid membrane-localized protein⁷¹. Xanthoxin is converted to ABA by a short-chain alcohol dehydrogenase/reductase (SDR) and abscisic aldehyde oxidase (AAO) in the cytoplasm.

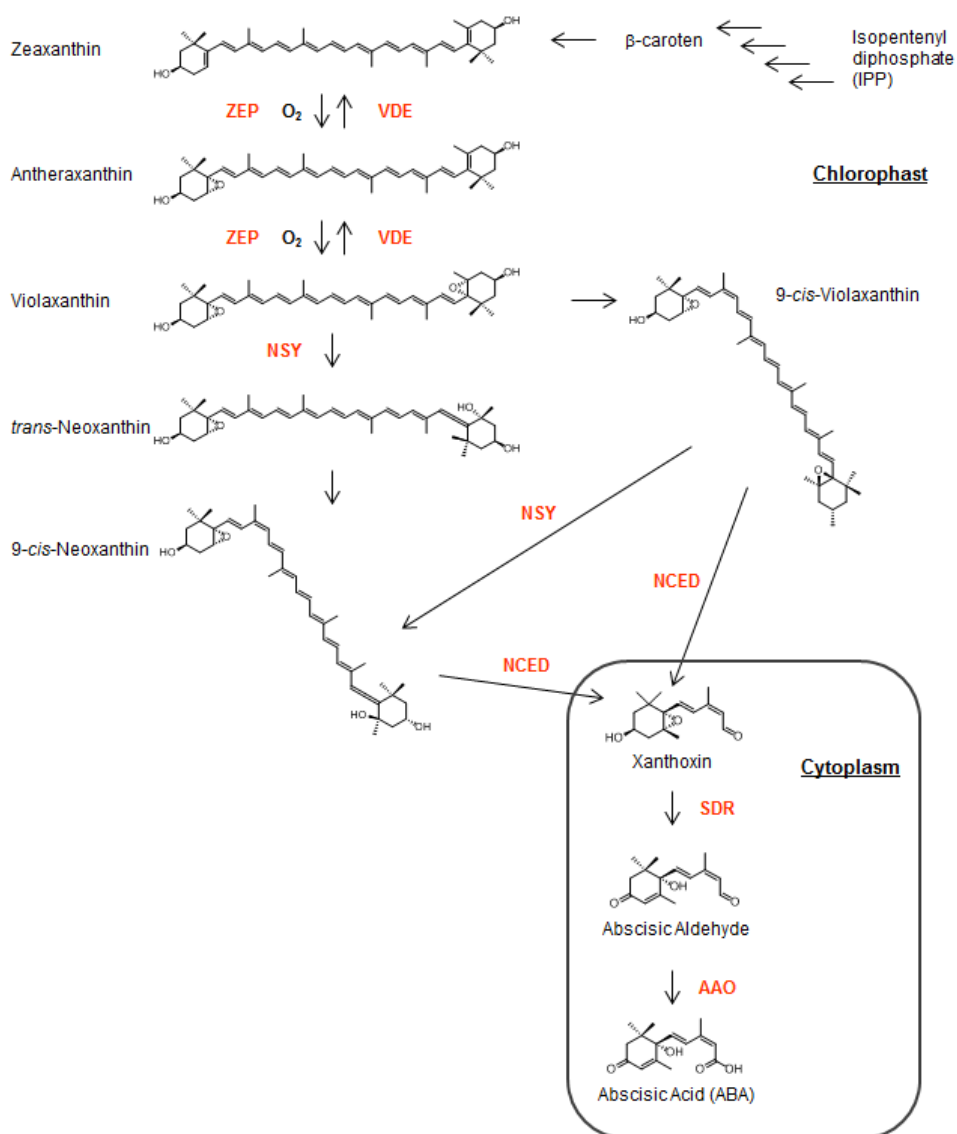


Figure 2 | Biosynthesis pathway of ABA in higher plants⁶⁹.

ZEP, zeaxanthin epoxidase; VDE, violaxanthin de-epoxidase; NSY, neoxanthin synthase; NCED, 9-*cis*-epoxycarotenoid dioxygenase; SDR, short-chain alcohol dehydrogenase/reductase; AAO: abscisic aldehyde oxidase.

1-4-2. Transportation

ABA biosynthetic enzymes NCED and SDR, as represented by AtABA2 and AAO, respectively, in *Arabidopsis*, are mainly expressed in vascular tissues; nevertheless, ABA acts in various cells, including guard cells^{72,73}. This suggests that the ABA synthesized in vascular tissues is transported to guard cell to induce stomatal closure. ABA is a weak acid ($pK_a = 4.7$), and thus, it exists in a protonated, uncharged form (ABA-H) or in an anionic form (ABA^-), depending on the compartmental pH, and ABA-H can move through the membrane lipid bilayer via a passive diffusion mechanism⁷⁴. Therefore, previously, most of the flow of ABA across membranes was assumed to occur as a result of diffusion⁷⁵. However, the pH of both the cell and apoplast implies that most of the ABA pools are of the ABA^- , charged and nondiffusible form. Thus, the diffusion processes through the membrane may be the limiting step for ABA transport, and ABA transporters could allow better access of ABA to intracellular receptors. ABA transporters may be particularly relevant during stress conditions, because such conditions are known to elevate the apoplast's pH, and this pH increase causes ABA-H to dissociate into its charged form, which cannot diffuse across the cell membrane.

So far, two ATP-binding cassette (ABC) transporters, AtABCG25 and AtABCG40, and a nitrate transporter, NPF4.6/AIT1, have been identified as ABA transporters in *Arabidopsis*. AtABCG25 acts as an efflux transporter that exports ABA from the vessels, whereas AtABCG40 and NPF4.6/AIT1 function in the uptake of ABA into subcellular compartments (Fig. 3). AtABCG25 was isolated from *Arabidopsis* by genetically screening for ABA sensitivity⁷⁶. When exogenous ABA was used to inhibit germination and early seedling growth, the *atabcg25* mutant was more sensitive to ABA than wild type. In contrast the AtABCG25-overexpressing plants resulted in an ABA-insensitive phenotype. Biochemical analyses indicated that AtABCG25 exported ABA from the inside to the outside of the cell, depending on the ATP concentration. The expression of AtABCG25 was detected mainly in vascular tissues, and it was increased by ABA. The AtABCG25-overexpressing plants showed higher leaf temperatures, probably as a result of inhibited transpiration. These results suggest that the export of ABA from vascular tissues via AtABCG25 is involved in intercellular ABA signaling.

AtABCG40 was identified by a forward genetics screen of *Arabidopsis* pleiotropic

drug resistance transporter (AtPDR) homozygous knockout mutants⁷⁷. Biochemical and expression analyses indicate that AtABCG40 imports ABA from the outside to the inside of cells, and it is expressed in the guard cells. In response to exogenous ABA, the *atabcg40* mutant showed lower expression levels of ABA responsive genes than those of wild type and impaired stomatal closure, which resulted in reduced drought tolerance. These results suggest that vascular tissues are the primary sites of ABA biosynthesis in response to drought stress and that synthesized ABA is then transported to the guard cells to close stomata.

NPF4.6/AIT1 was identified by using a modified yeast two-hybrid system, which was based on the ability of a protein to transport ABA and utilized the PYL–ABA– type 2C protein phosphatase (PP2C) interaction as a sensor to check for ABA levels in yeast cells⁷⁸. AIT1 has been characterized as the low-affinity nitrate transporter, but based on a comparison of the K_m values, ABA is likely a better substrate than nitrate. AIT1 is mainly expressed in vascular tissues and mediates ABA import at the plasma membrane. The *ait1* mutants showed less sensitivity to exogenous ABA than wild type in seed germination and seedling growth, whereas *AIT1*-overexpressing *Arabidopsis* showed ABA hypersensitivity. In addition, the surface temperature of inflorescence stems of the *ait1* and *AIT1*-overexpressing plants were lower than those of wild type, suggesting that AIT1 acts as a regulator of the ABA pool in vascular tissues.

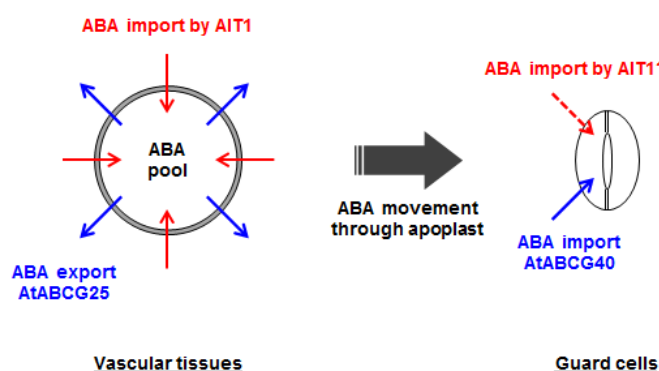


Figure 3 | Model for physiological roles of ABA transporters⁷⁸.

ATP-binding cassette (ABC) transporters, AtABCG25 and AtABCG40, and a nitrate transporter, NPF4.6/AIT1, have been identified as ABA transporters in *Arabidopsis*. AtABCG25 and AIT1 mediate ABA export and import, respectively, at the site of ABA biosynthesis (vascular tissues). AIT1 may contribute to maintaining the ABA pool size in this tissue. ABA synthesized in vascular tissues is transported toward the guard cells by an unknown mechanism. It is possible that ABA must remain in vascular tissues for efficient transport of ABA to guard cells. AtABCG40 mediates ABA uptake into guard cells to close stomata. AIT1 may also contribute to ABA uptake into guard cells

1-4-3. Catabolism

ABA is inactivated by two major path ways: (i) hydroxylation of ABA's C8' position and (ii) glycosylation of ABA's C1' position (Fig. 4). ABA-8'-hydroxylase is a P-450 type monooxygenase that is encoded by the CYP707A family, *CYP707A1–CYP707A4*^{79,80}. The gene expression levels of CYP707As are increased during drought stress and subsequent rehydration conditions, indicating that ABA levels are regulated through a continuous balance of synthesis and catabolism. The reaction product, 8'-hydroxy-ABA, is highly unstable and; therefore, it spontaneously isomerizes to phaseic acid (PA). Then, PA is converted to dihydro-PA and *epi*-dihydro-PA by the reduction of the C4' carbonyl group. Although 8'-hydroxy-ABA is the major product of CYP707A, this enzyme can hydroxylate at the C7' or C9' positions of ABA as a minor side reaction⁸¹.

ABA and its metabolites are also inactivated by conjugation to ABA-glucosyl ester (ABA-GE), which is stored in the vacuoles. Previously ABA-GE was considered a permanent inactivation form, but recent studies indicate that it is a storage or transport form of ABA. There are eight glucosyltransferases in *Arabidopsis* that can catalyze this reaction⁸². Under drought conditions, ABA-GE may be cleaved by β -glucosidases that are present in the endoplasmic reticulum (AtBG1)⁸³ and vacuoles (AtBG2)⁸⁴. The *atbg1* mutant caused defective stomatal closure, early germination, stress-sensitive phenotypes and lower ABA levels, whereas *AtBG1*-overexpressing plants accumulated higher ABA levels and had enhanced drought stress tolerance. Dehydration rapidly induces polymerization of AtBG1, resulting in an increase in enzymatic activity. These results indicated that the activation of ABA-GE by polymerized AtBG1 is a mechanism by which plants rapidly adjust ABA levels and respond to environmental stresses. In addition, the *atbg2* mutant also showed a high sensitivity to drought and NaCl stress, whereas *AtBG2*-overexpressing plants resulted in enhanced resistance to drought and NaCl stress. Taken together, these observations suggested that besides the *de novo* biosynthesis, ABA is produced in various organelles by organelle-specific β -glucosidases in response to many stresses.

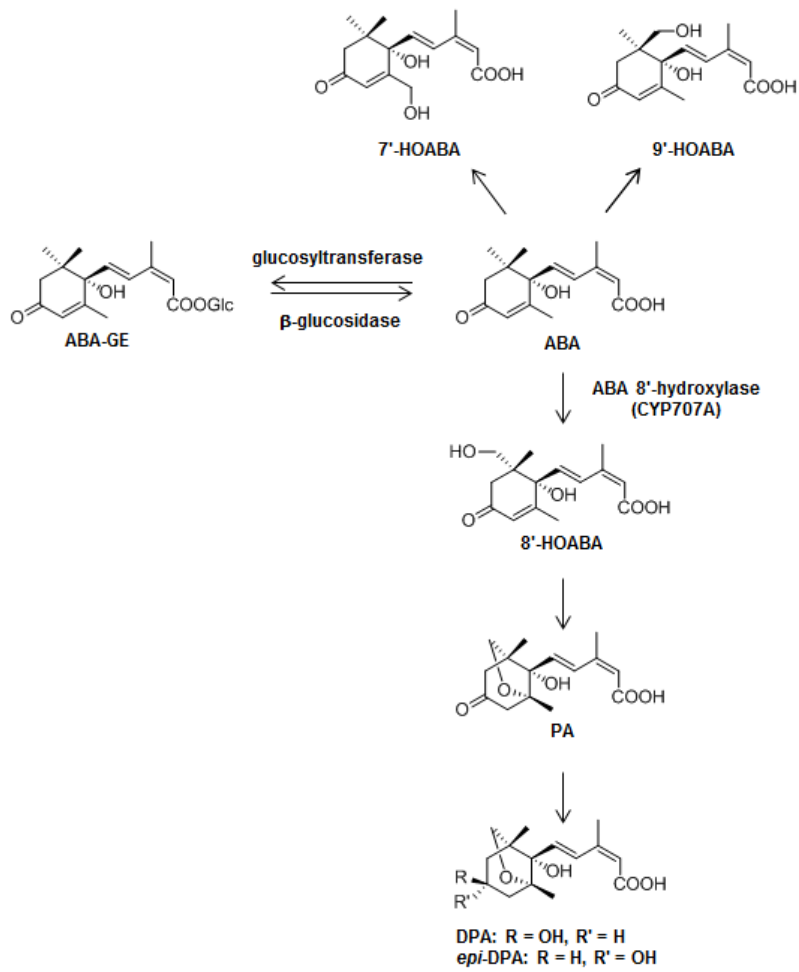


Figure 4 | ABA catabolic pathway in plants.

1-5. Identification of ABA receptors

More than 50 genes that are related to ABA signal transduction were identified from ABA sensitive mutants, and it was revealed that protein phosphatases and kinases play key roles in the ABA signaling pathway. However, ABA receptors were not identified by molecular genetic analyses because of the functional redundancy of homologous genes. Therefore, the understanding of ABA perception and signal transduction was delayed in comparison to those of other plant hormones.

Studies of ABA binding proteins have been performed since the 1970s. The first study using [³H] ABA indicated that ABA binds to membrane-rich fractions prepared from the leaves of *Vicia faba*⁸⁵. After that, a different group, studying guard cell protoplasts of *V. faba*, reported the existence of guard cell-specific ABA-binding proteins, which were located at the plasma membrane⁸⁶. In the 1990s, microinjection studies and the applications of ABA-protein conjugates suggested that ABA could be perceived at both intercellular and extracellular sites⁸⁷⁻⁸⁹, and an additional study using barley aleurone protoplasts suggested the existence of an ABA receptor protein at the plasma membrane⁹⁰. In 2006, the first ABA receptor was identified in barley by screening a cDNA expression library with an anti-idiotypic antibody⁹¹. Sequence analyses indicated that this protein was *Arabidopsis* FCA, an RNA-binding protein involved in flowering. After that, the H subunit of Mg-chelatase^{92,93} and G-protein coupled receptor GCR2⁹⁴ were reported as ABA receptors, but this was not by consensus. The FCA paper was retracted in 2008 because Risk et al. in their *Nature* paper reported that FCA did not bind ABA⁹⁵. In 2009, novel G-protein coupled receptor-type G proteins, GTG1 and GTG2, were reported as ABA receptors in *Cell*⁹⁶. The *Arabidopsis* *gtg1/gtg2* double mutants showed ABA hyposensitivity in seed germination, stomatal response, root growth and expression of ABA responsive genes. Thus, it has been considered that GTG1/GTG2 is involved in ABA signaling, although its signal transduction mechanism has remained unclear⁹⁷.

In the same year, 2009, two separate groups reported the cytoplasmic ABA receptor, PYR/PYL/RCAR. Ma et al. identified the regulatory component of ABA receptor 1 (RCAR1) that interacts with ABI2, a PP2C, using the yeast two-hybrid assay⁹⁸. In *Arabidopsis*, there are 13 genes markedly similar to RCAR1 (RCAR2–14). Biochemical and thermodynamic analyses indicated that RCARs bind to ABA and inhibit PP2C

activity in the presence of ABA. Park et al. found that pyrabactin functions as a selective ABA agonist in the chemical library, and identified *PYRABACTIN RESISTANCE 1* (*PYR1*) by a chemical genetics screening using pyrabactin⁹⁹. *PYR1* belongs to the START superfamily of ligand-binding proteins, and there are 13 homologs of *PYR1*, *PYR1*-like proteins 1–13 (*PYL1*–13), in *Arabidopsis*. It was discovered that *RCAR* and *PYR/PYL* are the same protein, and thus, it is referred to as *PYR/PYL/RCAR* (*PYL*).

1-6. The functions of *PYL* and ABA signal transduction

Arabidopsis *PYL*s are classified into two distinct subclasses: dimeric receptors, *PYR1* and *PYL1*–3, and monomeric receptors, *PYL4*–12^{100,101}. Recent studies suggested that *PYL13*, which differs from other *PYL*s in the highly conserved three residues (in *PYR1*: Lys 59, Leu 87 and Asn 151) of the ABA binding pocket, interacts with other *PYL* isoforms and specific PP2Cs to regulate ABA signaling¹⁰²⁻¹⁰⁴. Dimeric receptors, which are inactive in the absence of ABA, dissociate into corresponding monomers in response to a conformational change induced by ABA binding, which triggers the closure of a mobile gating loop. This gate is open in the apoenzyme state but closes to create an interaction surface that enables binding to the active site of the PP2Cs, negative regulators of ABA signaling^{98,99,104-110}. In *Arabidopsis*, nine PP2Cs belonged to group-A, and six PP2C (*ABI1*, *ABI2*, *HAB1*, *HAB2*, *PP2CA/AHG3* and *AHG1*) deletion variants showed ABA hypersensitive phenotypes in seed germination, whereas the highly ABA-induced mutants, *hai1*, *hai2* and *hai3*, did not affect the ABA sensitivity^{111,112}. A recent study suggested that these three PP2Cs functioned as vegetative-specific regulators of ABA signaling in response to water stress¹¹³. ABA-bound *PYL*s interact with and inhibit PP2Cs, which directly inactivate SNF1-related protein kinases (subclass III SnRK2s) in the absence of ABA, allowing the activation of SnRK2s via autophosphorylation^{109,114,115}. Activated SnRK2s phosphorylate basic-domain leucine zipper (bZIP)-type ABA-responsive element-binding protein/factor (*AREB/ABF*) transcription factors and S-type anion channels, including *SLAC1*, elicit ABA actions^{114,116-119}. In *Arabidopsis*, three proteins, SnRK2.2 (*SRK2D*), SnRK2.3 (*SRK2I*) and OST1/SnRK2.6 (*SRK2E*) belong to a subclass of the SnRK2 family, and the

srk2d/e/i triple mutant has a completely abolished ABA response^{113,119-121}. Thus, in this system, the activity of the key regulatory SnRK2 kinases is controlled by ABA-mediated inhibition of PP2C activity. In contrast to dimeric receptors, monomeric receptors are in an equilibrium between gate-opened and gate-closed conformers in the absence of ABA^{100,101}. Thus, the heterologously expressed monomeric receptors inactivate PP2C activity in the absence of ABA^{97,99-101}, although at much lower levels than observed in the presence of ABA¹⁰⁰. Previous studies have indicated that both dimeric and monomeric receptors are involved in plant ABA responses^{122,123}. The *pyl8* single mutant shows an ABA-insensitive phenotype in roots, and the *pyr1pyl1pyl2pyl3pyl5pyl8* sextuple mutant, which includes monomeric receptor mutations, enhances the *pyr1pyl1pyl2pyl4* quadruple mutant phenotype and shows an extreme ABA-insensitive phenotype. However, the physiological importance of ABA-independent PP2C inhibition by monomeric receptors remains unresolved. It has also been demonstrated that the selective chemical activation of the dimeric receptors elicits a nearly full ABA response, which points to the dimeric receptors as key factors in ABA signaling¹²⁴. The results obtained in this study might help to resolve this question (described below).

Since the PYL protein family was identified as the ABA receptor in *Arabidopsis*, several studies have addressed their functions in various plant species, including commercial crops¹²⁵. In rice, there are 12 orthologs of *Arabidopsis* PYL, which are classified into two subclasses: dimeric receptors (OsPYL1–3) and monomeric receptors (OsPYL6, 10, 11)¹²⁶. Dimeric receptors show ABA-dependent PP2C inhibition, whereas monomeric receptors can inhibit PP2C in the absence of ABA. The crystal structure of OsPYL2-ABA-OsPP2C06 indicated that ABA binds OsPYL2 in the same manner as the AtPYLs-ABA binding model. Additionally, OsPYL5 has been identified as a positive regulator of ABA signaling in seed germination and seedling growth^{127,128}. In soybean, 21 of 23 PYL orthologs, GmPYLs, were characterized¹²⁹. GmPYLs are categorized into three subgroups by protein sequence similarity. Subgroup I includes GmPYL1–14, and most of them interact with PP2C in an ABA-dependent manner. Subgroup II contains GmPYL15–20, and GmPYL15–18 can interact in an ABA-independent manner. Subgroup III consists of GmPYL21–23. GmPYL23 cannot interact with PP2Cs in either the presence or absence of ABA. In addition, it was confirmed that GmPYL1,

GmPYL16 and GmPYL21 suppress PP2C activity in an ABA-dependent manner *in vitro*. The tomato ABA receptor, SIPYL, is composed of 15 family members¹³⁰, and *SIPYL1*, *SIPYL2*, *SIPYL3* and *SIPYL6* are the major genes involved in fruit development¹³¹. The strawberry ABA receptors consist of a family of 11 genes¹³². Silencing of *FaPYR1* by RNAi not only reduced the ABA content, ABA sensitivity and expression of ABA-responsive genes but also significantly delayed fruit ripening, suggesting that *FaPYR1* acts as a positive regulator in strawberry fruit ripening. The grape ABA receptor family contains seven genes (*VvRCAR1–7*), and *VvRCAR5* and *VvRCAR6*, respectively, act as the major ABA receptors in roots and leaves¹³³. Thus, there are many PYL proteins in plants and their functions may be redundant, making the regulation of PYL functions by gene manipulation is difficult.

1-7. Objective

The technological ability to chemically control the functions of plant hormones would be useful in addressing biological questions in multiple plant species. However, the development of a key material, a small molecular compound, is greatly delayed. Several plant hormones function as natural modulators of protein-protein interactions (PPIs) and ultimately modulate the affinity of hormone receptors for their protein binding partners^{134,135}. Indole-3-acetic acid, jasmonate-isoleucine conjugate and brassinosteroids act as molecular glues that stabilize PPIs without causing major conformational changes of their receptor proteins, whereas ABA and GA are allosteric ligands that cause conformational changes in their receptors that are required for PPIs¹³⁶⁻¹³⁹. Although PPIs have recently emerged as attractive drug targets, the rational design of small molecules that act as positive or negative PPI modulators remains challenging, in part because of the difficulty in creating tight interactions with the relatively flat, large and featureless interfaces typical of PPIs¹⁴⁰. In the case of plant hormones, such as ABA and GA, the challenge is different because these hormones bind within a cavity and induce conformational changes, as opposed to binding between two flat surfaces. Given this feature, it may be easier to manipulate these types of PPIs. However, with the exception of a GA receptor inhibitor that was discovered using chemical screening¹⁴¹, the successful, rational design of PPI inhibitors has been limited to rigid receptors, which

do not induce conformational changes¹⁴²⁻¹⁴⁴. Alternative design strategies are thus required for creating allosteric modulators, and such efforts benefit from known structural details of ligand-induced conformational changes; the ABA receptor system currently provides this data better than any other plant system. Here, we focused on the structural properties of ABA, which acts as a positive allosteric regulator of the PYLs, and planned a study to develop a negative allosteric regulator that inhibits PYL-PP2C interactions and blocks ABA signaling.

With respect to ABA analogs, numerous ABA receptor agonists have been described^{51,145}, but little work has been done regarding antagonists. Given the numerous stress responses across virtually all land plants, a tool for inhibiting ABA signaling would be extremely valuable for dissecting the myriad roles of ABA, particularly in new systems lacking genetic resources. Additionally, ABA-receptor antagonists are of potential agrichemical value because the ability to control seed germination rates, which are affected by ABA, is important in a number of crop species. Moreover, recent findings demonstrate that stress tolerant cereal varieties have a strong ability to inactivate ABA in pollens¹⁴⁶ that highlights the usefulness of not only enhancing, but of also locally reducing, ABA activity to acquire better stress tolerant plants. It has been previously shown that the sulfonamide pyrabactin (PyrA) is a selective agonist of PYR1 and PYL1 and a weak antagonist of PYL2, but its stronger agonist activity dominates its effects, and it is an ineffective antagonist *in vivo*. Thus, there is a real need to create antagonists for use in multiple contexts.

As the actions of PYL proteins are connected to ligand-mediated gate closure, an effective antagonist might stabilize gate-opened conformers. That is, they might function as inverse agonists. Alternatively, antagonists might enable gate closure but block PP2C binding and inhibition. To rationally create ABA receptor antagonists, we focused on the crystal structures of PYL-ABA complexes and structure–activity relationship studies of ABA. They are described in detail below.

1-7-1. The structural basis for PYL-PP2C interactions

The crystal structures of PYLs were solved immediately after the identification of the PYL receptors^{46,101-103,105-108,147-150}. So far, PYR1, PYL1, PYL2, PYL3, PYL5, PYL9, PYL10 and PYL13 have been registered in the Protein Data Bank (PDB), and their

crystal structures were resolved as PYL-ABA, PYL-pyrabactin, PYL-ABA-PP2C, PYL-pyrabactin-PP2C, PYL-quinabactin-PP2C or PYL-PP2C complexes (Table 1). These crystal structures revealed that ABA acts as an allosteric modulator of PYL and induces the interaction between PYL and PP2C. The PYL structure is composed of three α -helices, including a 3_{10} -helix, denoted as η , and seven β -strands with the following N-terminal: $\alpha 1$ - $\beta 1$ - $\alpha 2$ - $\eta 1$ - $\beta 2$ - $\beta 3$ - $\beta 4$ - $\beta 5$ - $\beta 6$ - $\beta 7$ - $\alpha 3$. The seven β -strands wrap up the ABA binding pocket and form the anti-parallel β -sheet. The ABA binding pocket is created by the $\eta 1$ - $\beta 2$ loop, $\beta 3$ - $\beta 4$ loop, $\beta 7$ - $\alpha 3$ loop and the N-terminal part of $\alpha 3$. The major differences between ABA-free and -bound PYL are observed in the relative positions of the gate-like loop between $\beta 3$ and $\beta 4$ (Fig. 5). In apo-PYL, the gate has an open conformation that allows ABA access to the ligand binding pocket from outside. Whereas in the ABA-bound PYL, the gate has a closed conformation and ABA is almost completely surrounded by PYL's amino acid residues. The orientation of the side chains of the highly conserved proline and serine on the gate loop are changed in accordance with gate closure. In the gate open conformer, the side chains of proline and serine are facing outside and inside, respectively. On the contrary, in the gate closed conformer the side chains of proline and serine are facing inside and outside. Thus, the hydrophobicity of gate entrance is increased according to gate closure. Considering that a cyclohexenone ring of ABA is hydrophobic, ABA may be involved in the hydrophobic interactions of gate residues to induce gate closure. In addition, the serine residue in the gate closed conformer plays an important role in the interaction between PYL and PP2C and the inhibition of PP2C activity.

Table 1| Protein Data Bank codes for the crystal structures of PYR/PYL/RCAR (PYL), PYL-ligands and PYL-ligands- protein phosphatases 2C (PP2Cs).

	PYR1	PYL1	PYL2	PYL3	PYL5	PYL9	PYL10	PYL13
Apo		3KAY	3KDH 3KL1 3KAZ	3KLX	4JDL		3UQH 3RT2	
PYL-ABA	3K3K	3JRS	3KDI 3KB0	4DSB 4DSD		3W9R	3R6P	
PYL-ABA-PP2C	3QN1 3K90	3KDJ 3JRQ	3UJL 3KB3	4DS8		3OQU		
PYL-PP2C							3RT0	4N0G
PYL-pyrabactin	3NJO	3NEF 3NEG	3NR4 3NS2 3NJ0 3NMH	3OJI				
PYL-pyrabactin-PP2C		3NMN						
PYL-quinabactin-PP2C			4LA7 4LG5					
PYL(-)-ABA				4JDA				
PYL-AS6	3WG8							

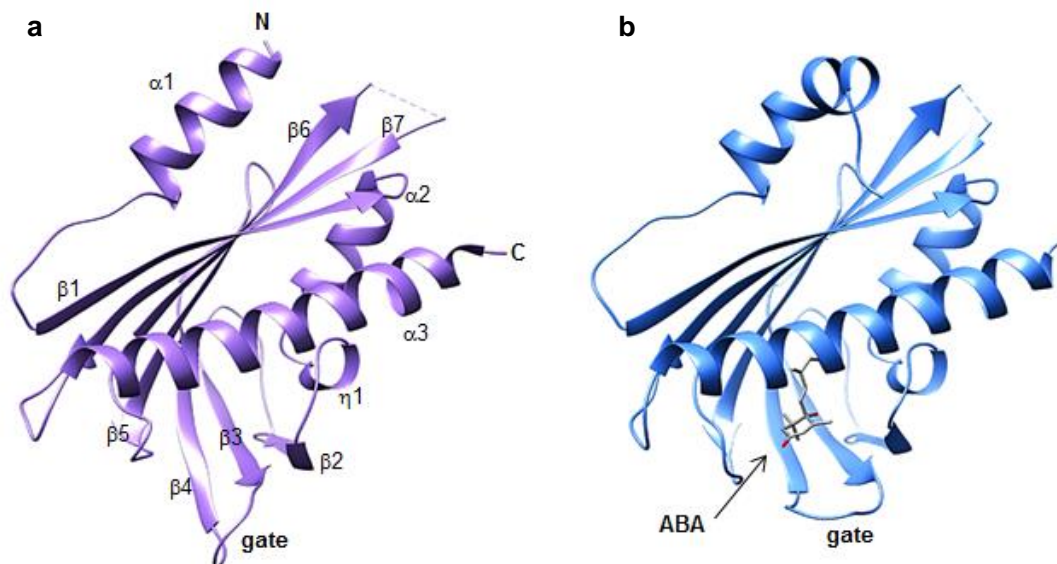


Figure 5 | Structure of apo-PYR/PYL/RCAR (PYL) receptor, PYL1 (a, PDB: 3KAY), and ABA-bound PYL1 (b, PDB: 3JRS).

In the PYL-ABA complex, PYL interacts with ABA through ion pairing, hydrogen-bond networks and hydrophobic contacts. The carboxyl group of ABA forms an ion pair with the side chain of lysine, which is highly conserved in the $\eta 1$ - $\beta 2$ loop. A PYL2 mutant, in which this lysine residue is mutated to alanine (PYL2^{K64A})¹⁰⁵, and PYL13, in which the equivalent lysine is replaced with glutamine¹⁰⁴, cannot bind to ABA. These results are consistent with the structure-activity relationship studies, in which the reduction, esterification and amidation of the carboxyl group of the ABA's side chains reduces the bioactivity⁵¹. Because the position of the lysine residue is not different between apo-PYL and ABA-bound PYL, this residue is not directly involved in the gate closing and interactions with the PP2Cs. As mentioned above, the ABA's ring moiety may be necessary to induce gate closure via hydrophobic interactions. ABA has three methyl groups in the ring moiety, and the C2'-binding methyl (C7' position) is the most important for bioactivity. The absence of C7' (7'-nor-ABA, **2**) almost eliminates ABA activity, whereas the elongation of the alkyl chain at C7' (7'-methy-ABA, **3**) retains the activity, although its activity is lower than that of ABA. The absence of the C6' geminal methyl group [C8' (**4**) or C9' (**5**)] has little effect on the activity, but the absence of both (**6**) dramatically reduces the activity. These observations suggest that the C2' and C3' positions of the ABA's ring participate in gate closure via hydrophobic contacts to hydrophobic residues on the gate loop. On the other hand, C8' and C9' methyl groups probably play important roles in placing the ABA ring in a compatible position in the PYL-ABA complexes.

The importance of hydrophobic contacts in gate closure is supported by the structural analyses of PYL-pyrabactin^{145,151}, PYL-quinabactin^{124,152} and PYL(-)-ABA⁴⁶ complexes. Pyrabactin acts as an agonist for PYR1 and PYL1, but an antagonist for PYL2. In the PYL1-pyrabactin complex, the gate loop adopts a closed conformation, whereas in the PYL2-pyrabactin complex the gate retains an open conformation. Furthermore the binding orientation of pyrabactin in PYL2 is rotated 180° from that of PYL1. The bromonaphthalene ring of pyrabactin in the PYL1-pyrabactin complex is located at the same position as the 2,6,6-trimethyl-cyclohexene ring of ABA in the PYL1-ABA complex. They may be the major driving forces to induce closed conformations through hydrophobic interactions with residues on the gate loop. On the other hand, in the PYL2-pyrabactin complex, a smaller pyridine ring is located at the

same position instead of a bromonaphthalene ring. This pyrabactin orientation cannot provide sufficient hydrophobic contacts to induce the gate closure.

Quinabactin, a dihydroquinolinone sulfonamide ABA analog is a strong agonist of PYR1, PYL1 and PYL2, and weakly activates PYL3 and PYL5. Based on comparisons with the crystal structures of PYL2-ABA-HAB1 and PYL2-quinabactin-HAB1, the 4-benzylmethyl substructure of quinabactin can be superimposed on the C6 methyl group of ABA. Considering that an ABA analog lacking C6 (6-nor-ABA, **7**) dramatically reduces bioactivity, this moiety may contribute to the hydrophobic contacts that induce conformational changes. In addition, quinabactin's dihydroquinolinone oxygen and ABA's cyclohexenone oxygen can be superimposed on each other, and they form a water-mediated hydrogen bond with tryptophan 385 from HAB1. Thus, quinabactin more closely mimics the interaction between ABA and PYLs than does pyrabactin.

A structural analysis of the PYL3-(–)-ABA complex indicated that the C8' and C9' methyl groups are positioned at the entrance of the ligand binding pocket, which is normally occupied by the C7' methyl group of (+)-ABA. (+)-8'-nor-ABA and (+)-9'-nor-ABA showed comparable activity levels to that of (+)-ABA. However, the (–)-ABA analog lacking the C8' methyl group reduced the bioactivity to less than 1/100 of that of (–)-ABA¹⁵³ (the activity of (–)-9'-nor-ABA has not been investigated). This data also suggests that the interaction between the ABA's cyclohexenone ring and the hydrophobic residues on the gate loop plays a key role in the conformational change.

Compared with the structures of the PYL-ABA and PYL-ABA-PP2C complexes, the conformation of PYL remains almost unchanged. The loops β 3- β 4 (gate) and β 7- α 3 are slightly shifted in ABA to form a tiny hydrophobic pocket. In the PYL-ABA-PP2C complex, PYL interacts with PP2Cs using mainly the gate loop and the N-terminal of the α 3 helix. A highly conserved serine residue in the gate loop has a key role in this interaction. Its hydroxyl group forms a hydrogen bond with the carboxyl group of glutamic acid, which composes an active site in the PP2Cs. A PYL1 mutant in which this serine residue was replaced with an alanine (PYL1^{S112A}) showed a reduced inhibitory activity against PP2Cs. In addition, the side chain of the conserved tryptophan in the PP2Cs is inserted into a narrow hydrophobic pocket of ABA-bound PYL to form hydrophobic contacts with PYL residues, including Phe159 (PYR1

numbering). In this hydrophobic pocket, the amino group of the indole ring of the tryptophan forms a water-mediated hydrogen bond with the carbonyl group of ABA.

1-7-2. Structure–Activity Relationships

Numerous ABA analogs have been synthesized to help clarify the structure–activity relationships and to develop more potent active compounds or biochemical tools for investigating the molecular mechanisms of ABA. The activities of these ABA analogs have been investigated under various conditions and in different plant species, making it difficult to quantitatively describe the structure–activity relationships. Therefore, the qualitative structural requirements for ABA activity are summarized in Fig. 6. The relationship between structures of ABA analogs and activities was reviewed by Addicott and Todoroki in detail^{51,154}; therefore, here they are described in terms of the activities combined with crystal structure analyses of PYL-ABA complexes.

The C1 carboxyl group is essential for binding to PYL, as mentioned above, but the alkyl esters of ABA (**8**), abscisic aldehyde (**9**) and ABA-alcohol (**10**) show similar activity levels as ABA in long-term assays, suggesting that these compounds are converted to ABA by hydrolysis or oxidation in plants. The C1' hydroxyl group acts as a proton donor and forms a water-mediated hydrogen bond with Glu 94 (PYR1 numbering). The absence of a hydroxyl group (1'-deoxy-ABA, **11**)¹⁵⁵ and replacement of a hydroxyl group with fluorine (1'-deoxy-1'-fluoro-ABA, **12**)¹⁵⁶, which can only act as a proton acceptor, reduces the ABA activity to 1/10–1/20 of its normal level. The activity of 1'-*O*-methyl-ABA (**13**) also has 1/10–1/100 the activity of ABA¹⁵⁷. The C4' carbonyl group acts as a proton acceptor. It forms a hydrogen bond with the backbone amide of Ala89 (PYR1 numbering) and a water-mediated hydrogen bond with the tryptophan residue of PP2C. Nevertheless, the 4'-reduced analogs, 1,4-diol-ABA (**14**, **15**) and 4'-deoxo-ABA (**16**), retain bioactivity, suggesting that these analogs are oxidized to the 4'-oxo-type in plants. On the other hand, 4'-methoxy-ABA (**17**) has a clearly reduced bioactivity¹⁵⁸.

The methyl groups C6, C7', C8' and C9' are involved in hydrophobic interactions with PYL's residues. In particular, the C6 and C7' methyl groups, which are located at the entrance of the ligand binding pocket, seem to be directly involved in gate closing, as described above. Consistent with this observation, the activity of 6-nor-ABA (**7**) and

7'-nor-ABA (**2**) are 1/100, or much less, than that of ABA.

The two conjugated double bonds of the side-chain (2*Z*, 4*E*) form an important moiety that determines the positions of the C6 methyl and C1 carboxyl groups of the PYL-ABA complexes. The geometric isomer of the 2C double bonds (2*E*-ABA, **18**) and C2 double bond reduced analogs (**19**, **20**) do not show ABA activity. On the other hand, the replacement of the C4 double bond by a triple bond (**21**) has little effect on the activity. Superpositioning **21** and ABA in the PYL-ABA complex indicates that the C6 methyl and C1 carboxyl groups of **21** reside in almost the same positions as those of ABA. The C2' double bond in the ring moiety plays an important role in determining the conformation of the cyclohexenone ring. The replacement of the C2' double bond with a single bond retains the activity level, but only when the C7' methyl is *cis* to the side-chain (**22**), which adopts an axial orientation.

In the PYL-ABA complex, ABA is bound in a half-chair conformation with an axial side-chain, which is consistent with the most thermodynamically stable conformer. The relationship between the ring conformation and activity were thoroughly investigated by Todoroki⁵¹. The ABA analogs with conformations that are constrained by a cyclopropyl ring (**23–26**) have reduced bioactivity and an increasing abundance of the conformer with an equatorial side-chain. These results are supported by the conformations of ABA analogs in the crystal structures of the PYL-ABA complex.

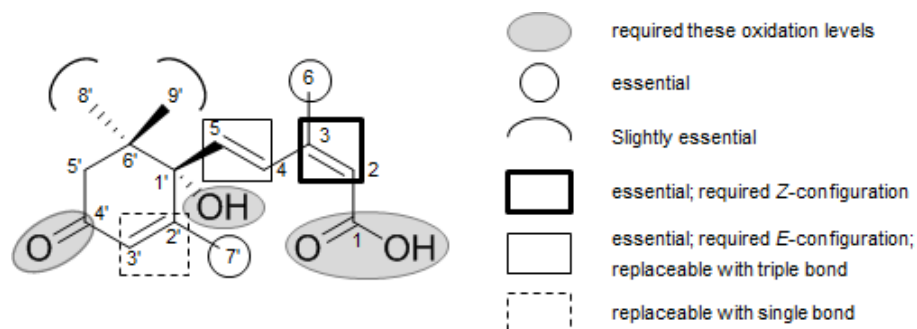


Figure 6 | Structural requirements for ABA activity.

Structural factors required for ABA activity: i) oxidized 1-carboxyl, 1'-hydroxyl, and 4'-carbonyl groups, ii) methyl groups (C6, C7', C8', and C9'), iii) C-C double bonds at C2 and C4, and iv) conformations of the six-membered ring and side-chain. The absence of any one functional group reduces activity, although to varying degrees.

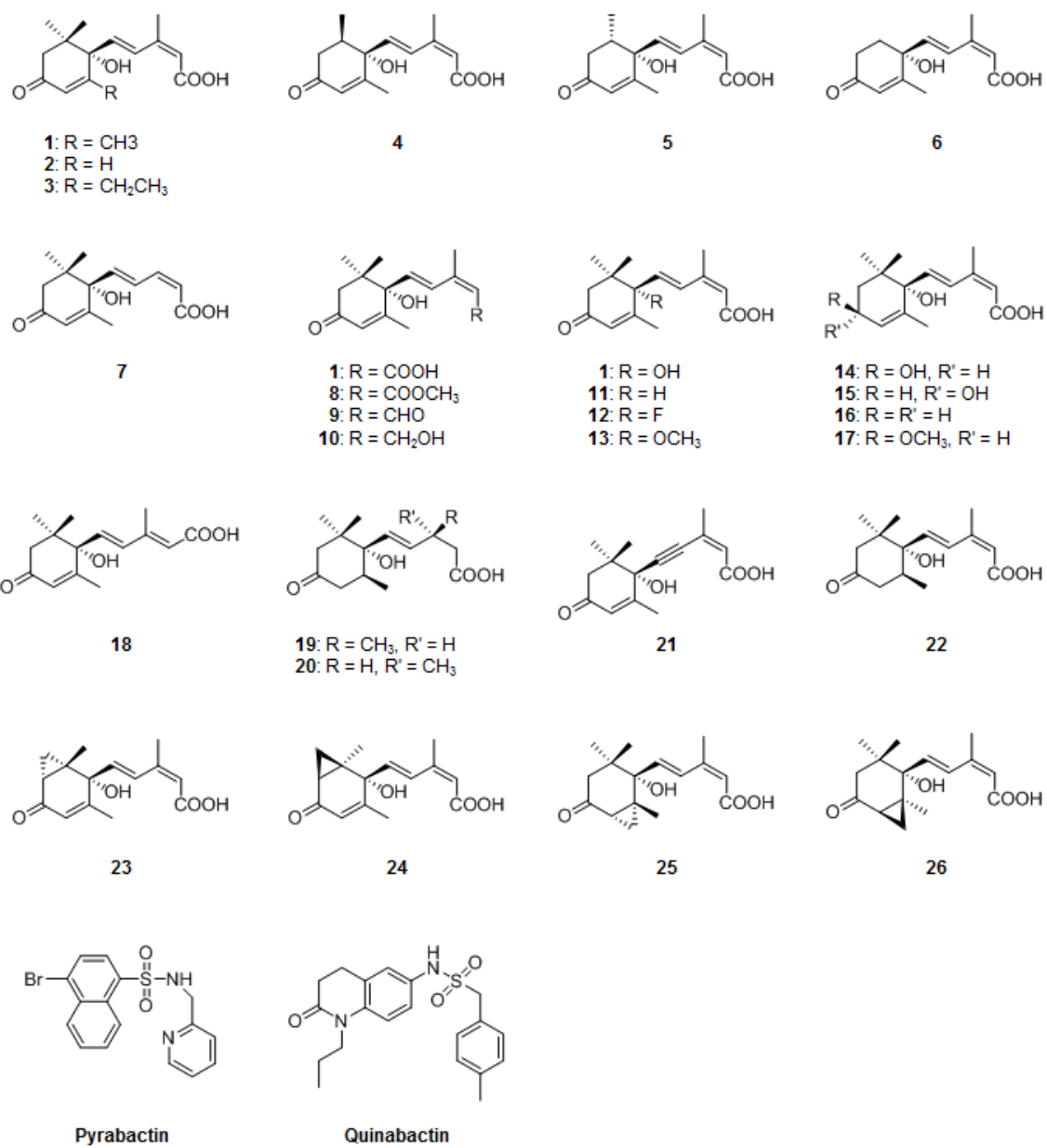


Figure 7 | Structures of ABA analogs.

2. Results

2-1. Design and synthesis

ABA interactions with the receptor in the PYL-ABA complex completely concur with those predicted based on the structure–activity relationship. Therefore, here we designed an ABA receptor antagonist based on molecular structure. An ABA receptor antagonist needs to bind strongly to PYL but not induce the interactions between PYL and PP2C. Considering that the affinity of the PYL-ABA-PP2C ternary complexes for ABA is 10-fold higher than that of PYL-ABA complexes, a PYL antagonist is needed at a concentration 10-fold greater than that of ABA to evenly antagonize the ABA action even if it has a comparable affinity to ABA. Thus, the design concept for a practical PYL antagonist should not reduce the affinity for PYL and, if possible, enhance the affinity by forming novel interactions.

In the PYL-ABA complexes, the side chain carboxylate of ABA was deeply intruded into the ligand binding pocket to form the salt bridge with Lys, thus any modifications of the side chain will reduce the affinity for PYLs, which are also supported by structure-activity relationship studies. On the other hand, the C2', C3' and C4' positions of ABA's ring were found to participate in gate closure via hydrophobic contacts to the gate loop, thus some structural modification of this portion can affect the conformational change of PYL. Furthermore, multiple PYL-ABA X-ray structures revealed that gate closure was accompanied by the formation of two small solvent-exposed tunnels adjacent to ABA's 3'-CH and 4'-C=O (Fig. 8a,b). The entrance to these tunnels (referred to as 3'- and 4'-tunnels) lay on the interface that normally contacted PP2C. Here we focused on the 3' tunnel that was a relatively simple cleft formed by five highly conserved hydrophobic residues (in PYR1: Phe61, Leu87, Pro88, Phe159 and Val163; Fig. 8c-f). Because some 3'-modified analogs of ABA retained activity (Table 2)^{51,159}, it was reasoned that the 3' tunnel might have accepted alkyl substituents at the 3' position that could then form hydrophobic contacts with the tunnel. One might have expected such derivatives to potentially stabilize the gate-closed conformer, interfere with gate closure or, in the case of longer chains, protrude through the tunnel and prevent PP2C binding. Thus, alterations of chain length could conceivably have resulted in both agonists and antagonists, making this an interesting site for ABA modifications.

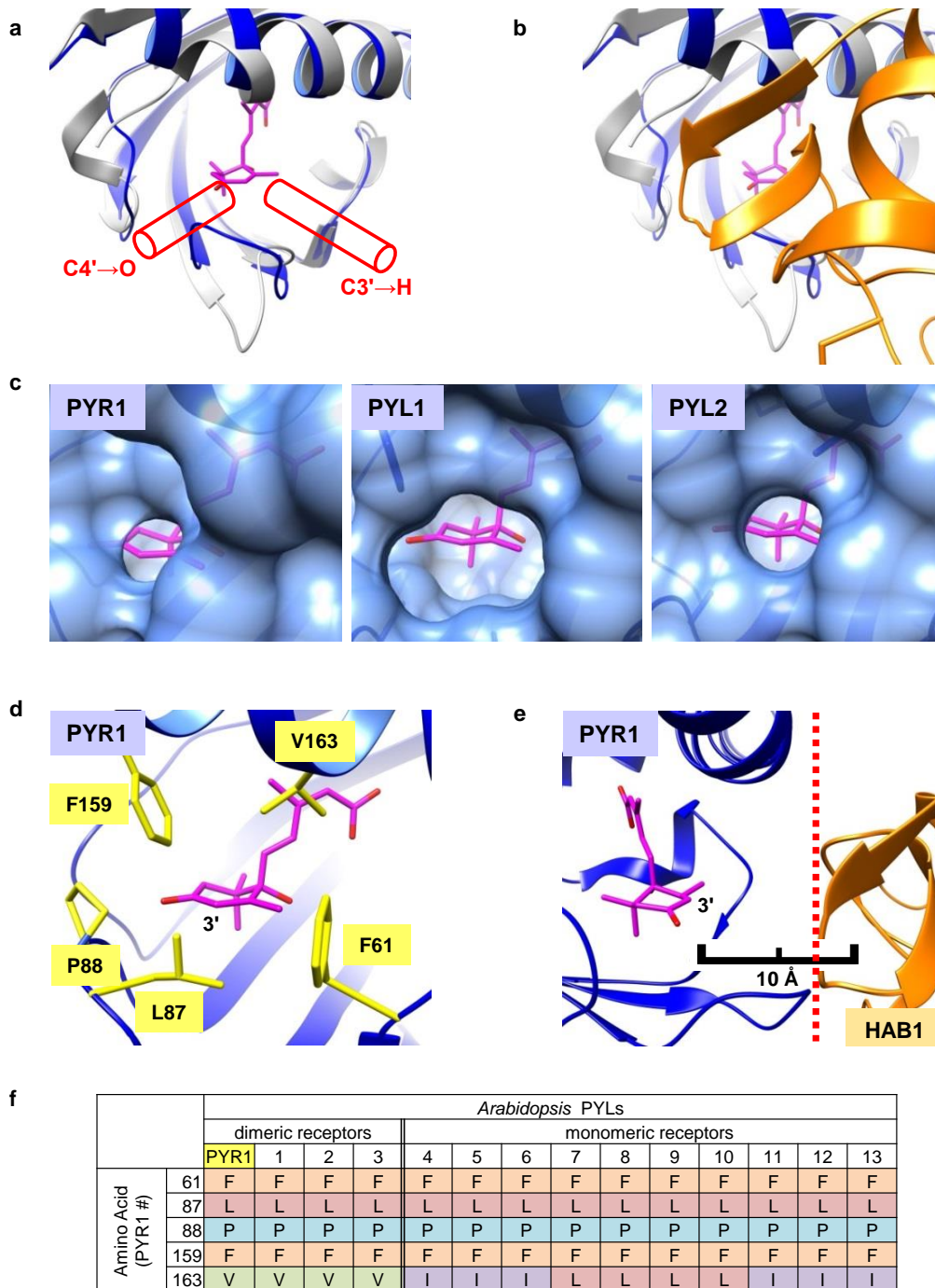


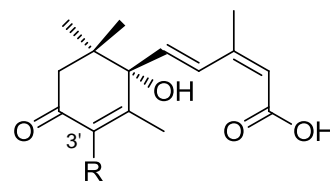
Figure 8 | Existence of small tunnels in PYL-ABA complexes.

a, Superimposition of the apoenzyme (gray) and ABA-bound (blue) PYR1 structure (PDB code: 3K90). Small tunnels highlighted by red cylinders and ABA, magenta sticks. **b**, HAB1 binds to the PYR1-ABA complex and covers these tunnels (3QN1). HAB1, orange, displayed in same view as in **(a)**. **c**, Close-up view of 3'-tunnel in PYR1-ABA (3K90), PYL1-ABA (3JRS), and PYL2-ABA (3KDI) complexes. Solvent-accessible surfaces (probe radius: 0.9, 1.4, and 1.4 Å, respectively) prepared with Chimera software¹⁶⁰. **d**, 3'-tunnel composed of well-conserved hydrophobic amino acids. **e**, Distance between C3'-position of ABA and PPI interfaces of HAB1 in PYR1-ABA-HAB1 complex (3QN1). **f**, Sequence alignment of residues composing 3'-tunnel.

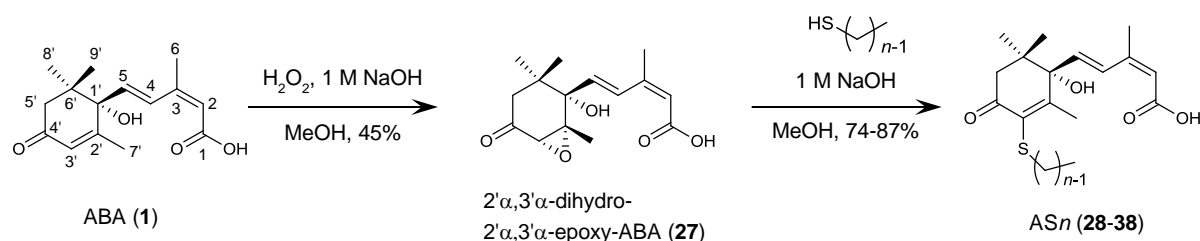
Table 2 | Biological activity of 3'-modified ABA.

Compounds	Bioactivity ^a
ABA (assay control): R = H	+++
3'-fluoro-ABA: R = F	+++
3'-chloro-ABA: R = Cl	+++
3'-bromo-ABA: R = Br	+++
3'-iodo-ABAR = I	++
3'-azido-ABA: R = N ₃	+++
3'-methyl-ABA: R = CH ₃	+++
ABA-3'- <i>n</i> -butyl thiol: S(CH ₂) ₄ SH	++
ABA-3' dimer: S(CH ₂) ₄ S-3'-ABA	-

^a The activity in rice seedling elongation assay: +++, 1; ++, 1/10; +, 1/100; -, <1/100.



On the basis of the above considerations, 3'-alkylsulfanyl ABAs were designed by nucleophilic addition of alkyl thiolate to the 2',3'-epoxides **27**, prepared from ABA (**1**; Fig. 9) using the most simple and selective method^{161,162}. For simplicity, these are called the AS_{*n*} compound series (**28-38**), where *n* denotes the alkyl chain length. Before preparing these compounds, a model of a PYR1–AS₆ complex was constructed on the basis of crystal structures of PYR1–ABA complexes^{47,147}, to estimate an appropriate length of alkyl chain of AS_{*n*}. This model suggested that a hexyl chain was of sufficient length to protrude through the PYR1 surface (Fig. 10a) and occupy a position normally occupied by the highly conserved PP2C residue Val393 (HAB1 numbering; Fig. 10b). Therefore, AS₆ was predicted to bind PYR1's ligand-binding pocket and disrupt PP2C binding. These analyses also suggested that compounds with *n* < 4 might stabilize gate closure and act as agonists. The validity of these predictions was established by the synthesis and characterization of 11 AS_{*n*} compounds (*n*=2–12; Fig. 9).

**Figure 9 | Synthesis of AS_{*n*} compounds (*n*=2-12).**

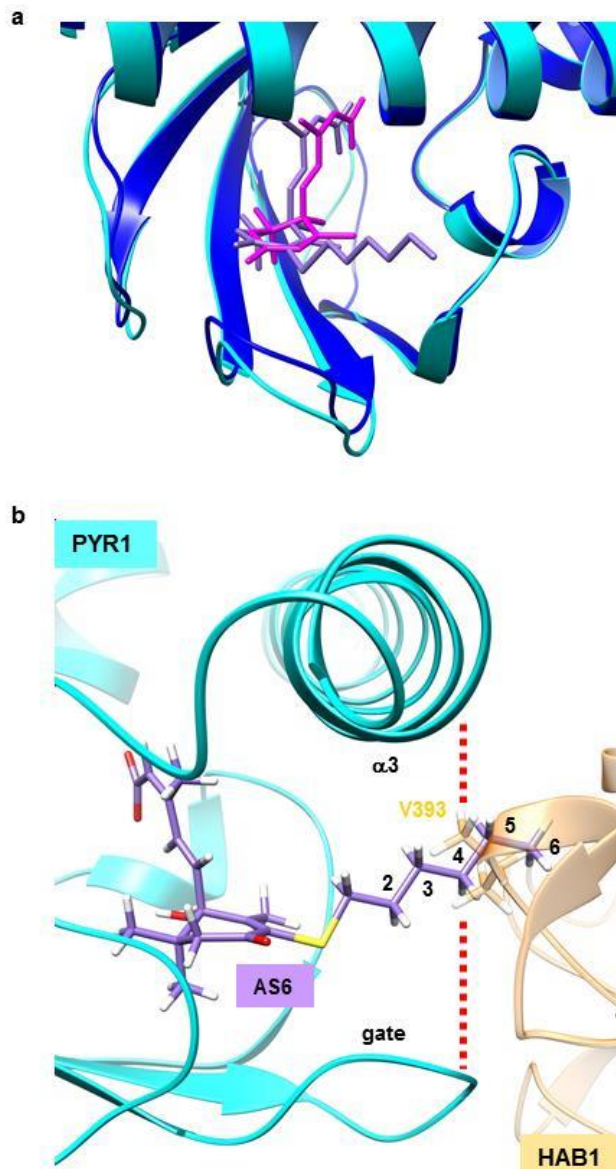


Figure 10 | A homology model of AS6-bound PYR1 constructed based on the crystal structure of PYR1-ABA complex (PDB code: 3K90).

a, Superimposition of PYR1-ABA complex (cyan) and a homology model of PYR1-AS6 complex (blue). ABA, magenta sticks and AS6, purple sticks. **b**, AS6 is overlaid on ABA in PYR1-ABA-HAB1 complex, hexyl chain overlaps with HAB1 residue.

2-2. Physiological effects of AS_n on plants

As these compounds' activities *in vivo* were of paramount importance, the effects of AS_n compounds were examined first using seed germination assays, which rely on ABA's inhibitory effect on germination to distinguish between antagonist or agonist activities. Here, agonists inhibit seed germination, and antagonists relieve this inhibition when coapplied with ABA. These experiments showed that AS2 and AS3 inhibited *Arabidopsis* seed germination and early seedling growth and that the potency of AS2 was greater than that of ABA (Fig. 11a and Fig. 12). *In vivo*, ABA is inactivated by cytochrome P450-mediated hydroxylation by CYP707A enzymes^{79,80}. Although the catabolic rate of AS_n compounds in plants was not examined, the inhibition activity against recombinant *Arabidopsis* CYP707A3 suggested that the affinity of AS2 and AS6 (K_i value = 56 and 48 μ M, respectively) for the enzyme active site are 10-fold lower than that of ABA (K_m = 4.8 μ M) (Table 3). Therefore, the enhanced catabolic stability compared to ABA should be taken into consideration in evaluating the *in vivo* activity of AS_n compounds. AS4 was a weaker agonist than AS2 and AS3, and molecules with $n > 4$ did not inhibit germination. AS2–AS4 enhanced and AS5–AS12 suppressed ABA's effect on germination and early seedling growth in coapplications with ABA (Fig. 11b and Fig. 12). Although the suppression effect was not very strong in an early stage of the assay, the effect of ABA was almost completely relieved eventually (Fig. 13), probably because the co-applied ABA was inactivated more promptly than AS_n compounds. The suppression of ABA effects by AS5–AS12 suggested that they were receptor antagonists.

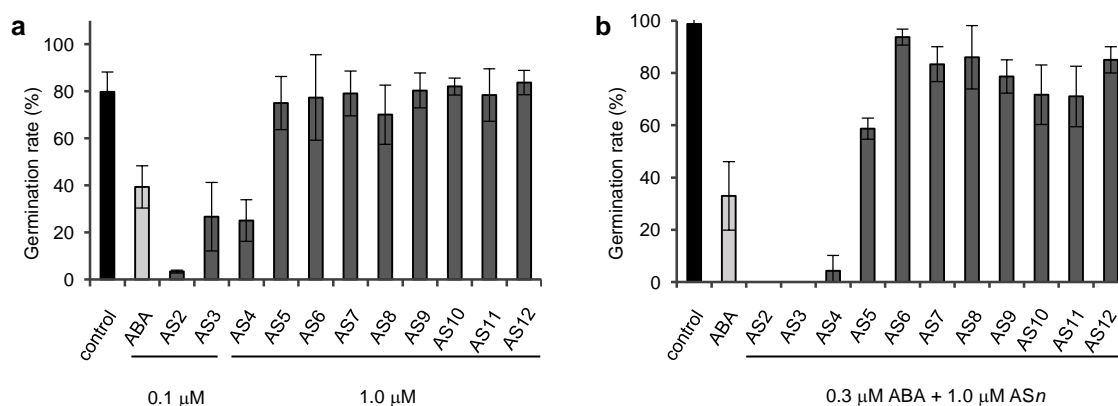


Figure 11 | The effects of AS_n on *Arabidopsis* seed germination.

a, Seed germination rate in the presence of AS_n at 24 h after stratification ($n=3$; error bars represent, s.d.). **b**, Seed germination rate in presence of 0.3 μ M ABA and 1.0 μ M AS_n at 36 h after stratification ($n=3$; error bars represent, s.d.).

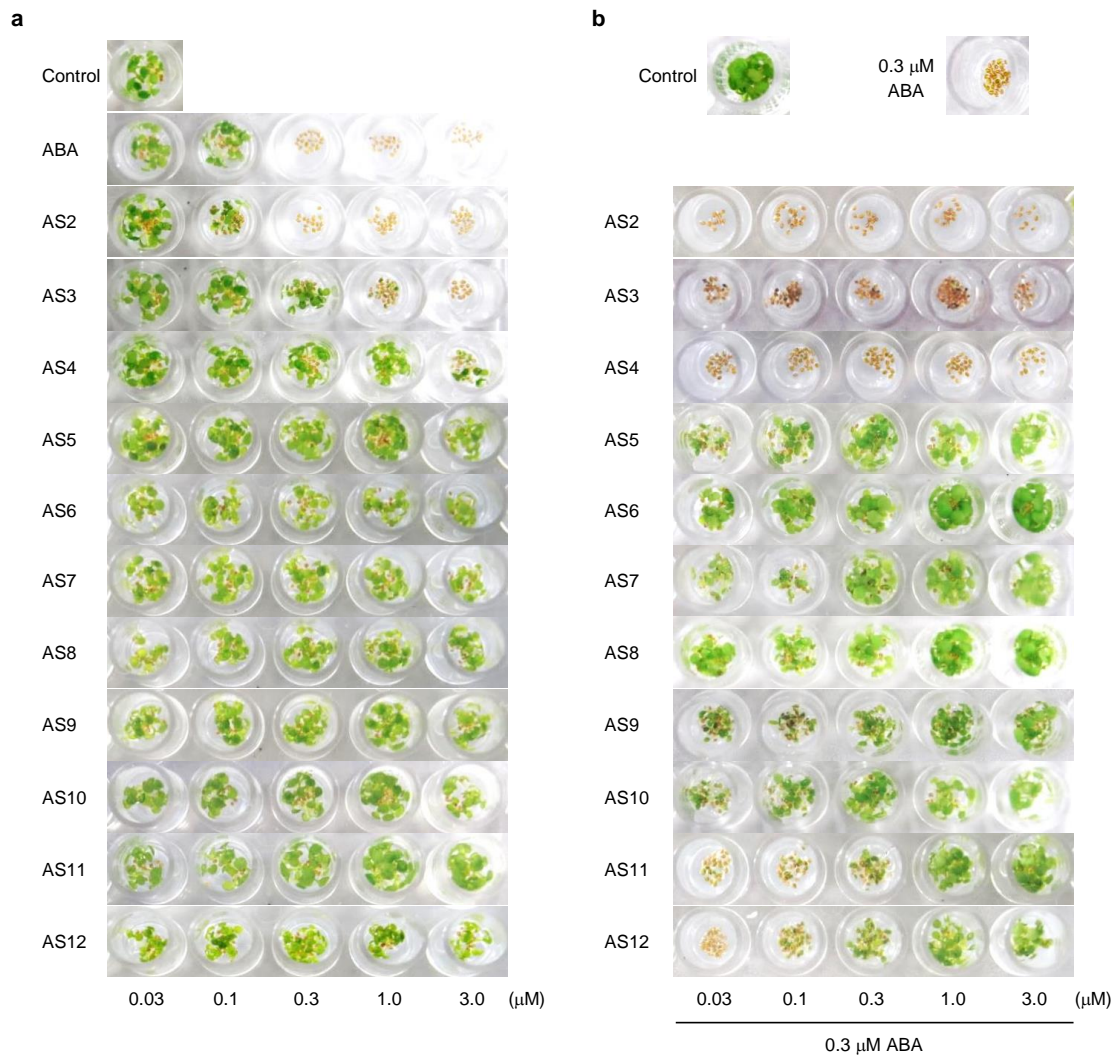


Figure 12 | Effects of AS n on early seedling growth of *Arabidopsis*.

AS2-AS4 exhibited an inhibitory effects, although to various degrees, whereas AS5-AS12 relieved ABA-inducible inhibition. **a**, Seedlings grown on test media agar containing indicated AS n concentrations for 5 d. **b**, Seedlings grown on test media agar containing 0.3 μM ABA and indicated AS n concentrations for 10 d. Similar results obtained from three independent experiments using different seed batches.

Table 3 | Inhibitory activity of AS2 and AS6 for 8'-hydroxylase.

Compounds	CYP707A3 ^a inhibition ratio K_i (μM)
AS2	56
AS6	48
Abz-E2B ^b	0.036

^a *Arabidopsis* recombinant CYP707A3 expressed in *E. coli*.

^b A selective inhibitor of ABA 8'-hydroxylase CYP707A¹⁶³

The K_m value of ABA was determined to be 4.8 μM in this assay.

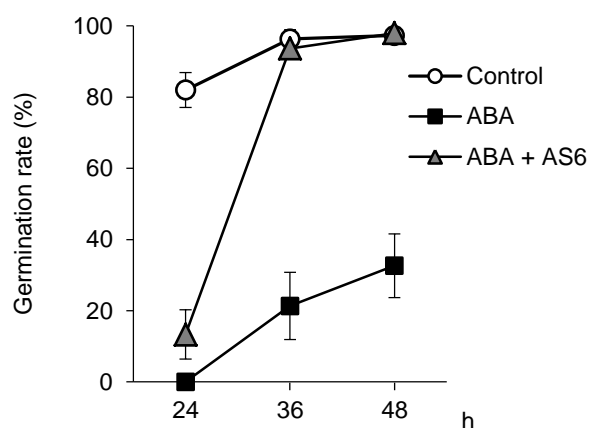


Figure 13 | Antagonistic effects of AS6 on *Arabidopsis* seed germination.

Seed germination rate in presence of 0.3 μM ABA and 1.0 μM AS6 at 24, 36, and 48 h after stratification. Seed germination rate in presence of 0.3 μM ABA also shown. ($n=3$; error bars, s.d.).

A similar trend was observed in studies with *Lactuca sativa* (lettuce), which showed that AS n compound effects were not restricted to *Arabidopsis* (Figs. 14 and 15). Interestingly, AS4 showed the opposite effect in seed germination and early seedling growth, that is, AS4 inhibited lettuce seed germination whereas it suppressed ABA's effect on seedling growth. The effects of AS2, AS4 and AS6 were also tested on *Raphanus sativus* (radish) seedling drought tolerance. Treatments with AS2 reduced water loss and enhanced drought tolerance (Table 4 and Fig. 16), as expected of an agonist. Conversely, AS6-treated seedlings lost water more rapidly, showed reduced leaf temperatures (owing to increased evaporative cooling) and wilted more quickly than mock-treated controls (Figs. 16 and 17), consistent with expected antagonist effects.

Thus, the AS_n compound series contained both agonist and antagonist activities with good bioavailabilities and activities beyond the model plant.

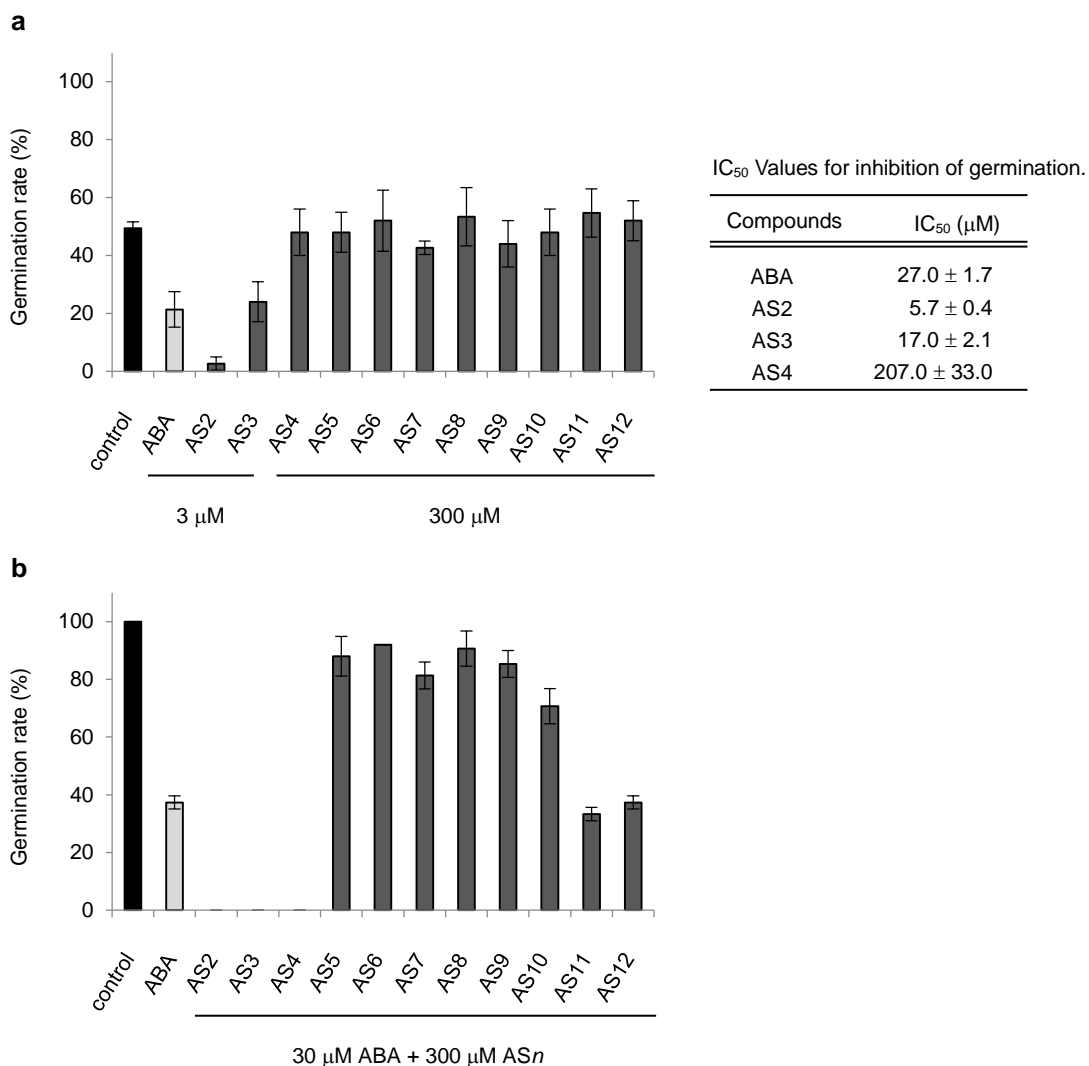


Figure 14 | Effects of AS_n compounds on lettuce seed germination.

AS_n exhibited similar effects as *Arabidopsis* seed germination. **a**, Seed germination rate in presence of AS_n at time when germination rate of control plant is at 50%. Inhibitor concentrations resulting in 50% inhibition (IC₅₀) of ABA, AS2, AS3, and AS4 at 72 h after seed sowing indicated. **b**, Seed germination rate in presence of 30 μ M ABA and 300 μ M AS_n at time when germination rate of only ABA-treated plant is at 40% ($n=3$; error bars, s.d.).

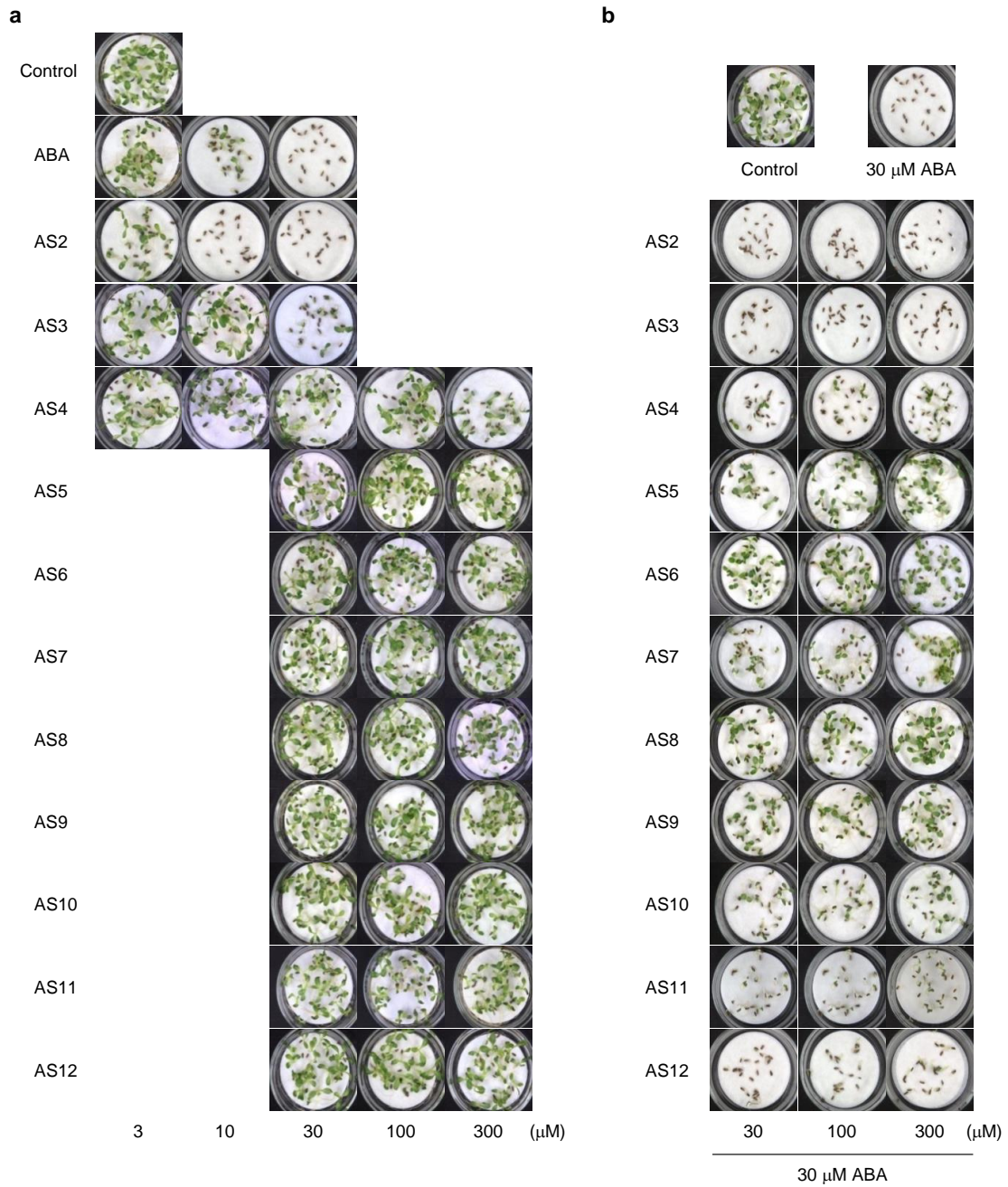


Figure 15 | Effects of AS n on early seedling growth of lettuce (*grand rapids*).

a, Seedlings grown on filter paper soaked in solutions containing indicated AS n concentrations for 14 d. **b**, Seedlings grown on filter paper soaked in solutions containing 30 μM ABA and indicated AS n concentration for 14 d. Similar results obtained from three independent experiments using different seed batches.

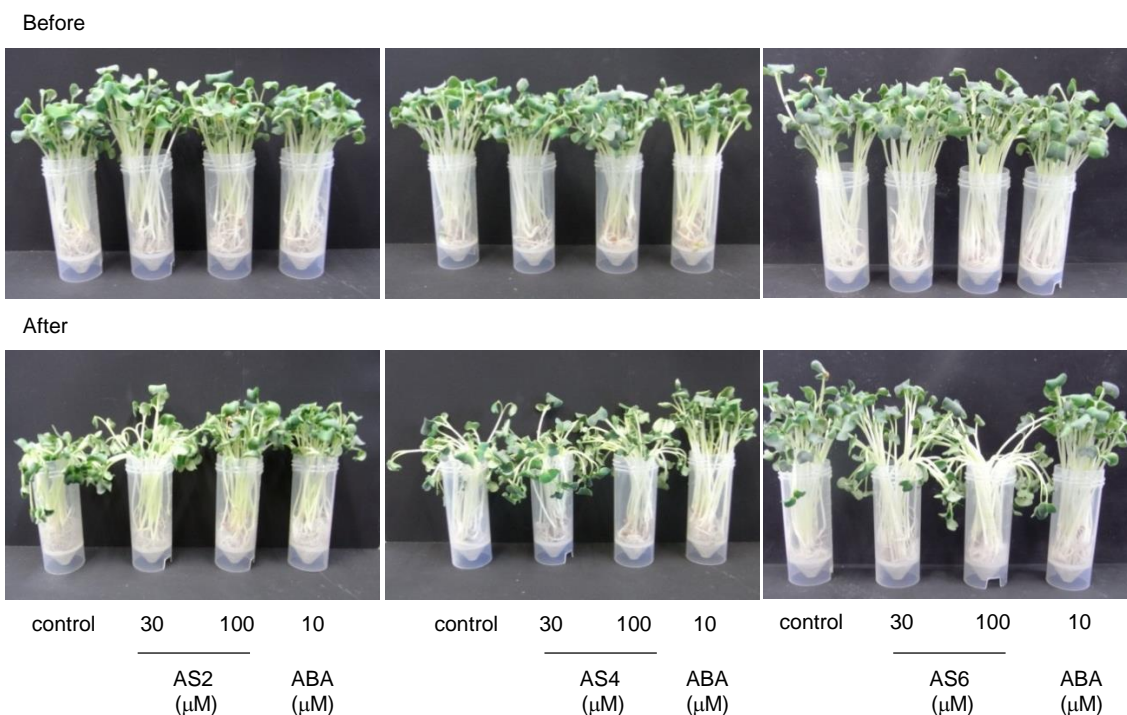


Figure 16 | Effects of AS2, AS4 and AS6 on drought tolerance.

Seven-day-old radish seedlings treated with AS n solutions for 12 h, transferred to empty tubes and left for 8, 4, or 3 h (left, middle, and right, respectively).

Table 4 | Effect of AS2, AS4 and AS6 on transpirational water loss.

	Conc. (μM)	Relative rate of water loss (%) ^a
control		100
ABA	10	53 ± 6.6
AS2	30	71 ± 3.7
AS4	100	63 ± 12
AS6	30	95 ± 11
	100	92 ± 9.7
	30	108 ± 11
	100	127 ± 15

The data represent means ±s.d. of three replications.

^aRelative reduction rate normalized to control (untreated) value of 100%.

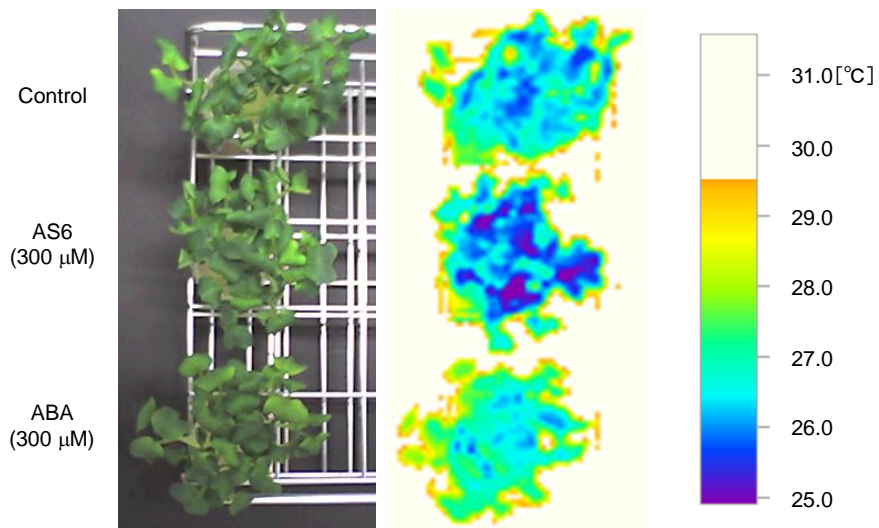


Figure 17 | Leaf surface temperature determined by infrared thermal imaging. Leaf temperature of radish seedlings monitored after treatment of AS6 (300 μM), ABA (300 μM), or water (control). Similar results obtained from three independent experiments.

The molecular bases of AS2, AS4 and AS6 actions *in vivo* were further characterized in *Arabidopsis*. AS2 was found to induce expression of ABA-responsive genes and the β -glucuronidase (GUS) gene on an ABA-responsive, transcriptional, reporter line with slightly stronger activity than ABA, which was consistent with the seed germination data (Fig. 18a,b). With AS4, clear expression of ABA-responsive genes was not observed by qRT-PCR, but weak reporter gene activation was detected in root tissues (Fig. 18a,b). As expected, AS6 was not able to induce obvious ABA responses, as measured by both qRT-PCR gene expression and reporter line assays (Fig. 18a,b). AS2 enhanced expression of ABA-inducible genes, whereas AS4 and AS6 lessened their expression in cotreatment with ABA (Fig. 18c,d). This antagonist effect was stronger for AS6 than AS4, the latter only partially decreasing expression of these genes. Notably, AS6 also repressed expression of stress-induced ABA-responsive genes in response to treatment with mannitol, which induced ABA synthesis by mimicking the water loss caused by drought (Fig. 19). These physiological data suggested that AS2 and AS6 functioned as a PYL agonist and antagonist, respectively, whereas AS4 exhibited an intermediate effect, consistent with predictions based on the present PYR1–AS6 model (Fig. 10).

PyrA is a synthetic PYL agonist but not an ABA analog and inhibits seed germination primarily by activating PYR1⁹⁹. In contrast to seeds, PyrA is not able to induce ABA response in vegetative tissues. Additionally, it has weak antagonist activity in assays with PYL2 *in vitro*, which perhaps explains its inability to trigger a strong ABA response in adult plant tissues. Given this, the two compounds were compared, and, consistent with previous reports^{99,124}, PyrA was observed not to induce strong ABA responses in vegetative tissues. More notably, PyrA, unlike AS6, did not block induction of ABA-inducible genes by either exogenous ABA treatment or endogenous stimulation by mannitol treatment (Figs. 18c,d and Fig. 19). Therefore, the previously reported PYL2-selective antagonist activity of PyrA¹⁴⁵ seemed not to be physiologically relevant, and, notably, the reported activity required a high molar excess of PyrA relative to ABA *in vitro* to be observed. These results suggest that functional ABA antagonist in physiological levels might be required to target on all expressing ABA receptors *in vivo*.

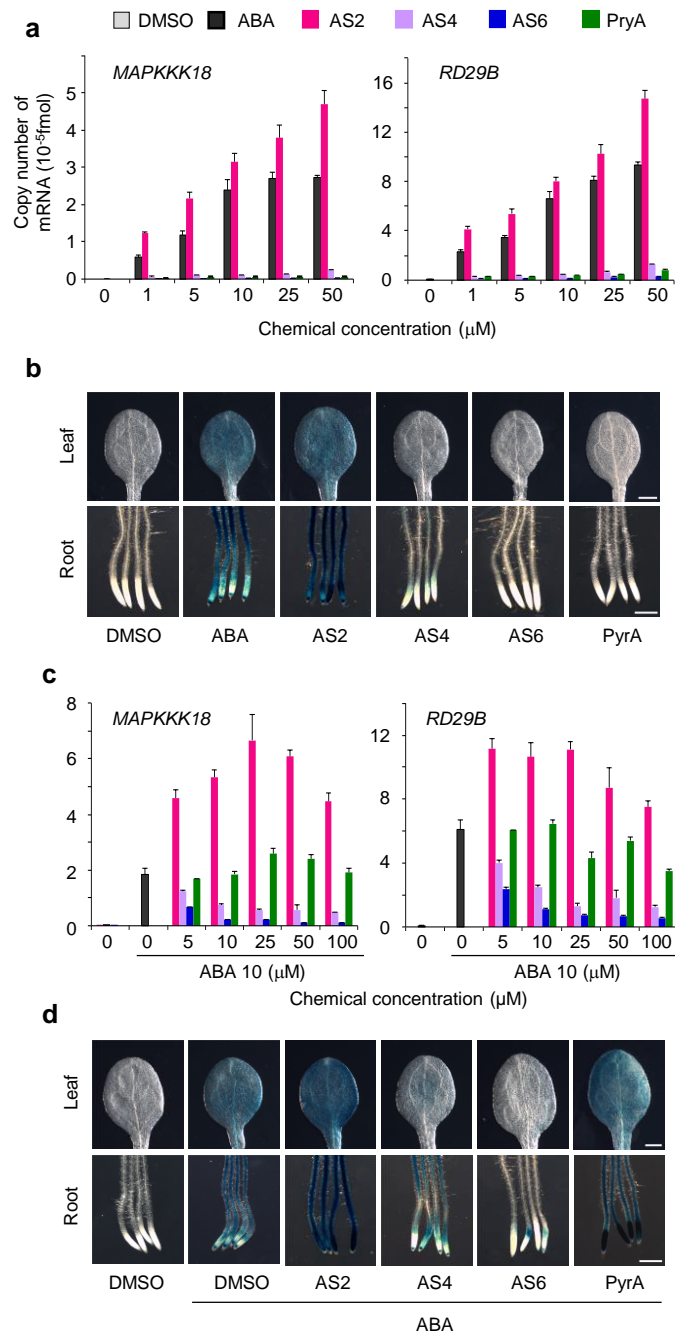


Figure 18 | Effects of AS_n compounds on expression of *Arabidopsis* ABA-responsive genes.

a, Expression of ABA-responsive genes after chemical treatments. Chemical concentrations were tested at 0 μM, 1 μM, 5 μM, 10 μM, 25 μM and 50 μM. **b**, Spatial expression pattern of *MAPKKK18* after 5 μM chemical treatment. **c**, Expression of ABA-responsive genes after cotreatment with ABA and AS_n or PyrA. AS_n compounds were tested at 0 μM, 1 μM, 5 μM, 10 μM, 25 μM and 50 μM in presence of 10 μM ABA. **d**, Spatial expression pattern of *MAPKKK18* after cotreatment with 5 μM ABA and 50 μM AS_n or PyrA. In **a–d**, 6-d-old *Arabidopsis* wild-type (Columbia accession) and promoter *MAPKKK18::GUS* transgenic seedlings incubated in solution containing chemicals in 0.5x MS and 0.5% sucrose for 6 h were used. In **a** and **c**, $n=3$, and error bars represent s.d. In **b** and **d**, scale bars represent 0.5 mm.

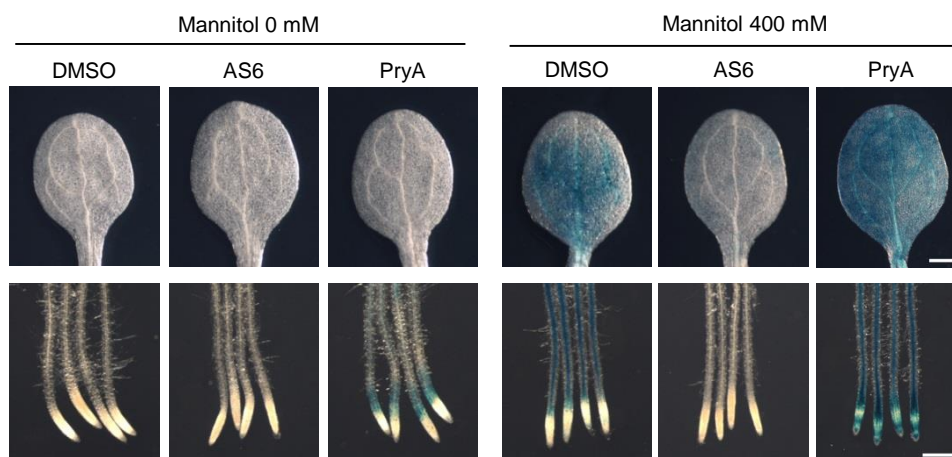


Figure 19 | AS6 antagonized endogenous ABA activity.

Transgenic *Arabidopsis* (*pMAPKKK18::GUS*) subjected to 400 mM mannitol or control solutions, in presence of 50 μ M AS6 or pyrabactin (PyrA) for 4 h. Scale bars, 0.5 mm.

2-3. Biochemical characterization of AS n

The 3' tunnel is enclosed by highly conserved residues, and therefore it was expected that AS n compounds might have broad-spectrum activity across the receptor family. Thus, the effects of AS n s on 11 of the 13 *Arabidopsis* receptors were examined using phosphatase assays (PYL7 and PYL12 have remained recalcitrant to expression as active proteins in our hands). In these assays, receptor activation was monitored by PP2C activity inhibition, and effective agonists exhibited near-complete PP2C activity inhibition at saturating concentrations, whereas partial agonists failed to completely inhibit PP2C activity. AS2 activated dimeric receptors (PYR1 and PYL1–3) with potencies comparable to that of ABA (Fig. 20a) and showed incomplete activation of the monomeric receptors PYL4, PYL5 and PYL11; thus, AS2 was not a broad-spectrum agonist. The recently reported agonist quinabactin also primarily activates dimeric receptors, and the AS2 effects observed here provided independent evidence for the sufficiency of dimeric receptors to activate ABA responses¹²⁴. AS4 displayed incomplete activation of dimeric receptors compared to ABA, and AS6 was also able to partially cause activation. Although AS6 bound to PYLs with affinity comparable to ABA, as described below, its effects included less than 50% PP2C inhibition, which suggested that AS6 acted as a weak partial agonist.

The antagonist activities of these compounds *in vitro* were characterized by examining their ability to reverse ABA-mediated PP2C inhibition. These experiments showed that AS2 slightly antagonized monomeric receptors, especially PYL10, whereas AS4 and AS6 antagonized ABA-dependent PP2C inhibition for all of the receptors tested, indicating broad-spectrum antagonist activity (Figs. 20b and 21). AS6's effects were greater than those of AS4, but neither enabled full recovery of PP2C activity, even when present at a 20-fold excess over ABA. This might be explained by the intrinsic partial-agonist activity of AS6 and, thus, in the presence of ABA, AS6 only enabled PP2C activity recovery to ~50% of the inhibition observed in the presence of AS6 alone. This partial antagonism of AS6 in the PP2C assay is not always consistent with the results obtained in the physiological assays, suggesting that a partial release of active PP2C from PYL might be sufficient to dephosphorylate SnRK2 to block ABA signal transduction.

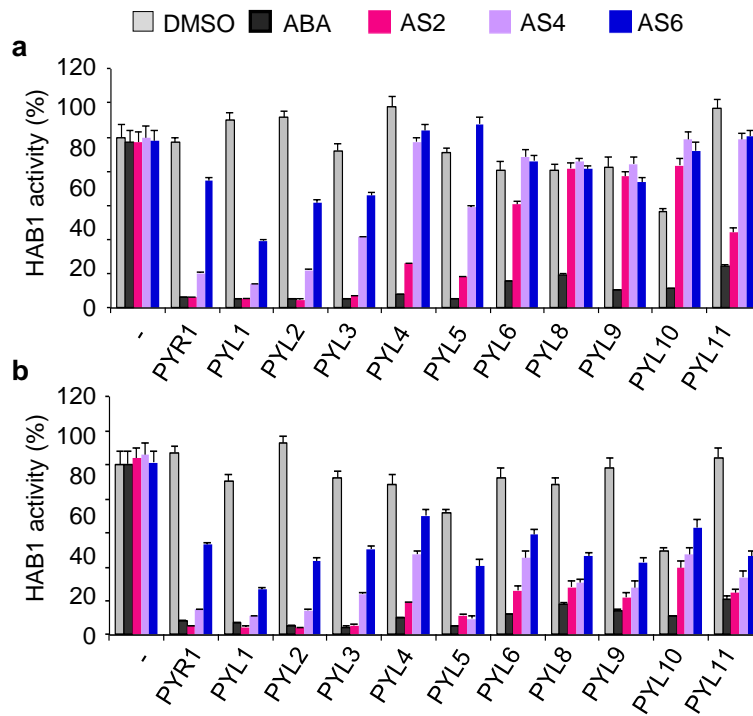


Figure 20 | Effects of AS_n on HAB1 inhibition by ABA receptors.

a, Chemical-dependent inhibition of HAB1 by various ABA receptors. Assays were conducted in presence of 25 μ M of each test chemical. **b**, Antagonistic effect of 50 μ M AS_n compounds. This assay conducted in presence of both 5 μ M ABA and 50 μ M AS_n compounds. PYL and HAB1 proteins were used at the same molar ratio at 60 pmol; $n = 3$; error bars represent s.d.

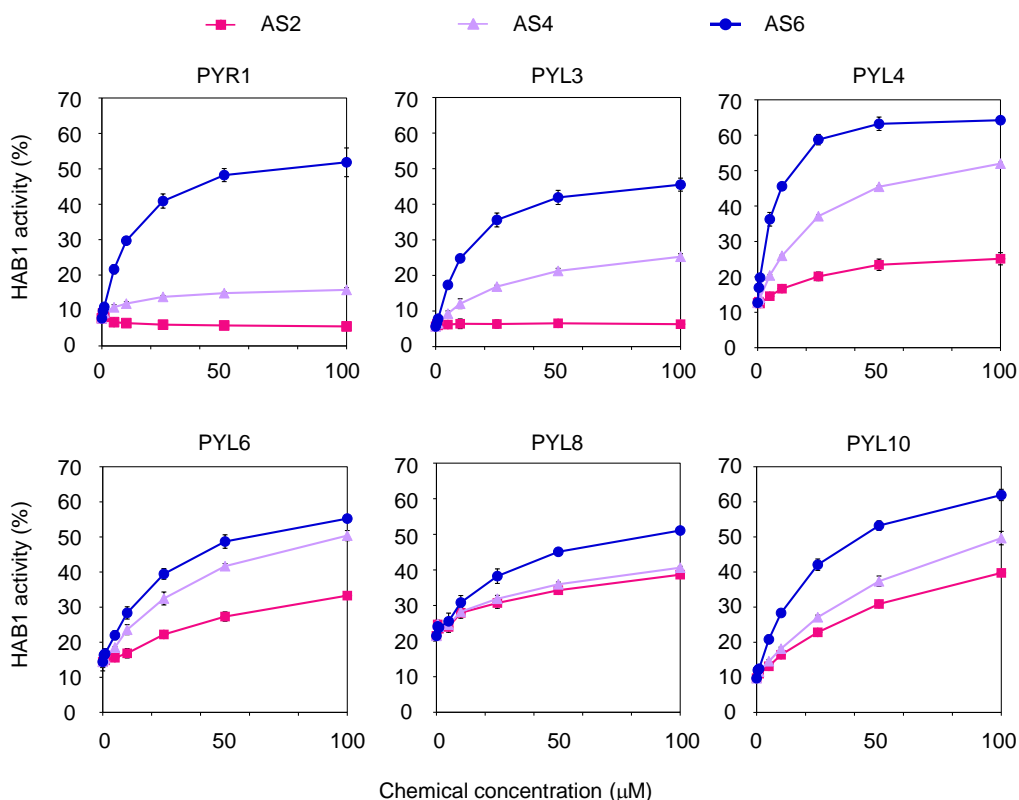


Figure 21 | Antagonist effects of AS_n on HAB1 inhibition by ABA receptors.

AS_n compounds were tested at 0 μM, 0.5 μM, 2.5 μM, 5 μM, 10 μM, 25 μM, 50 μM and 100 μM, whereas ABA was used at 5 μM in reactions. HAB1 activity in absence of receptor protein and chemical are shown as 100% of enzyme activity. PYL and HAB1 proteins were used at the same molar ratio at 60 pmol; *n* = 3; error bars represent s.d.

The mechanism of AS₆ antagonist activity was further characterized by pull-down assays *in vitro* using recombinant PYLs in combination with HAB1. PYR1, PYL3 and PYL4 did not bind to HAB1 in the absence of ABA but did in its presence (Fig. 22). In addition, AS₆ slightly promoted the binding of PYLs to HAB1, consistent with HAB1 phosphatase assay. In cotreatment experiments, AS₆ blocked ABA-induced PYL-PP2C interactions in a dose-dependent manner (Fig. 22). We observed that PYL6, PYL8 and PYL10 bind HAB1 in the absence of ABA, consistent with previous reports^{99,100,110}. Interactions between these receptors and HAB1 were modestly enhanced in response to ABA and as expected AS₆ reversed this to the basal levels that they show in the absence of ABA, but did not block ABA-independent interaction of these monomeric receptors with HAB1. Collectively, these biochemical data showed that AS₆ acted as an antagonist by blocking ABA-induced PYL-PP2C interactions.

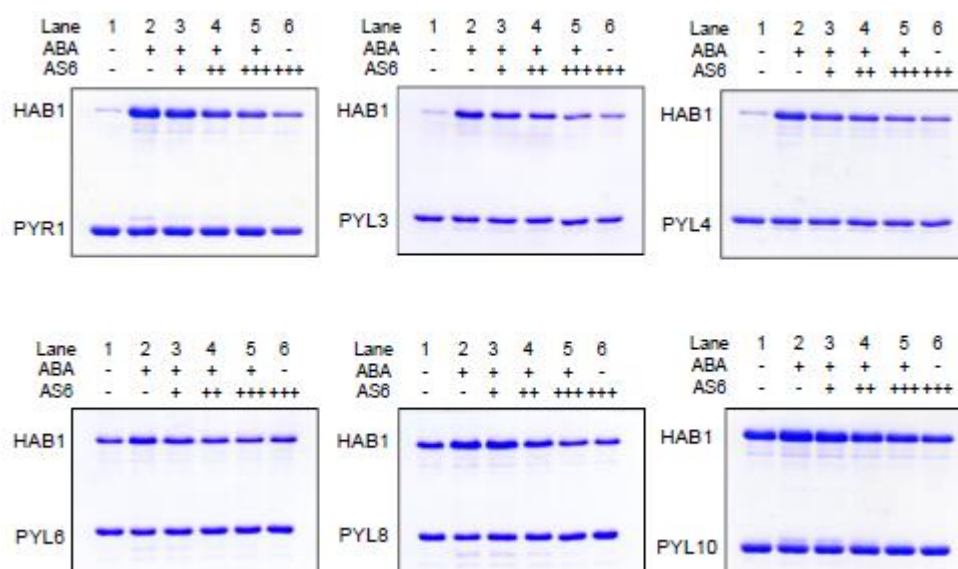


Figure 22 | Effects of AS n compounds on PYL-PP2C interactions *in vitro*.

Antagonistic effect of AS6 on ABA-mediated PYL-PP2C interaction. Pull-down assay performed using purified glutathione S-transferase (GST)-HAB1 and 6xHis-tagged PYLs (100 and 20 μg , respectively). Signals = (-) for 0 μM ; (+) for 25 μM ; (++) for 100 μM ; and (+++) for 250 μM .

2-4. Thermodynamic and structural analysis of PYL-AS6

Isothermal titration calorimetry was next used to characterize AS6 binding with monomeric receptors, which were selected over dimeric receptors because they display simple ligand association and dissociation and lack a dimer dissociation step. These analyses revealed apparent dissociation constants (K_d) of $0.48 \pm 0.10 \mu\text{M}$ (s.e.m.) and $1.28 \pm 0.72 \mu\text{M}$ (PYL5 and PYL10, respectively) with negative enthalpies, indicating an exothermic binding process (Fig. 23 and Table 5). These values were comparable to those of ABA ($0.88 \pm 0.11 \mu\text{M}$ and $0.78 \pm 0.12 \mu\text{M}$ for PYL5 and PYL10, respectively). In comparison to ABA, AS6 binding to PYL5 is associated a larger negative enthalpy ($\Delta H = -9.7$ vs. $-7.8 \text{ kcal mol}^{-1}$), whereas as entropy for AS6 is less than that for ABA. This was not the case for AS6-PYL10 interactions; the ΔH for AS6 is less negative ($-6.9 \text{ kcal mol}^{-1}$) than that for ABA ($-10.9 \text{ kcal mol}^{-1}$), but on the contrary, as $-T\Delta S$ for AS6 is greater than that of ABA. These observations suggested that there might have been subtle mechanistic differences in the AS6 gate-closing dynamics for different receptors.

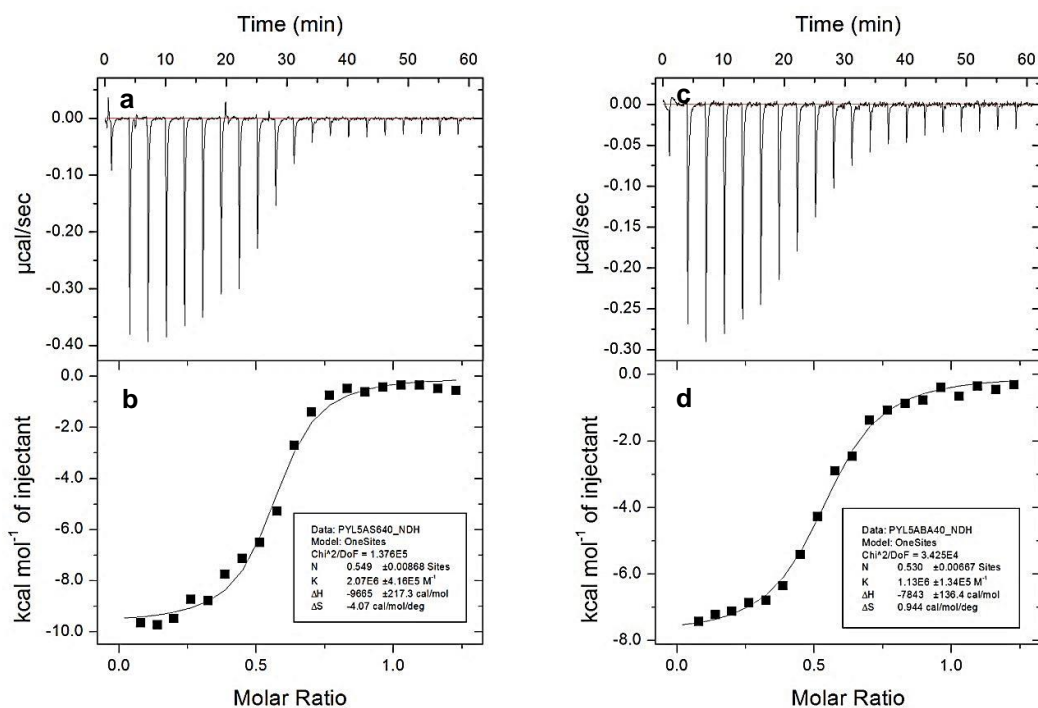


Figure 23 | Isothermal titration calorimetry profiles and thermodynamic data for AS6-PYL5 binding experiments.

a, Raw data for 20 sequential injections of 1.25 μL of 0.4 mM AS6 stock solution into cell containing 40 μM 6xHis-tagged PYL5 in phosphate buffer, pH 8.0. Injections performed over a period of 5 sec. with 3 min intervals between injections. **b**, Plot of heat evolved (kcal) per mole of AS6 dilution, against molar ratio of AS6 to PYL5. Data fitted using software 'one set of sites' and solid line represents best fit. **c**, Raw data for 20 sequential injections of 0.4 mM ABA stock solution into cell containing 40 μM 6xHis-tagged PYL5 in phosphate buffer. **d**, Plot of heat evolved (kcal) per mole of ABA added, corrected for heat of ABA dilution, against molar ratio of ABA to PYL5.

Table 5 | Apparent AS6 and ABA binding affinity for PYLs.^a

Receptors	Compounds	K_d (μM)	ΔH (kcal/mol)	$-T\Delta S^b$ (kcal/mol)	ΔG^c (kcal/mol)
PYL5	ABA	0.88 ± 0.11	-7.8 ± 0.1	-0.3	-8.1 ± 0.1
PYL5	AS6	0.48 ± 0.10	-9.7 ± 0.2	1.2	-8.5 ± 0.1
PYL10	ABA	0.78 ± 0.12	-10.9 ± 0.3	2.7	-8.2 ± 0.1
PYL10	AS6	1.28 ± 0.72	-6.9 ± 0.5	-1.0	-7.9 ± 0.3

^a K_d , ΔH obtained from single-set-of-sites fit to date.

^b $T\Delta S = \Delta H - \Delta G$

^c $\Delta G = -RT \ln(1/K_d)$. Uncertainties for K_d , ΔH , and ΔG calculated by curve fitting program of MicroCal Origin 7.0.

The molecular mechanism of AS6 activity was then clarified by determining the crystal structure of recombinant PYR1 bound to AS6 at 2.3-Å resolution, using molecular replacement and starting from published PYR1–ABA coordinates PDB code 3K90; refinement and structure statistics are summarized in [Table 6](#)). The PYR1–AS6 complex was found to resemble very closely that of the PYR1–ABA complex ([Fig. 24a](#)), and AS6’s ABA-skeleton resided in almost the same position normally occupied by ABA ([Fig. 24b](#)). Consistent with the present model-based predictions, the gate loop adopted a closed conformation, and the 3’ tunnel accommodated the AS6 *S*-hexyl chain, which also protruded out onto PYR1’s PP2C-interaction surface ([Figs. 24c,d](#) and [26](#)). A significant difference with the PYR1-ABA is the 90 degrees flipped orientation of the phenyl side chain of the conserved Phe residue of α 3 helix, which may have been induced due to the interaction with *S*-hexyl chain of AS6 ([Fig. 24b](#)). These observations provided direct evidence that AS6 induced the gate-closed conformer and that the *S*-hexyl chain was positioned to interfere with PP2C binding through steric effects.

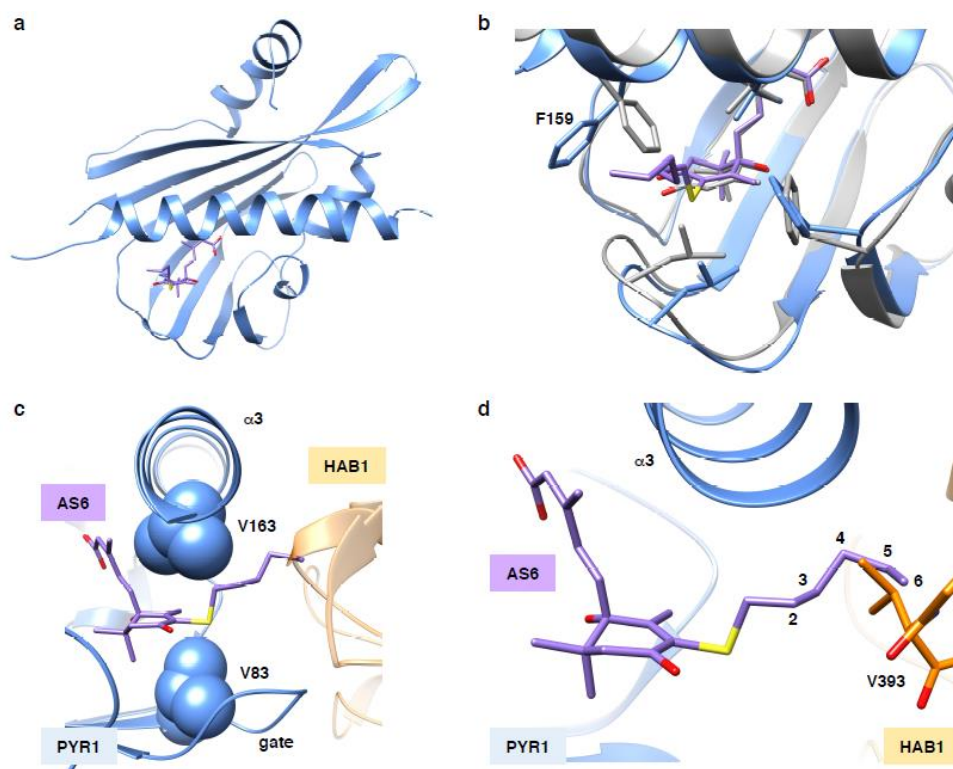


Figure 24 | Crystal structure of PYR1-AS6 complex.

a, Overall structure of AS6-bound PYR1. AS6 is shown as purple sticks. **b**, Superposition of the PYR1–AS6 complex (cyan) and PYR1–ABA complex (gray, PDB code 3K90) at the ligand binding pocket. **c,d**, Superposition of the PYR1–AS6 complex and the PYR1–ABA–HAB1 (orange, PDB code 3QN1) complex. The gate loop of the PYR1–AS6 complex adopted a closed conformation, and the AS6 S-hexyl chain passed through the 3' tunnel to protrude over the PYR1 surface. In **c**, Val163 in the $\alpha 3$ helix and Val83 at the N terminus of the gate loop region are located at the top and bottom of the tunnel, respectively, and are highlighted in spheres. In **d**, the S-hexyl chain tip collided with HAB1 Val393, which is well conserved among PP2Cs (**d**).

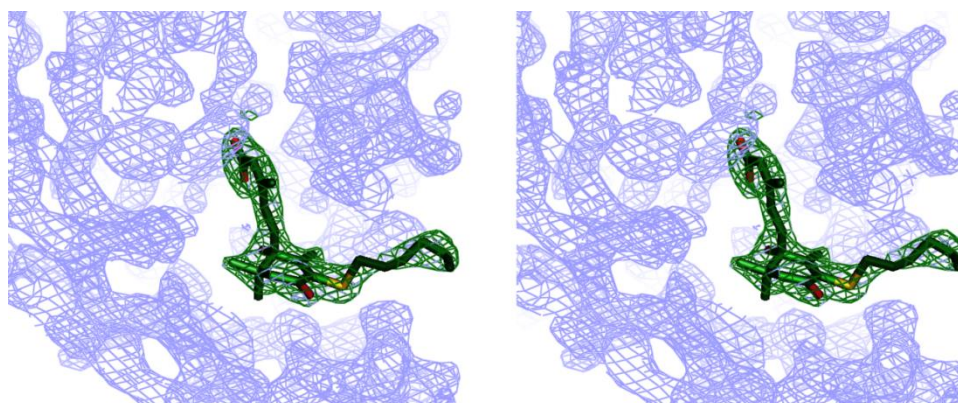


Figure 25 | A stereo view of the 2Fo-Fc omit electron density maps for AS6-bound PYR1 centering on AS6.

The 2Fo-Fc map, contoured at 1.3σ , in blue mesh for protein and green mesh for AS6.

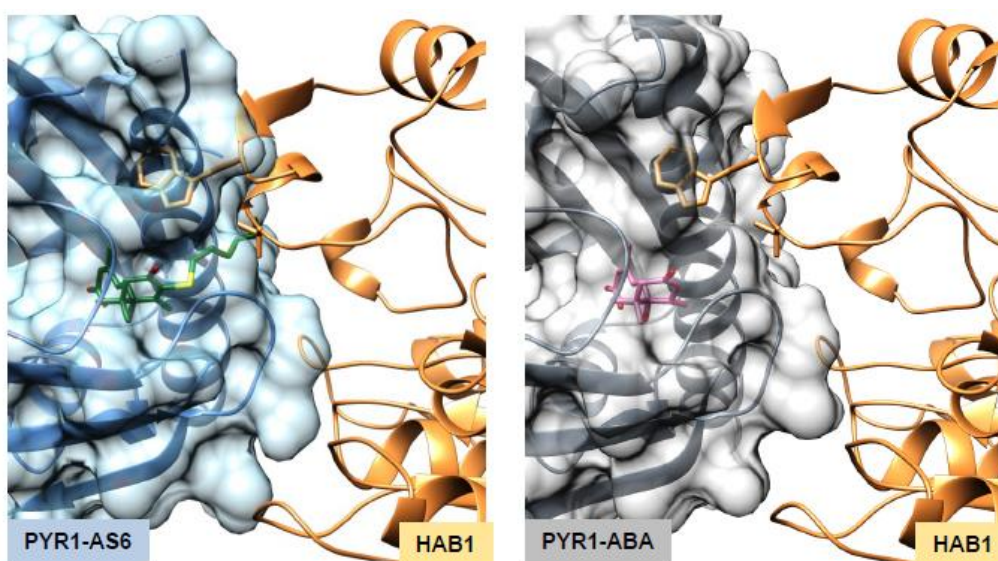


Figure 26 | PP2C binding surface of PYR1-AS6 complex was identical to that of PYR1-ABA complex.

a, Superposition of PYR1-AS6 complex (cyan) and PYR1-ABA-HAB1 (orange, 3QN1) complex. AS6, green sticks. **b**, Crystal structure of PYR1-ABA-HAB1 (3QN1) complex. ABA, magenta sticks.

Table 6 | Data collection and refinement statistics (molecular replacement).

	PYR1-AS6 PBD ID: 3WG8
Data collection	
Space group	$P3_121$
Cell dimensions	
<i>a</i> , <i>b</i> , <i>c</i> (Å)	66.93, 66.93, 78.24
α , β , γ (°)	90, 90, 120
Resolution (Å)	58.0-2.3 (2.38-2.3) *
R_{sym} or R_{merge}	0.084 (0.709)
$I / \sigma I$	38.5 (4.3)
Completeness (%)	98.7 (98.6)
Redundancy	7.2 (7.1)
Refinement	
Resolution (Å)	32.45-2.3
No. reflections	8811
$R_{\text{work}} / R_{\text{free}}$	23.8/28.1
No. atoms	
Protein	1408
Ligand/ion	26
Water	33
<i>B</i> -factors	
Protein	49.29
Ligand/ion	42.75
Water	46.49
R.m.s. deviations	
Bond lengths (Å)	0.015
Bond angles (°)	1.843

*Values in parentheses are for highest-resolution shell.
Single crystal was used for data collection.

2-5. The functional selectivity of AS n

The compounds in the AS n series were structurally nearly identical to ABA, with the exception of their 3'-alkyl chains. Although direct evidence was developed here for receptor-mediated physiological effects by these compounds, it is conceivable that activity at other ABA binding sites could have contributed to their effects *in vivo*. Thus, the effects of AS2 and AS6 on two well-characterized, nonreceptor ABA-binding sites were characterized, and, as described above, AS n compounds were not potent inhibitors of ABA catabolic CYP707A enzymes. Moreover, endogenous ABA concentrations in *Arabidopsis* seedlings treated with AS2 or AS6 were investigated to examine whether these concentrations were altered by AS n compounds. No significant differences ($P > 0.1$ by one-way analysis of variance; $n = 5$ or 6) were observed in ABA concentrations between AS n and mock-treated controls (Fig. 27), suggesting that AS n exerted little effect on ABA metabolism. Recently, two ATP-binding cassette (ABC) transporters, AtABCG25⁷⁶ and AtABCG40⁷⁷, and the nitrate transporter NPF4.6 (also known as AIT1)⁷⁸ were described as ABA transporters. The effect of AS6 on AIT1, whose assay system has been established uniquely among the ABA transporters, was examined, and AS6 was found not to substantially inhibit ABA transport activity by AIT1 when present at equimolar concentrations to ABA; however, it weakly inhibited transport when present in tenfold excess (Fig. 28). These data suggest that AS6 is not a strong inhibitor of ABA transport activity.

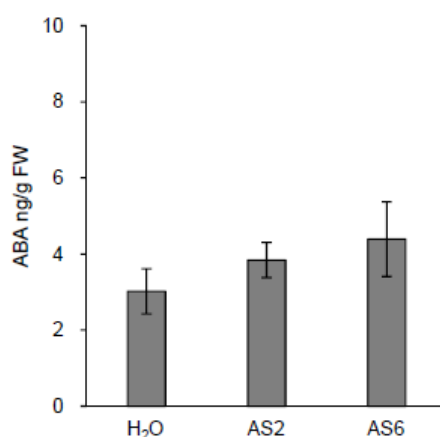


Figure 27 | Effects of AS2 and AS6 on endogenous ABA concentration.

Ten-day old seedlings incubated with 10 μ M AS2 or AS6 solution, or water as control, for 6 h. Data analyzed by one-way ANOVA ($n=5-6$, mean \pm s.e.m.).

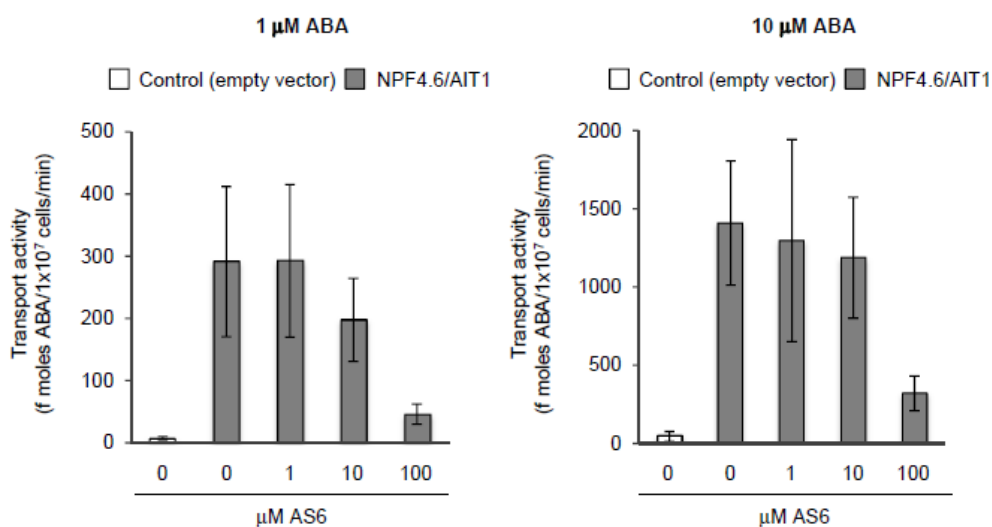


Figure 28 | Effects of AS6 on ABA transporter NPF4.6/AIT1.

ABA import activity (fmoles ABA/1x10⁷ cells/min) of NPF4.6/AIT1 in presence of ABA and AS6 determined by analyzing ABA incorporated into yeast cells. Amounts of ABA incorporated into cells with empty vector also shown (Control). AS6 tested at 0, 1, 10, and 100 μM in presence of 1 or 10 μM ABA ($n=3$; error bars, s.d.).

2-6. Molecular determination for the functional selectivity of AS2

In the PP2C assay, AS2 showed different function for different subclasses/subtypes of PYLs (Fig. 20), which indicates that the agonistic/antagonistic properties of AS n do not always depend only on the length of the *S*-alkyl chain. Based on the PYR1-AS6 structure, the *S*-ethyl chain of AS2 is estimate to be too short to directory interfere with binding to PP2Cs, as is the case of monomeric receptors. Therefore, another mechanism is required to explain the functional selectivity of AS2. When focusing on the residues comprising the 3'-tunnel, the only difference among the subclasses/subtypes is found in the $\alpha 3$ helix. This residue, which is located on the C3'-position of ABA, is a Val in the dimeric receptors and a Leu (PYL7-10) or Ile (PYL4-6, PYL11 and PYL12) in the monomeric receptors (Fig. 29). Because of the steric bulkiness, which is greatest in Leu, less in Ile, and the least in Val, this residue can interfere with the *S*-ethyl chain. The steric interference may prevent the closure of the gate by pushing the AS2 *S*-ethyl chain to the gate loop (Fig. 30).

To validate this hypothetical mechanism, we prepared PYL9 and PYL10 mutants in

which the $\alpha 3$ Leu was replaced by a smaller residue, Ala. ABA, but not AS2, inhibited HAB1 activity via PYL9 and PYL10, and ABA-independent inhibition of HAB1 was observed in PYL10 as reported previously (Fig. 31a,e)¹⁰¹. The antagonistic effect of AS2 is significant for PYL10, whereas it is not significant for PYL9 (Fig. 31b,f). This difference may result from the difference in a residue at the N-terminus of the gate loop region. This residue, which sandwiches the C3' of the ABA ring with $\alpha 3$ Val/Ile/Leu, is Val in all of the receptors, except for PYL10, in which the corresponding residue is Leu (Fig. 31c). This means that PYL10 facilitates the hydrophobic interaction between the $\alpha 3$ helix and gate loop, more easily than PYL9, to induce the gate-closed conformer even in the absence of ABA¹⁰¹. However, this also means that PYL10 has more difficulty accommodating the *S*-ethyl of AS2 in the gate-closed form. PYL9^{L165A} was insensitive, and PYL10^{L159A} was only slightly sensitive to ABA, probably because Ala is too small to facilitate the hydrophobic interactions with the gate loop via the ABA ring to maintain the gate closed (Fig. 31c,g). On the other hand, AS2 was not antagonistic but agonistic for both mutants, probably because the *S*-ethyl chain compensated for the hydrophobic interactions that had been diminished by the Ala replacement (Fig. 31d,h).

The structural and mutational analyses collectively support the notion that the functional selectivity of AS2 is controlled by a combination of the two residues that induce gate closure by sandwiching the C3' of the ABA ring: Val/Ile/Leu in the $\alpha 3$ helix and Val/Leu at the N-terminus of the gate loop region. For the dimeric receptors with the smallest combination, Val-Val, AS2 strongly induces the conformational shift from the gate-opened to the gate-closed conformers. For the monomeric receptors with Ile-Val, PYL4–6 and PYL11, AS2 stabilizes the gate-closed conformers slightly more than in the case of the apo state, whereas in those with Leu-Val, PYL8 and PYL9, AS2 has little effect on the equilibrium. In the case of PYL10 with the largest combination, Leu-Leu, AS2 changes the equilibrium to increase the gate-opened conformer, that is, functions as an inverse agonist.

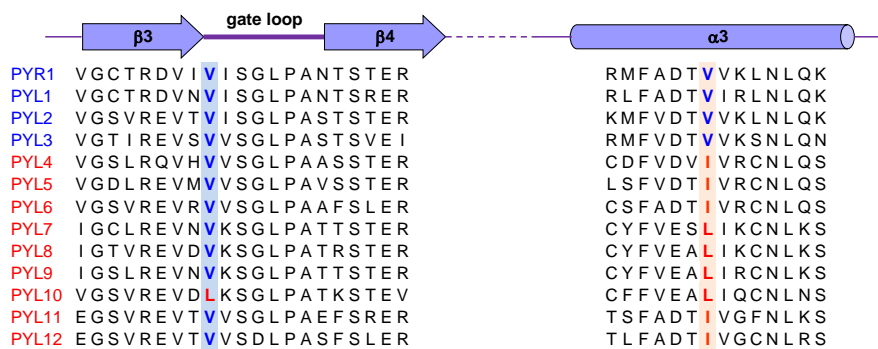


Figure 29 | Sequence alignment around the gate loop and $\alpha 3$ helix of PYR/PYL/RCAR (PYL) receptors. The functional selectivity of AS2 is controlled by a combination of the two amino acid residues: Val/Ile/Leu in the $\alpha 3$ helix and Val/Leu at the N-terminus of the gate loop region.

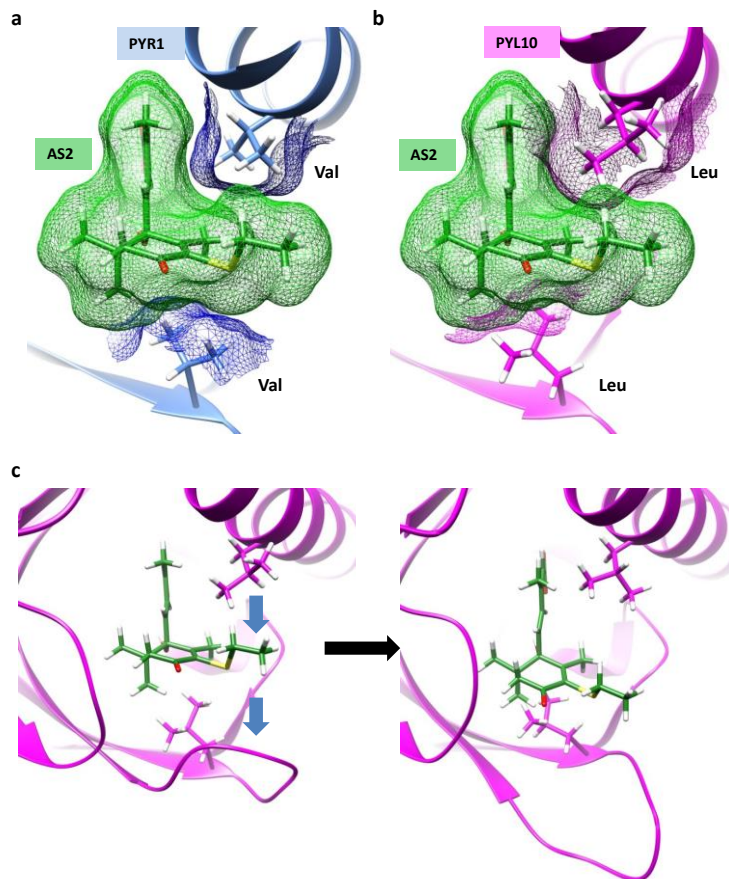


Figure 30 | A putative mechanism for AS2, preventing the gate-closing motion of monomeric PYR/PYL/RCAR (PYL) receptors, especially PYL10.

a,b, AS2 was overlaid on ABA in the PYR1-ABA complex (3K90) (**a**), and the PYL10-ABA complex (3R6P) (**b**). The solvent accessible surface areas of AS2 and two amino acid residues that induce the gate conformational shift by sandwiching the C3' of ABA ring are shown as mesh. **c**, The steric interference with the S-ethyl chain of AS2 by L159 in the $\alpha 3$ helix of PYL10 may prevent the gate closure by pushing the S-ethyl chain to the gate loop.

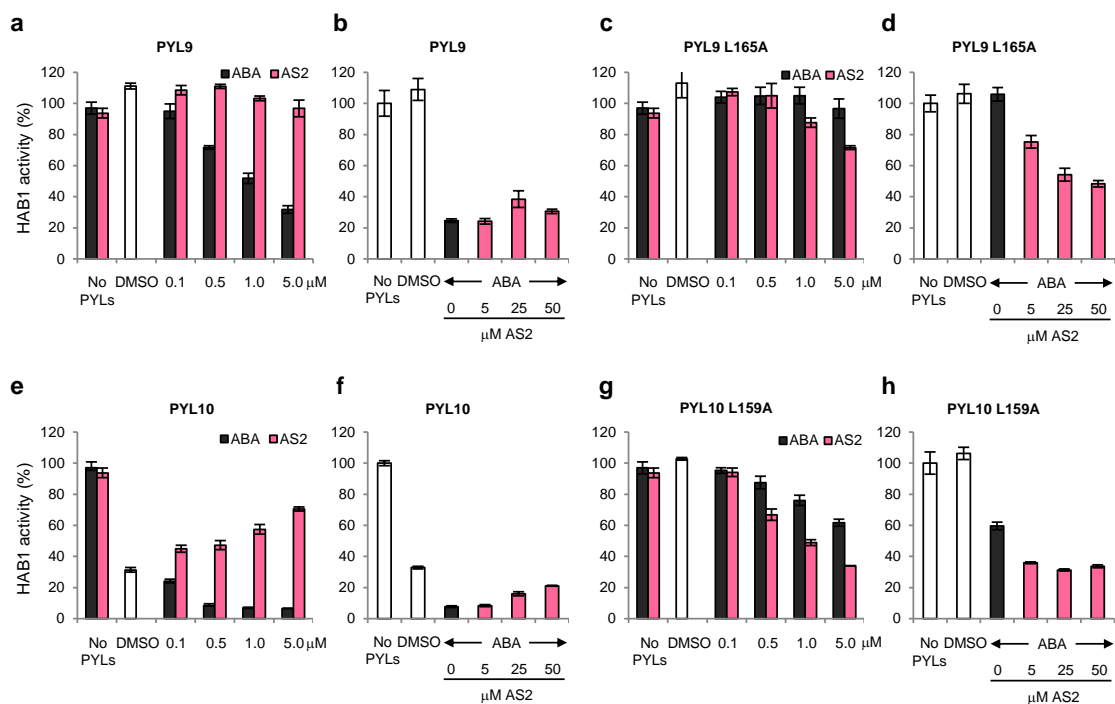


Figure 31 | The replacement of the $\alpha 3$ Leu by Ala converts PYL9 and PYL10 to AS2-activated receptors.

a,b, AS2 has little effect on the interaction between PYL9 and the protein phosphatase 2C (PP2C), HAB1, as determined by phosphatase activity assays in the both absence (**a**) and presence (**b**) of ABA ($n = 3$, error bars = standard deviation; s.d.). **c,d**, AS2 slightly inhibits HAB1 phosphatase activity by PYL9 L165A in the absence (**c**) and presence (**d**) of ABA ($n = 3$, error bars = s.d.). **e,f**, AS2 relieves the ABA-independent (**e**) and ABA-dependent (**f**) inhibition of HAB1 phosphatase activity by PYL10 ($n = 3$, error bars = s.d.). **g**, AS2 inhibits HAB1 phosphatase activity by PYL10 L159A ($n = 3$, error bars = s.d.). **h**, AS2 enhances the ABA-dependent inhibition of HAB1 phosphatase activity by PYL10 L159A ($n = 3$, error bars = s.d.). Reactions contained 5 μ M ABA and the indicated concentrations of AS2 (**b,d,f,h**).

3. Discussion

A structure-guided design was used to rationally and successfully create an ABA receptor antagonist, demonstrating that this allosteric ligand could be modified relatively easily to yield a protein-protein interaction (PPI) inhibitor. Consistent with the present PYR1–AS6 model (Fig. 10), the AS n analog series, prepared by 3' *S*-alkylation of ABA, yielded agonists when $n < 4$ and yielded antagonists when $n > 4$. Thus, the 3' position of ABA's ring was found to be a versatile ABA modification site. The present structural, thermodynamic, biochemical and physiological data demonstrated that AS6 bound to PYLs with affinity comparable to ABA and prevented formation of ABA-induced PYL-PP2C complexes by direct steric hindrance of its *S*-hexyl chain. However, AS6 did not completely abolish PYL-PP2C interactions owing to its basal partial agonist activity. Notably, this partial agonist activity *in vitro* did not correspond to partial activation of ABA responses *in vivo*, suggesting that partial reversal of ABA-induced PP2C inhibition was sufficient to block ABA signal transduction *in vivo*. The incomplete inhibition of ABA-induced PYL-PP2C interactions by AS6 might have been sufficient to displace PP2C toward the native substrates, including SnRK2s and OST1. In the PP2C assay, an artificial, small, phosphorylated molecule, *p*-nitrophenylphosphate (*p*NPP), was used as a substrate instead of phosphorylated proteins. PP2C affinity for this small substrate might have been much lower than to native protein substrates¹⁶⁴, in which case, even if a PYL-AS6 complex bound weakly to PP2C, the weak ligand of PP2C should have been easily replaced by native substrates to form stable complexes. Thus, the weak activity of PYL-AS6 *in vitro* might have been similar to the basal activity of monomeric PYL proteins *in vitro*, which has not been proven with phosphorylated proteins^{123,165}. This implies that even if monomeric receptors can partially inhibit PP2C in an ABA-independent manner in plants, this activity may not be sufficient for activating SnRK2s and inducing physiological ABA responses.

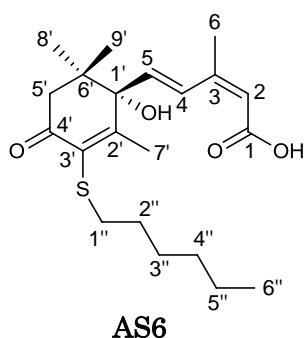
A good deal of the current understanding of ABA's functions *in vivo* has come from analyses of mutants of model organisms that are defective in either ABA signaling or biosynthesis. The present creation and characterization of AS6 now makes feasible studies of ABA signaling in nonmodel organisms. It was shown here using AS6, for example, that blocking of ABA signaling in *R. sativus* increased water loss and, in *L.*

sativa, blocked ABA's effects on seed germination. Although these results were not surprising, they highlight the portability of this new tool for answering biological questions in nonmodel systems. Furthermore, the steric strategy for controlling PPIs presented here might be generally applicable to the design of other allosteric modulators of PPIs.

4. Experimental

General procedures

ABA was a gift from Dr. Y. Kamuro and Toray Industries, Inc., Tokyo, Japan. ^1H NMR spectra were recorded with tetramethylsilane as the internal standard using JEOL JNM-EX270 (270 MHz) and JNM-LA500 (500 MHz) NMR spectrometers (JEOL Ltd., Tokyo, Japan). ^{13}C NMR and 2D-correlation NMR experiments were recorded using a JNM-LA500 (500 MHz) NMR spectrometer (JEOL Ltd.). All peak assignments refer to the numbering in structure **AS6**. High resolution mass spectra were obtained with a JEOL JMS-T100LC AccuTOF mass spectrometer (ESI-TOF, positive mode; JEOL Ltd.). Column chromatography was performed using silica gel (Wakogel C-200, Wako Pure Chemical Industries, Ltd., Osaka, Japan).



Synthesis of **AS_n** ($n = 2-12$)

2' α ,*3'* α -dihydro-2' α ,*3'* α -epoxy-ABA (**27**)¹⁶¹

With stirring at 0 °C, 1 M NaOH (3 mL, 3 mmol) and H₂O₂ (1 mL, 12.4 mmol) were added to an ABA solution (200 mg, 0.758 mmol) in methanol (MeOH, 15 mL) and the mixture stirred for 25.5 h at the same temperature. After quenching with 1 M HCl (6 mL) at 0°C, the resulting mixture was diluted with H₂O (150 mL) and extracted thrice with ethyl acetate (EtOAc, 50 mL \times 3). The organic layer was then washed with brine, dried over Na₂SO₄, and concentrated *in vacuo*. The residual oil was purified by silica gel column chromatography eluted with 25% EtOAc in hexane (v/v) containing 0.1% acetic acid (AcOH, by vol) to obtain **27** (95 mg, 45%) as a colorless oil. ^1H NMR (270 MHz, CDCl₃): δ 0.90 (3H, s, H₃-9'), 1.04 (3H, s, H₃-8'), 1.37 (3H, s, H₃-7'), 1.86 (1H, d, $J = 15.2$ Hz, H-5'), 2.04 (3H, d, $J = 1.0$ Hz, H₃-6), 2.85 (1H, d, $J = 15.2$ Hz, H-5'), 3.19 (1H, s, H-3'), 5.75 (1H, s, H-2), 5.75 (1H, d, $J = 16.2$ Hz, H-5), and 7.92 (1H, d, $J =$

16.2 Hz, H-4); ^{13}C NMR (68 MHz, CDCl_3): δ 21.1, 21.4, 24.0, 24.8, 44.3, 46.0, 64.2, 68.9, 76.4, 118.0, 128.7, 135.3, 151.1, 170.7, and 205.6; HRMS (m/z): $[\text{M}+\text{Na}]^+$ calc'd. for $\text{C}_{15}\text{H}_{20}\text{O}_5\text{SNa}$, 303.1208; found, 303.1205.

3'-ethylsulfanyl-ABA, AS2 (28)

With stirring at room temperature, 1 M NaOH (10 mL, 10 mmol) and ethyl mercaptan (900 μL , 12.2 mmol) was added to a solution of **27** (500 mg, 1.79 mmol) in MeOH (50 mL) and the mixture stirred for 1 h at room temperature¹⁶². After quenching with 1 M HCl (20 mL), it was then diluted with H_2O (400 mL) and extracted thrice with EtOAc (150 mL \times 3). The organic layer was washed, dried, and concentrated, as described above. The residual oil was purified by silica gel column chromatography eluted with 25% EtOAc in hexane containing 0.1% AcOH to obtain **AS2** (479 mg, 83%) as a colorless oil. ^1H NMR (500 MHz, CDCl_3): δ 1.03 (3H, s, $\text{H}_{3-9'}$), 1.10 (3H, s, $\text{H}_{3-8'}$), 1.18 (3H, t, $J = 7.6$ Hz, $\text{H}_{3-2''}$), 2.04 (3H, d, $J = 0.9$ Hz, H_{3-6}), 2.23 (3H, s, $\text{H}_{3-7'}$), 2.45 (1H, d, $J = 16.8$ Hz, $\text{H}_{-5'}$), 2.56 (1H, d, $J = 16.8$ Hz, $\text{H}_{-5'}$), 2.79 (2H, m, $\text{H}_{-1''}$), 3.49 (1H, s, $\text{HO}-1'$), 5.77 (1H, brs, H_{-2}), 6.16 (1H, d, $J = 16.2$ Hz, H_{-5}), and 7.78 (1H, d, $J = 16.2$ Hz, H_{-4}); ^{13}C NMR (125 MHz, CDCl_3): δ 15.2 ($\text{C}_{2''}$), 18.9 ($\text{C}_{7'}$), 21.4 (C_6), 23.0 (C_8), 24.3 ($\text{C}_{9'}$), 27.7 ($\text{C}_{1''}$), 40.9 (C_6'), 49.7 (C_5'), 81.1 (C_1'), 118.0 (C_2), 128.4 (C_4), 132.0 (C_3'), 136.9 (C_5), 151.6 (C_3), 165.0 (C_2'), 170.8 (C_1), and 193.7 (C_4'); UV λ_{max} (MeOH) nm (ϵ): 251.4 (17,900); HRMS (m/z): $[\text{M}+\text{Na}]^+$ calc'd. for $\text{C}_{17}\text{H}_{24}\text{O}_4\text{SNa}$, 347.1293; found, 347.1291.

3'-propylsulfanyl-ABA, AS3 (29)

With stirring at room temperature, 1 M NaOH (400 μL , 400 μmol) and 1-propanethiol (45 μL , 500 μmol) was added to a solution of **27** (20 mg, 71 μmol) in MeOH (2 mL) and the mixture stirred for 1 h at room temperature. After quenching with 1 M HCl (2 mL), it was then diluted with H_2O (60 mL) and extracted thrice with EtOAc (30 mL \times 3). The organic layer was washed, dried, and concentrated as above. The residual oil was purified by silica gel column chromatography eluted with 25% EtOAc in hexane containing 0.1% AcOH to obtain **AS3** (20 mg, 83%) as a colorless oil. ^1H NMR (500 MHz, CDCl_3): δ 0.95 (3H, t, $J = 7.3$ Hz, $\text{H}_{3-3''}$), 1.02 (3H, s, $\text{H}_{3-9'}$), 1.09 (3H, s, $\text{H}_{3-8'}$), 1.51 (2H, tq, $J = 7.3$ and 7.3 Hz, $\text{H}_{2-2''}$), 2.04 (3H, d, $J = 1.2$ Hz, H_{3-6}), 2.22 (3H, s,

H₃-7'), 2.45 (1H, d, *J* = 16.8 Hz, H-5'), 2.56 (1H, d, *J* = 16.8 Hz, H-5'), 2.74 (2H, m, H-1''), 5.77 (1H, brs, H-2), 6.14 (1H, d, *J* = 15.9 Hz, H-5), and 7.79 (1H, d, *J* = 15.9 Hz, H-4); ¹³C NMR (125 MHz, CDCl₃): δ 13.3 (C3''), 18.8 (C7'), 21.4 (C6), 23.0 (C8'), 23.4 (C2''), 24.3 (C9'), 35.6 (C1''), 40.9 (C6'), 49.8 (C5'), 81.1 (C1'), 118.0 (C2), 128.4 (C4), 132.3 (C3'), 136.8 (C5), 151.6 (C3), 164.6 (C2'), 170.6 (C1), and 193.7 (C4'); UV λ_{max} (MeOH) nm (ε): 253.4 (17,600); HRMS (*m/z*): [M+Na]⁺ calc'd. for C₁₈H₂₆O₄SNa, 361.1450; found, 361.1453.

3'-butylsulfanyl-ABA, AS4 (30)

With stirring at room temperature, 1 M NaOH (6.4 mL, 6.4 mmol) and 1-butanethiol (860 μL, 8.03 mmol) was added to a solution of **27** (290 mg, 1.04 mmol) in MeOH (30 mL) and the mixture stirred for 1 h at room temperature. After quenching with 1 M HCl (12 mL), it was then diluted with H₂O (200 mL) and extracted thrice with EtOAc (80 mL × 3). The organic layer was washed, dried, and concentrated as above. The residual oil was purified by silica gel column chromatography eluted with 20% EtOAc in hexane (v/v) containing 0.1% AcOH to obtain **AS4** (294 mg, 80%) as a colorless oil. ¹H NMR (500 MHz, CDCl₃): δ 0.87 (3H, t, *J* = 7.3 Hz, H₃-4''), 1.02 (3H, s, H₃-9'), 1.09 (3H, s, H₃-8'), 1.37 (2H, tq, *J* = 7.3 and 7.3 Hz, H₂-3''), 1.47 (2H, tt, *J* = 7.3 and 7.3 Hz, H₂-2''), 2.04 (3H, d, *J* = 0.9 Hz, H₃-6), 2.22 (3H, s, H₃-7'), 2.45 (1H, d, *J* = 16.8 Hz, H-5'), 2.56 (1H, d, *J* = 16.8 Hz, H-5'), 2.76 (2H, m, H-1''), 5.77 (1H, brs, H-2), 6.15 (1H, d, *J* = 16.2 Hz, H-5), and 7.80 (1H, d, *J* = 16.2 Hz, H-4); ¹³C NMR (125 MHz, CDCl₃): δ 13.7 (C4''), 18.7 (C7'), 21.4 (C6), 21.7 (C3''), 23.0 (C8'), 24.3 (C9'), 32.2 (C2''), 33.3 (C1''), 40.9 (C6'), 49.7 (C5'), 81.1 (C1'), 117.8 (C2), 128.4 (C4), 132.3 (C3'), 136.7 (C5), 151.6 (C3), 164.7 (C2'), 170.6 (C1), and 196.7 (C4'); UV λ_{max} (MeOH) nm (ε): 253.4 (19,100); HRMS (*m/z*): [M+Na]⁺ calc'd. for C₁₉H₂₈O₄SNa, 375.1606; found, 375.1602.

3'-pentylsulfanyl-ABA, AS5 (31)

With stirring at room temperature, 1 M NaOH (300 μL, 300 μmol) and 1-pentanethiol (40 μL, 340 μmol) was added to a solution of **27** (16 mg, 57 μmol) in MeOH (1.5 mL) and the mixture stirred for 2 h at room temperature. After quenching with 1 M HCl (2 mL), it was then diluted with H₂O (30 mL) and extracted thrice with EtOAc (20 mL × 3). The organic layer was washed, dried, and concentrated as above. The residual oil

was purified by silica gel column chromatography eluted with 20% EtOAc in hexane containing 0.1% AcOH to obtain **AS5** (17 mg, 81%) as a colorless oil. ^1H NMR (500 MHz, CDCl_3): δ 0.86 (3H, t, $J = 7.3$ Hz, $\text{H}_3\text{-5}''$), 1.02 (3H, s, $\text{H}_3\text{-9}'$), 1.09 (3H, s, $\text{H}_3\text{-8}'$), 1.28 (2H, m, $\text{H}_3\text{-4}''$), 1.33 (2H, m, $\text{H}_3\text{-3}''$), 1.48 (2H, tt, $J = 7.3$ and 7.3 Hz, $\text{H}_2\text{-2}''$), 2.04 (3H, d, $J = 0.9$ Hz, $\text{H}_3\text{-6}$), 2.22 (3H, s, $\text{H}_3\text{-7}'$), 2.45 (1H, d, $J = 16.8$ Hz, $\text{H-5}'$), 2.56 (1H, d, $J = 16.8$ Hz, $\text{H-5}'$), 2.74 (2H, m, $\text{H}_2\text{-1}''$), 5.77 (1H, brs, H-2), 6.14 (1H, d, $J = 16.2$ Hz, H-5), and 7.80 (1H, d, $J = 16.2$ Hz, H-4); ^{13}C NMR (125 MHz, CDCl_3): δ 13.9 ($\text{C5}''$), 18.7 ($\text{C7}'$), 21.4 (C6), 22.3 ($\text{C4}''$), 23.0 ($\text{C8}'$), 24.3 ($\text{C9}'$), 29.8 ($\text{C3}''$), 30.8 ($\text{C2}''$), 33.6 ($\text{C1}''$), 40.9 ($\text{C6}'$), 49.7 ($\text{C5}'$), 81.1 ($\text{C1}'$), 118.1 (C2), 128.5 (C4), 132.3 ($\text{C3}'$), 136.6 (C5), 151.4 (C3), 164.7 ($\text{C2}'$), 170.7 (C1), and 193.7 ($\text{C4}'$); UV λ_{max} (MeOH) nm (ϵ): 252.2 (19,200); HRMS (m/z): $[\text{M}+\text{Na}]^+$ calc'd. for $\text{C}_{20}\text{H}_{30}\text{O}_4\text{SNa}$, 389.1763; found, 389.1769.

3'-hexylsulfanyl-ABA, AS6 (32)

With stirring at room temperature, 1 M NaOH (22 mL, 22 mmol) and 1-hexanethiol (3 mL, 21 mmol) was added to a solution of **27** (1000 mg, 3.6 mmol) in MeOH (100 mL) and the mixture stirred for 1 h at room temperature. After quenching with 1 M HCl (22 mL), it was then diluted with H_2O (400 mL) and extracted with EtOAc (150 mL \times 3). The organic layer was washed, dried, and concentrated as above. The residual oil was purified by silica gel column chromatography eluted with 20% EtOAc in hexane containing 0.1% AcOH to obtain **AS6** (1200 mg, 87%) as a colorless oil. ^1H NMR (500 MHz, CDCl_3): δ 0.86 (3H, t, $J = 7.0$ Hz, $\text{H}_3\text{-6}''$), 1.02 (3H, s, $\text{H}_3\text{-9}'$), 1.09 (3H, s, $\text{H}_3\text{-8}'$), 1.20 - 1.29 (4H, m, $\text{H}_2\text{-4}''$ and $\text{5}''$), 1.35 (2H, tt, $J = 7.0$ and 7.0 Hz, $\text{H}_3\text{-3}''$), 1.48 (2H, tt, $J = 7.0$ and 7.0 Hz, $\text{H}_2\text{-2}''$), 2.04 (3H, d, $J = 1.2$ Hz, $\text{H}_3\text{-6}$), 2.22 (3H, s, $\text{H}_3\text{-7}'$), 2.44 (1H, d, $J = 16.8$ Hz, $\text{H-5}'$), 2.56 (1H, d, $J = 16.8$ Hz, $\text{H-5}'$), 2.75 (2H, m, $\text{H}_2\text{-1}''$), 5.77 (1H, brs, H-2), 6.15 (1H, d, $J = 15.9$ Hz, H-5), and 7.80 (1H, d, $J = 15.9$ Hz, H-4); ^{13}C NMR (125 MHz, CDCl_3): δ 14.0 ($\text{C6}''$), 18.7 ($\text{C7}'$), 21.4 (C6), 22.5 ($\text{C4}''$), 23.0 ($\text{C8}'$), 24.3 ($\text{C9}'$), 28.3 ($\text{C3}''$), 30.1 ($\text{C2}''$), 31.4 ($\text{C5}''$), 33.6 ($\text{C1}''$), 40.9 ($\text{C6}'$), 49.8 ($\text{C5}'$), 81.1 ($\text{C1}'$), 117.9 (C2), 128.5 (C4), 132.3 ($\text{C3}'$), 136.8 (C5), 151.7 (C3), 164.6 ($\text{C2}'$), 170.7 (C1), and 193.7 ($\text{C4}'$); UV λ_{max} (MeOH) nm (ϵ): 257.0 (18,000); HRMS (m/z): $[\text{M}+\text{Na}]^+$ calc'd. for $\text{C}_{21}\text{H}_{32}\text{O}_4\text{SNa}$, 403.1919; found, 403.1909.

3'-heptylsulfanyl-ABA, AS7 (33)

With stirring at room temperature, 1 M NaOH (300 μ L, 300 μ mol) and 1-heptanethiol (75 μ L, 432 μ mol) was added to a solution of **27** (15 mg, 54 μ mol) in MeOH (1.5 mL) and the mixture stirred for 1 h at room temperature. After quenching with 1 M HCl (2 mL), it was then diluted with H₂O (50 mL) and extracted with EtOAc (25 mL \times 3). The organic layer was washed, dried, and concentrated as above. The residual oil was purified by silica gel column chromatography with 20% EtOAc in hexane containing 0.1% AcOH to obtain **AS7** (17 mg, 80%) as a colorless oil. ¹H NMR (500 MHz, CDCl₃): δ 0.86 (3H, t, J = 7.3 Hz, H₃-7"), 1.02 (3H, s, H₃-9'), 1.09 (3H, s, H₃-8'), 1.20 - 1.29 (6H, m, H₂-4", 5" and 6"), 1.32 (2H, tt, J = 7.0 and 7.0 Hz, H₂-3"), 1.48 (2H, tt, J = 7.0 and 7.0 Hz, H₂-2"), 2.04 (3H, d, J = 1.2 Hz, H₃-6), 2.22 (3H, s, H₃-7'), 2.45 (1H, d, J = 17.1 Hz, H-5'), 2.56 (1H, d, J = 17.1 Hz, H-5'), 2.76 (2H, m, H₂-1"), 5.77 (1H, brs, H-2), 6.14 (1H, d, J = 15.9 Hz, H-5), and 7.81 (1H, d, J = 15.9 Hz, H-4); ¹³C NMR (125 MHz, CDCl₃): δ 14.0 (C7"), 18.7 (C7'), 21.4 (C6), 22.6 (C4", 5" or 6"), 23.0 (C8'), 24.3 (C9'), 28.6 (C4", 5" or 6"), 28.9 (C3"), 30.1 (C2"), 31.7 (C4", 5" or 6"), 33.6 (C1"), 40.9 (C6'), 49.8 (C5'), 81.1 (C1'), 117.9 (C2), 128.4 (C4), 132.3 (C3'), 136.8 (C5), 151.6 (C3), 164.6 (C2'), 170.5 (C1), and 193.6 (C4'); UV λ_{\max} (MeOH) nm (ϵ): 253.2 (18,500); HRMS (m/z): [M+Na]⁺ calc'd. for C₂₂H₃₄O₄SNa, 417.2076; found, 417.2072.

3'-octylsulfanyl-ABA, AS8 (34)

With stirring at room temperature, 1 M NaOH (320 μ L, 320 μ mol) and 1-octanethiol (60 μ L, 350 μ mol) was added to a solution of **27** (15 mg, 54 μ mol) in MeOH (1.5 mL) and the mixture stirred for 2 h at room temperature. After quenching with 1 M HCl (2 mL), it was diluted with H₂O (60 mL) and extracted thrice with EtOAc (25 mL \times 3). The organic layer was washed, dried, and concentrated as above. The residual oil was purified by silica gel column chromatography eluted with 20% EtOAc in hexane containing 0.1% AcOH to obtain **AS8** (18 mg, 82%) as a colorless oil. ¹H NMR (500 MHz, CDCl₃): δ 0.87 (3H, t, J = 7.0 Hz, H₃-8"), 1.02 (3H, s, H₃-9'), 1.10 (3H, s, H₃-8'), 1.24 - 1.28 (8H, m, H₂-4", 5", 6" and 7"), 1.34 (2H, m, H₂-3"), 1.48 (2H, tt, J = 7.3 and 7.3 Hz, H₂-2"), 2.04 (3H, brs, H₃-6), 2.22 (3H, s, H₃-7'), 2.45 (1H, d, J = 16.8 Hz, H-5'), 2.57 (1H, d, J = 16.8 Hz, H-5'), 2.75 (2H, m, H₂-1"), 5.77 (1H, brs, H-2), 6.15 (1H, d, J = 16.2 Hz, H-5), and 7.80 (1H, d, J = 16.2 Hz, H-4); ¹³C NMR (125 MHz, CDCl₃): δ 14.0 (C8"), 18.7 (C7'), 21.4 (C6), 22.6 (C4", 5", 6" or 7"), 23.0 (C8'), 24.2 (C9'), 28.6

(C3''), 29.1 (C4'', 5'', 6'' or 7''), 29.1 (C4'', 5'', 6'' or 7''), 30.0 (C2''), 31.7 (C4'', 5'', 6'' or 7''), 33.6 (C1''), 40.9 (C6'), 49.7 (C5'), 81.0 (C1'), 117.9 (C2), 128.4 (C4), 132.2 (C3'), 136.8 (C5), 151.6 (C3), 164.8 (C2'), 170.8 (C1), and 193.7 (C4'); UV λ_{\max} (MeOH) nm (ϵ): 250.2 (19,000); HRMS (m/z): $[M+Na]^+$ calc'd. for $C_{23}H_{36}O_4SNa$, 431.2232; found, 431.2227.

3'-nonanylsulfanyl-ABA, AS9 (35)

With stirring at room temperature, 1 M NaOH (300 μ L, 300 μ mol) and 1-nonanethiol (75 μ L, 400 μ mol) was added to a solution of **27** (15 mg, 54 μ mol) in MeOH (1.5 mL) and the mixture stirred for 1 h at room temperature. After quenching with 1 M HCl (2 mL), it was diluted with H₂O (50 mL) and extracted thrice with EtOAc (20 mL \times 3). The organic layer was washed, dried, and concentrated as above. The residual oil was purified by silica gel column chromatography eluted with 15% EtOAc in hexane (v/v) containing 0.1% AcOH to obtain **AS9** (17 mg, 74%) as a colorless oil. ¹H NMR (500 MHz, CDCl₃): δ 0.87 (3H, t, $J = 7.3$ Hz, H₃-9''), 1.02 (3H, s, H₃-9'), 1.09 (3H, s, H₃-8'), 1.24 (10H, m, H₂-4'', 5'', 6'', 7'' and 8''), 1.34 (2H, m, H₂-3''), 1.47 (2H, tt, $J = 7.3$ and 7.3 Hz, H₂-2''), 2.04 (3H, d, $J = 1.2$ Hz, H₃-6), 2.22 (3H, s, H₃-7'), 2.45 (1H, d, $J = 16.8$ Hz, H-5'), 2.56 (1H, d, $J = 16.8$ Hz, H-5'), 2.76 (2H, m, H₂-1''), 3.49 (1H, s, HO-1'), 5.77 (1H, brs, H-2), 6.14 (1H, d, $J = 16.2$ Hz, H-5), and 7.81 (1H, d, $J = 16.2$ Hz, H-4); ¹³C NMR (125 MHz, CDCl₃): δ 14.1 (C9''), 18.7 (C7'), 21.4 (C6), 22.6 (C4'', 5'', 6'', 7'' or 8''), 23.0 (C8'), 24.3 (C9'), 28.7 (C3''), 29.2 (C4'', 5'', 6'', 7'' or 8''), 29.3 (C4'', 5'', 6'', 7'' or 8''), 29.5 (C4'', 5'', 6'', 7'' or 8''), 30.1 (C2''), 31.8 (C4'', 5'', 6'', 7'' or 8''), 33.7 (C1''), 40.9 (C6'), 49.8 (C5'), 81.1 (C1'), 117.9 (C2), 128.4 (C4), 132.4 (C3'), 136.8 (C5), 151.6 (C3), 164.6 (C2'), 170.3 (C1), and 193.6 (C4'); UV λ_{\max} (MeOH) nm (ϵ): 253.2 (18,500); HRMS (m/z): $[M+Na]^+$ calc'd. for $C_{24}H_{38}O_4SNa$, 445.2389; found, 445.2381.

3'-decanyl-sulfanyl-ABA, AS10 (36)

With stirring at room temperature, 1 M NaOH (400 μ L, 400 μ mol) and 1-decanethiol (105 μ L, 500 μ mol) was added to a solution of **27** (20 mg, 71 μ mol) in MeOH (2 mL) and the mixture stirred for 1 h at room temperature. After quenching with 1 M HCl (2 mL), it was diluted with H₂O (70 mL) and extracted thrice with EtOAc (30 mL \times 3). The organic layer was washed, dried, and concentrated as above. The residual oil was

purified by silica gel column chromatography eluted with 20% EtOAc in hexane containing 0.1% AcOH to obtain **AS10** (26 mg, 82%) as a colorless oil. ¹H NMR (500 MHz, CDCl₃): δ 0.87 (3H, t, *J* = 7.0 Hz, H₃-10"), 1.02 (3H, s, H₃-9'), 1.09 (3H, s, H₃-8'), 1.24 – 1.29 (12H, m, H₂-4", 5", 6", 7", 8" and 9"), 1.34 (2H, m, H₂-3"), 1.48 (2H, tt, *J* = 7.0 and 7.0 Hz, H₂-2"), 2.03 (3H, brs, H₃-6), 2.21 (3H, s, H₃-7'), 2.45 (1H, d, *J* = 16.8 Hz, H-5'), 2.56 (1H, d, *J* = 16.8 Hz, H-5'), 2.75 (2H, m, H₂-1"), 5.77 (1H, brs, H-2), 6.14 (1H, d, *J* = 16.2 Hz, H-5), and 7.81 (1H, d, *J* = 16.2 Hz, H-4); ¹³C NMR (125 MHz, CDCl₃): δ 14.1 (C10"), 18.7 (C7'), 21.4 (C6), 22.6 (C3", 4", 5", 6", 7", 8" or 9"), 23.1 (C8'), 24.3 (C9'), 28.7 (C3", 4", 5", 6", 7", 8" or 9"), 29.2 (C3", 4", 5", 6", 7", 8" or 9"), 29.3 (C3", 4", 5", 6", 7", 8" or 9"), 29.5 (C3", 4", 5", 6", 7", 8" or 9"), 29.5 (C3", 4", 5", 6", 7", 8" or 9"), 30.1 (C2"), 31.9 (C3", 4", 5", 6", 7", 8" or 9"), 33.6 (C1"), 40.8 (C6'), 49.8 (C5'), 81.0 (C1'), 118.2 (C2), 128.4 (C4), 132.2 (C3'), 136.6 (C5), 151.3 (C3), 164.8 (C2'), 170.6 (C1), and 193.7 (C4'); UV λ_{max} (MeOH) nm (ε): 251.6 (18,300); HRMS (*m/z*): [M+Na]⁺ calc'd. for C₂₅H₄₀O₄SNa, 459.2545; found, 459.2545.

3'-undecanylsulfanyl-ABA, AS11 (37)

With stirring at room temperature, 1 M NaOH (400 μL, 400 μmol) and 1-undecanethiol (110 μL, 500 μmol) was added to a solution of **27** (20 mg, 71 μmol) in MeOH (2 mL) and the mixture stirred for 1 h at room temperature. After quenching with 1 M HCl (2 mL), it was then diluted with H₂O (70 mL) and extracted with EtOAc (25 mL × 3). The organic layer was washed, dried, and concentrated as above. The residual oil was purified by silica gel column chromatography eluted with 20% EtOAc in hexane containing 0.1% AcOH to obtain **AS11** (24 mg, 75%) as a colorless oil. ¹H NMR (500 MHz, CDCl₃): δ 0.88 (3H, t, *J* = 7.0 Hz, H₃-11"), 1.02 (3H, s, H₃-9'), 1.09 (3H, s, H₃-8'), 1.24 (12H, brs, H₂-4", 5", 6", 7", 8" and 9"), 1.30 (2H, m, H₂-10"), 1.34 (2H, m, H₂-3"), 1.48 (2H, tt, *J* = 7.0 and 7.0 Hz, H₂-2"), 2.04 (3H, brs, H₃-6), 2.22 (3H, s, H₃-7'), 2.45 (1H, d, *J* = 16.8 Hz, H-5'), 2.56 (1H, d, *J* = 16.8 Hz, H-5'), 2.75 (2H, m, H₂-1"), 3.49 (1H, s, HO-1'), 5.77 (1H, brs, H-2), 6.14 (1H, d, *J* = 15.9 Hz, H-5), and 7.81 (1H, d, *J* = 15.9 Hz, H-4); ¹³C NMR (125 MHz, CDCl₃): δ 14.1 (C11"), 18.7 (C7'), 21.4 (C6), 22.7 (C3"), 23.0 (C8'), 24.3 (C9'), 28.7 (C4", 5", 6", 7", 8" or 9"), 29.3 (C10"), 29.3 (C4", 5", 6", 7", 8" or 9"), 29.5 (C4", 5", 6", 7", 8" or 9"), 29.6 (C4", 5", 6", 7", 8" or 9"), 29.6 (C4", 5", 6", 7", 8" or 9"), 30.1 (C2"), 31.9 (C4", 5", 6", 7", 8" or 9"), 33.6 (C1"), 40.9 (C6'),

49.8 (C5'), 81.1 (C1'), 117.9 (C2), 128.4 (C5), 132.3 (C3'), 136.8 (C4), 151.6 (C3), 164.6 (C2'), 170.6 (C1), and 193.6 (C4'); UV λ_{\max} (MeOH) nm (ϵ): 253.4 (17,100); HRMS (m/z): $[M+Na]^+$ calc'd. for C₂₆H₄₂O₄SNa, 473.2702; found, 473.2703.

3'-dodecanylsulfanyl-ABA, AS12 (38)

With stirring at room temperature, 1 M NaOH (400 μ L, 400 μ mol) and 1-dodecanethiol (120 μ L, 500 μ mol) was added to a solution of **27** (20 mg, 71 μ mol) in MeOH (2 mL) and the mixture stirred for 1 h at room temperature. After quenching with 1 M HCl (2 mL), it was then diluted with H₂O (60 mL) and extracted with EtOAc (25 mL \times 3). The organic layer was washed, dried, and concentrated as above. The residual oil was purified by silica gel column chromatography with 20% EtOAc in hexane containing 0.1% AcOH to obtain **AS12** (27 mg, 82%) as a colorless oil. ¹H NMR (500 MHz, CDCl₃): δ 0.88 (3H, t, J = 7.0 Hz, H₃-12''), 1.02 (3H, s, H₃-9'), 1.09 (3H, s, H₃-8'), 1.24 (14H, brs, H₂-4'', 5'', 6'', 7'', 8'', 9'' and 10''), 1.30 (2H, m, H₂-11''), 1.34 (2H, m, H₂-3''), 1.48 (2H, tt, J = 7.0 and 7.0 Hz, H₂-2''), 2.04 (3H, d, J = 0.9 Hz, H₃-6), 2.22 (3H, s, H₃-7'), 2.45 (1H, d, J = 16.8 Hz, H-5'), 2.56 (1H, d, J = 16.8 Hz, H-5'), 2.75 (2H, m, H₂-1''), 3.49 (1H, s, HO-1'), 5.77 (1H, brs, H-2), 6.15 (1H, d, J = 16.2 Hz, H-5), and 7.81 (1H, d, J = 16.2 Hz, H-4); ¹³C NMR (125 MHz, CDCl₃): δ 14.1 (C12''), 18.7 (C7'), 21.4 (C6), 22.6 (C3'', 4'', 5'', 6'', 7'', 8'', 9'', 10'' or 11''), 23.0 (C8'), 24.3 (C9'), 28.7 (C3'', 4'', 5'', 6'', 7'', 8'', 9'', 10'' or 11''), 29.2 (C3'', 4'', 5'', 6'', 7'', 8'', 9'', 10'' or 11''), 29.3 (C3'', 4'', 5'', 6'', 7'', 8'', 9'', 10'' or 11''), 29.5 (C3'', 4'', 5'', 6'', 7'', 8'', 9'', 10'' or 11''), 29.6 (C3'', 4'', 5'', 6'', 7'', 8'', 9'', 10'' or 11''), 29.6 (C3'', 4'', 5'', 6'', 7'', 8'', 9'', 10'' or 11''), 29.6 (C3'', 4'', 5'', 6'', 7'', 8'', 9'', 10'' or 11''), 30.1 (C2''), 31.9 (C3'', 4'', 5'', 6'', 7'', 8'', 9'', 10'' or 11''), 33.6 (C1''), 40.9 (C6'), 49.8 (C5'), 81.0 (C1'), 117.9 (C2), 128.4 (C4), 132.3 (C3'), 136.8 (C5), 151.6 (C3), 164.6 (C2'), 170.7 (C1), and 193.6 (C4'); UV λ_{\max} (MeOH) nm (ϵ): 250.0 (17,200); HRMS (m/z): $[M+Na]^+$ calc'd. for C₂₇H₄₄O₄SNa, 487.2858; found, 487.2856.

Molecular modeling of a PYR1–AS6 complex.

The initial structure of AS6 was built by adding an *S*-hexyl chain onto the 3'-carbon of ABA in GaussView 5¹⁶⁶ before it was fully optimized through density functional theory, using the Becke three parameter hybrid functional (B3LYP) method and the 6-31G (d)

basis set in Gaussian 09¹⁶⁷. The RESP charge distributions of AS6 were obtained using R.E.D. Server¹⁶⁸, a web service for deriving RESP charges. Hydrogen molecules were added to a gate-closed conformer of PYR1, and water molecules were added to the PYR1–ABA complex (PDB code 3K3K) using the AddH function in Chimera. The AS6 molecule was manually inserted into the ABA-binding site in this modified PYR1, and the PYR1–AS6 complex was minimized using the Tinker program¹⁶⁹ with amber99 and modified amber gaff parameters with the GB/SA model.

***Arabidopsis* seed germination assay.**

Twenty-five to forty seeds (Columbia accession) were sterilized successively with soaking in 70% aqueous ethanol (EtOH, v/v) for 30 min and reagent-grade EtOH for 1 min. They were then soaked in 250 µl of a test solution and incubated in darkness at 5 °C for 3 d. The stratified seeds in the test solution were transferred onto two pieces of filter paper in 24-well plates and allowed to germinate under continuous illumination at 22 °C for 24 h or 36 h. All of the assays were conducted at least three times.

***Arabidopsis* early growth assay.**

Twenty to thirty seeds (Columbia accession) were sterilized successively with 70% aqueous EtOH (v/v) for 30 min and reagent-grade EtOH for 1 min. They were then were soaked in 100 µl of a test medium liquid agar in 96-well plates and allowed to germinate and grow at 22 °C and under continuous illumination for 5 d or 10 d. All of the assays were conducted at least three times.

Lettuce seed germination and early growth assay.

Twenty-five seeds (*Lactuca sativa* L. cv. Grand Rapids) were placed in a dish on two sheets of filter paper soaked in 2 ml of a test solution and allowed to germinate and grow at 22 °C and under continuous illumination for 14 d. The germination rate was determined as the time when the germination rate of the control plant was 50% or the germination rate of only ABA-treated plants was 40%. All of the assays were conducted at least three times.

Radish seedling water-loss assay.

Radish seeds (*Raphanus sativus* L. var. raphanistroides (Makino) Sinsk.) were soaked in water at 25 °C in darkness for 2 d and allowed to germinate and grow under continuous illumination for 5 d. Seven-day old seedlings were placed in a plastic tube containing 15 ml of a test solution and incubated at 25 °C and under continuous illumination for 12 h. The plants were transferred to empty tubes and exposed to drought stress under same conditions for 4 h. Water content was expressed as a relative reduction rate normalized to a control (untreated) value of 100%.

Thermal imaging.

Seven-day old radish seedlings (sp. and var. as above) grown under continuous illumination at 25 °C were placed in plastic tubes containing 15 ml of a test solution and were incubated in darkness at 25 °C for 12 h. Thermal images were obtained using Testo 881-2 thermography (Testo, Inc., Sparta, NJ, USA). Images were saved in a computer memory card and analyzed using the IRSoft software (Testo, Inc.).

CYP707A3 inhibition assay.

Reaction mixtures containing 25 µg ml⁻¹ of CYP707A3 microsomes (coexpressed with AR2 in *E. coli*)¹⁷⁰, ABA (final concentration 1–64 µM), inhibitors (0 for control, 50–100 µM in 5 µl dimethylformamide (DMF)) and 130 µM NADPH in 100 mM potassium phosphate buffer (pH 7.25) were incubated at 30 °C for 10 min. Reactions were initiated by adding NADPH, stopped by addition of 50 µl of 1 M NaOH and then acidified with 100 µl of 1 M HCl. Reaction products were extracted by loading the mixture onto an Oasis HLB cartridge (1 ml, 30 mg; Waters Corp., Milford, MA, USA) and were washed with 1 ml of 10% MeOH in H₂O (v/v) containing 1% AcOH (v/v). The enzyme products were then eluted with 1 ml of MeOH containing 1% AcOH, and the eluate was concentrated *in vacuo*. The dried sample was then dissolved in 50 µl of MeOH, and a 20-µl volume was subjected to HPLC (Prominence; Shimadzu Corp., Kyoto, Japan). HPLC conditions were as follows: the octadecylsilyl (ODS) column was composed of Hydrosphere C18 (150 × 6.0 mm, YMC Co., Ltd., Kyoto, Japan), solvent comprised 17% acetonitrile (MeCN) in H₂O containing 0.05% AcOH (v/v), the flow rate was 1.0 ml min⁻¹, and detection was at 254 nm. Enzyme activity was evaluated by determining the amount of phaseic acid in control experiments before each set of measurements. The

inhibition constants for AS2 and AS6 were determined using the Enzyme Kinetics module of SigmaPlot 10 software (Systat Software, Inc., San Jose, CA, USA) after determining the inhibition mode by plotting the reaction velocity in the presence and absence of inhibitor on a double-reciprocal plot. All of the tests were conducted at least three times.

qRT-PCR analysis.

Total RNA was isolated using Plant RNA Purification reagent (Invitrogen Corp., Carlsbad, CA, USA), according to the manufacturer's protocol. cDNA was synthesized using the QuantiTec reverse transcription kit (Qiagen GmbH, Hilden, Germany). Real-time PCR using Maxima SYBR Green/Fluorescein qPCR Master Mix (Thermo Fisher Scientific, Inc., Pittsburgh, PA, USA) was performed with the iQ5 real-time PCR detection system (Bio-Rad Laboratories, Inc., Hercules, CA, USA). The relative amount of target mRNA was based on a standard curve and normalized to the relative amount of internal control mRNA. Biological triplicate experiments were performed, and primer sets were used as previously described¹²⁴. Pyrabactin (98%) was purchased from Sigma-Aldrich, Inc. (St. Louis, MO, USA).

GUS staining assay.

For ABA-responsive reporter gene analyses, transgenic *Arabidopsis* expressing β -glucuronidase (GUS) under the control of the AtMAPKKK18 promoter were used, as previously described¹²⁴. Six-day-old seedlings were used in this study, and GUS staining was performed in a reaction buffer composed of 50 mM sodium phosphate buffer, pH 7.0, 0.05% Tween-20, 2.5 mM potassium ferrocyanide, 2.5 mM potassium ferricyanide and 1 mM X-gluc. After incubation at 37 °C, the reaction was stopped by EtOH addition, and green pigments in the sample were extracted into EtOH with incubation at 65 °C.

PP2C enzyme assay.

For production of PP2C protein, GST-HAB1 was cloned into pGex-2T, as previously described⁹⁵. For ABA receptor proteins, PYL cDNAs were cloned into pET28 vector, whereas PYL11 cDNA was cloned into pMAL-c vector^{99,124}. Functional PYL7 and

PYL12 were not obtained in this expression system using pET28 or pMAL-c vectors. HAB1 and PYL proteins were expressed and purified, as previously described¹²⁴. Briefly, plasmids were transformed into BL21[DE3]pLysS, the resulting transformant cells were precultured overnight in 10 ml LB medium, and then cells were grown in 800 ml medium at 30 °C to an OD₆₀₀ ~0.5. Protein expression was induced by IPTG addition, and inductions were conducted at 15 °C for 16 h. Cells were harvested, frozen, thawed and sonicated, and the constituent proteins were purified by affinity column chromatography. Purified proteins were preincubated in 80 µl of buffer containing 12.5 mM MnCl₂, 0.125% 2-mercaptoethanol and test compound at 22 °C for 30 min. After adding 20 µl of substrate buffer (165 mM Tris-acetate, pH 7.9, 330 mM potassium acetate, 0.1% BSA and 250 mM *p*NPP), reactions were immediately monitored for hydrolysis of *p*NPP at 405 nm. The PP2C assay was performed using 60 pmol each of PP2C and PYL.

Pull-down assay.

Here, 100 µg and 20 µg of purified GST-HAB1 and His₆-tagged PYLs, respectively, were incubated in 200 µl of Tris-buffered saline (TBS) containing 100 µg BSA, 0.025% 2-mercaptoethanol, 10 mM MnCl₂ and 10 mg PrepEase His-tagged protein purification resin (Affymetrix, Inc., Santa Clara, CA, USA) in the presence or absence of test compounds with gentle shaking at 4 °C for 60 min. The resin was then washed five times with TBS containing 0.025% 2-mercaptoethanol and 10 mM MnCl₂, while held on ice. The bound proteins were eluted in 60 µl of SDS-sample buffer with 250 mM imidazole and denatured at 95 °C for 5 min. Then, 10 µl of eluate was loaded on a 13% SDS-PAGE gel, and proteins were detected after development by Coomassie brilliant blue staining.

Isothermal titration calorimetry.

ASn-binding studies were performed by isothermal titration calorimetry (ITC) using an iTC₂₀₀ calorimeter (Microcal, GE Healthcare Bio-Sciences AB) and were conducted at 20 °C and with a solvent of 100 mM phosphate buffer, pH 8.0. His₆-tagged PYL5 or His₆-tagged PYL10 were assayed at a concentration of 40 µM and 50 µM, respectively, with AS6 and ABA stock solutions in the injection syringe at tenfold higher

concentrations than the proteins. All of the titrations were carried out via a series of 20 injections of 1.25 μl each. The data were corrected by subtracting the mixing enthalpies for the AS6 or ABA solutions into protein-free solutions and fitted by Origin for ITC (GE Healthcare Bio-Sciences AB) with a 1/1 binding model.

Protein preparation and crystallization.

For crystallization of the PYR1–AS6 complex, PYR1 was cloned into a pET-28 vector, as previously described⁹⁹. The plasmid was then transformed into *E. coli* strain BL21-CodonPlus (DE3)-RIPL (Agilent Technologies, Santa Clara, CA, USA), and transformed cells were incubated at 30 °C to an $\text{OD}_{600} \sim 0.5$. Protein expression was induced by IPTG addition and incubation at 16 °C for 16 h, after which cells were harvested, frozen, thawed and sonicated. Protein was then purified from this preparation using a Ni-Sepharose resin (GE Healthcare Bio-Sciences AB) and eluted with binding buffer (150 mM phosphate, pH 8.0, and 300 mM NaCl) supplemented with 250 mM imidazole. The protein was further purified using a Resource Q column (GE Healthcare Bio-Sciences AB) and eluted with binding buffer (10 mM Tris-HCl, pH 8.0) supplemented with 150 mM NaCl. Peak fractions were concentrated using an Amicon Ultrafilter (30,000 MWCO, Millipore Corp., Billerica, MA, USA).

Crystallization was performed using the hanging-drop vapor-diffusion method at 20 °C, and crystallization buffer comprised 100 mM HEPES (pH 7.5) with 20% (v/v) PEG 10,000 as the reservoir buffer. Drops of protein solution (1.5 μl , 10 mg ml^{-1}) containing 1 mM AS6 were mixed with 1.5 μl of reservoir buffer. Crystals were flash-frozen at 100 K under a cold stream of nitrogen gas without cryoprotectant.

Data collection, structure determination and refinement.

Diffraction data of PYR1 cocrystallized with AS6 were collected on beamline 17A at the Photon Factory (Tsukuba, Japan), and data sets were processed with the program HKL2000¹⁷¹. The initial structure of the complex was solved by molecular replacement using the program MOLREP^{172,173} in the CCP4 suite¹⁷⁴ with the PYR1 coordinates (PDB code 3K90) as a target model. Refinements were carried out with the program REFMAC5¹⁷⁵ in the CCP4 suite, and the restraint file for the AS6 molecule was obtained at thePRODRG server¹⁷⁶. Manual model building was performed using Coot¹⁷⁷,

and the structure was refined at 2.3 Å to $R_{\text{work}}/R_{\text{free}}$ factors of 23.8%/28.1%. The statistics for data collection and refinement are provided in **Table 5**.

Quantitative analysis of endogenous ABA.

Measurement of endogenous ABA has been described elsewhere^{178,179}. Briefly, 10-d-old plants (0.5–1 g) were incubated for 6 h in a 10 µM AS2 or AS6 solution or water as a control. These plants were homogenized in 80% aqueous acetone (v/v) containing 0.1 mg/ml 2,6-di-*tert*-butyl-4-methylphenol as an antioxidant. A 5.0 ng of [3',5',5',7',7',7'-²H₆]ABA (*d*₆-ABA), as the internal standard, was added to a homogenized sample before the following extraction procedure. The homogenate was centrifuged at 5,000g and 4 °C for 15 min, and the supernatant was reduced to the aqueous phase *in vacuo*. After washing with hexane, the pH was adjusted to 2 using 0.5 M phosphoric acid, and ABA was extracted into EtOAc. The solvent was removed from this extract *in vacuo*, and the residue was dissolved in 110 µl of 10% MeOH containing 0.1% AcOH (v/v) and introduced into a HPLC. HPLC conditions were as follows: ODS column with Hydrosphere C18 (150 × 6.0 mm, YMC Co.), a solvent gradient program of MeOH containing 0.1% AcOH (35–60% MeOH over 30 min), flow rate of 1.0 ml min⁻¹ and detection at 254 nm. The fraction containing ABA standard was collected, dried *in vacuo* and then methylated with trimethylsilyldiazomethane. The resulting methylated samples were dissolved in 10 µl of EtOAc and analyzed by gas chromatography-MS on a QP5050A system (Shimadzu Corp., Kyoto, Japan) using an Equity-5 column (Supelco Inc., Bellefonte, PA, USA; 0.25 mm i.d. × 30 m, 0.25-µm film thickness) and helium carrier gas at linear and total flow rates of 35.6 cm s⁻¹ and 50 ml min⁻¹, respectively. The column flow rate was set at 1.0 ml min⁻¹, and splitless injection mode was used with a 2-min sampling time at 200 kPa. The programmed column temperature was a step gradient of 60 °C for 2 min, 60–270 °C at 10 °C min⁻¹ and then 270 °C for 35 min. The system was set with a 70-eV electron potential and 0.5-s signal sampling rate, and qualitative analysis was performed in selected-ion monitoring mode. Samples (2.5 µl) of material were injected onto the column and *d*₀-ABA and *d*₆-ABA methyl esters detected with retention times of 22.54 min and 22.49 min, respectively. The mass chromatogram peak area of the [M-C₅H₁₂O]⁺ ion (*m/z* 190) derived from *d*₀-ABA methyl ester was compared to that of *d*₆-ABA methyl ester (*m/z*

194). Concentrations were calculated using a linear regression equation based on different concentrations of the methylated standards ABA and d_6 -ABA. Identification of ABA methyl ester in samples was conducted in total ion monitoring mode through comparison of the fragmentation pattern with that of the standard.

Statistical analyses.

All statistical analyses were performed using R version 3.0.2 software, and Grubbs' test was used to detect outliers. Normal distributions and assumptions regarding variance homogeneities in ABA concentrations from each treatment were checked using the Shapiro-Wilk test and Bartlett's test, respectively. Differences in ABA concentrations between treatments were tested using one-way ANOVA.

Transport assay.

ABA transport activities of NPF4.6/AIT1 in a yeast system were determined by directly analyzing ABA taken into cells by LC/MS/MS, as described previously⁷⁸, but with some modifications. Potassium phosphate buffer at pH 5.8, instead of pH 7.5, was used for the assays. ABA was extracted from yeast cells at $-30\text{ }^{\circ}\text{C}$ overnight in 1 ml of 80% aqueous acetone containing 1% acetic acid (v/v), with d_6 -ABA as an internal standard. Supernatants were collected after centrifugation, and acetone was evaporated using a SpeedVac (Thermo Fisher Scientific Inc.) to obtain aqueous extracts containing acetic acid. Solutions were adjusted to 1 ml with 1% acetic acid and applied to Oasis WAX cartridge columns (30 mg, 1 ml; Waters Corp.) prewashed successively with 1 ml of MeCN and methanol, regenerated with 0.5 ml of 0.1 M NaOH and equilibrated with 1 ml of 1% acetic acid. After washing successively with 3-ml volumes of 1% acetic acid and methanol, the fractions containing ABA were eluted with 2 ml of 80% MeCN containing 1% acetic acid (v/v). The eluates were taken to dryness and dissolved in 0.5 ml of chloroform containing 49% ethyl acetate and 1% acetic acid (v/v). They were then loaded on Sep-Pak silica (100 mg; Waters Corp.) cartridge columns prewashed with 3 ml of chloroform and equilibrated with 1 ml of chloroform containing 1% acetic acid. Fractions containing ABA were eluted with 2 ml of chloroform containing 49% ethyl acetate and 1% acetic acid (v/v). The samples were next taken to dryness and dissolved in 20 μl of water containing 1% acetic acid (v/v) before injection into the LC/MS/MS. A

Nexera (Shimadzu Corp., Kyoto, Japan)/Triple TOF 5600 (AB SCIEX, Framingham, MA, USA) system equipped with an ACQUITY UPLC BEH phenyl column (Waters Corp.) was used to quantify ABA, as described previously⁷⁸, except that the desolvation temperature was 600 °C instead of 700 °C.

Summary

The plant hormone ABA is critical for plant growth and several abiotic stress responses. ABA signaling is normally repressed by group-A PP2Cs, which are negative regulators of the ABA response. A stress-induced ABA binds PYL receptors, which triggers the conformational change associated with gate closure to create an interaction surface with the PP2Cs. ABA-bound PYLs bind and inhibit PP2Cs, including HAB1, ABI1, and ABI2, which directly inactivate SnRK2s, to allow the activation of SnRK2s via autophosphorylation. Activated SnRK2s phosphorylate transcription factors and S-type anion channels to elicit ABA responses such as seed dormancy and stomatal closing. By focusing on the structural properties of ABA, which acts as a positive allosteric regulator of PYLs, we have developed a negative allosteric regulator that retains the high selectivity for PYLs but does not activate PYLs.

In the PYL-ABA complexes, ABA intrudes deeply into the ligand binding pocket to be tightly packed by PYL's residues. The C2', C3' and C4' positions of ABA's ring were found to participate in gate closure via hydrophobic contacts with the gate loop, and furthermore, the X-ray structures of several PYL-ABA complexes revealed a small tunnel above ABA's 3' ring that opens at the PP2C binding interface. Here, ABA analogs with sufficiently long 3' alkyl chains were predicted to traverse this tunnel and block PYL-PP2C interactions. To test this, a series of 3'-alkylsulfanyl ABAs were synthesized with different alkyl chain lengths by nucleophilic addition of alkyl thiolate to the 2',3'-epoxide, prepared from ABA. For simplicity, there are called the AS n compound series, where n denotes the alkyl chain length. Before preparing these compounds, a model of a PYR1-AS6 complex was constructed on the basis of the crystal structures of PYR1-ABA complexes. This model suggested that alkyl chains of compounds with $n > 4$ protrude through the PYR surface and block the interactions with PP2C, whereas the compounds with $n < 4$ might stabilize gate closure and act as agonists.

In seed germination and a seedling growth assay using *Arabidopsis* and lettuce, AS2 and AS3 acted as ABA mimics, where AS5–AS12 suppressed ABA's effect in coapplications with ABA. Radish seedlings treated with AS2 enhanced drought tolerance, whereas AS6-treated seedlings wilted more quickly than non-treated controls.

In addition, AS2 induced the expression of ABA-responsive genes and the β -glucuronidase gene on an ABA-responsive, transcriptional, reporter line, as expected of an agonist. Conversely, AS4 and AS6 lessened the expression levels of ABA-responsive genes and the β -glucuronidase gene in cotreatments with ABA. This antagonist effect was stronger for AS6 than AS4. Notably, AS6 also repressed the expression levels of stress-induced ABA-responsive genes in response to treatments with mannitol, which induced ABA synthesis by mimicking the water loss caused by drought. These physiological data suggested that AS2 and AS6 functioned as a PYL agonist and antagonist, respectively, whereas AS4 exhibited an intermediate effect.

The effects of AS n on 11 of the 13 *Arabidopsis* receptors were examined using receptor-mediated phosphatase assays. AS2 activated PYR1 and PYL1–3 with potencies comparable to that of ABA, but did not show the activation of PYL8–10; thus, AS2 was not a broad-spectrum agonist. On the other hand, AS6 antagonized the ABA-dependent PP2C inhibition for all of the receptors tested in a cotreatment assay, indicating a broad-spectrum antagonist activity. The mechanism of the AS6 antagonist activity was further characterized by a pull-down assay. In cotreatment experiments, AS6 blocked ABA-induced PYL-PP2C interactions in a dose-dependent manner. These biochemical results indicated that AS6 acts as an antagonist by blocking ABA-induced PYL-PP2C interactions.

Isothermal titration calorimetry was next used to characterize AS6 binding with PYL5 and PYL10. These analyses revealed apparent dissociation constants of AS6 (0.4–1.3 μ M) with negative enthalpies, indicating an exothermic binding process. These values were comparable to those of ABA (0.8 μ M). The molecular mechanism of AS6 activity was then clarified by determining the crystal structure of recombinant PYR1 bound to AS6 (Protein Data Bank code 3K90). The PYR1-AS6 complex was found to very closely resemble the PYR1-ABA complex. Consistent with the present model-based predictions, the gate loop adapted a closed conformation, and the 3' tunnel accommodated the AS6 *S*-hexyl chain, which also protruded out onto PYR1's PP2C-interaction surface. These observations provide direct evidence that AS6 induces the gate-closed conformer but the *S*-hexyl chain interferes with the PYL-PP2C interactions.

To examine the functional selectivity of AS n , the effects of AS2 and AS6 on two

well-characterized, non-receptor ABA binding sites were characterized. Both compounds were found not to be potent inhibitors of the ABA metabolic CYP707A enzyme. No significant differences were observed in endogenous ABA concentrations between ASn and non-treated *Arabidopsis* seedlings. In addition, AS6 did not substantially inhibit the ABA transport activity of NPF4.6/AIT1. These data suggest that ASn has little effect on ABA metabolism and transportation.

This study provides a new approach for the design of ABA analogs, and the results validated structure-based designs of this target class.

Acknowledgments

This study was carried out in the Laboratory of Natural Products Organic Chemistry, Department of Bioscience, Graduate School of Science and Technology, Educational Division, Shizuoka University from 2011 to 2014.

The author wishes to thank Professor Yasushi Todoroki, for his guidance, encouragement and practical advice, which have been indispensable to the continuation of this study. The author also thanks Dr. Toshiyuki Ohnishi of the Laboratory of Natural Products Organic Chemistry for his encouragement and practical advice, and Professor Naoharu Watanabe of the Laboratory of Bioorganic Chemistry at Shizuoka University for helpful suggestion and comments.

The author thanks Dr. Masanori Okamoto of Arid Land Research Center at Tottori University for his collaboration and helpful discussions, Professor Shunsuke Yajima of Department of Bioscience at Tokyo University of Agriculture for his collaboration, Dr. Masayuki Sue of Department of Applied Biology and Chemistry at Tokyo University of Agriculture for analyzing the crystal structure, and Mr. Tomonori Akiyama of Department of Bioscience at Tokyo University of Agriculture for creating the crystal structure. The author thanks Dr. Mitsunori Seo and Ms. Yuri Kanno of RIKEN Center for Sustainable Resource Science for analyzing of ABA transport assay, Dr. Kamo Tsunashi of National Institute for Agro-Environmental Sciences for analyzing of endogenous ABA. The author thanks Dr. Akira Endo of Crop Breeding Research Division at National Agricultural Research Organization for Hokkaido Region and Professor Eiji Nambra of Department of Cell and Systems Biology at University of Toronto and Professor Nobuhiro Hirai of Graduate School of Agriculture at Kyoto University for their collaboration, and Professor Sean R Cutler of Department of Botany and Plant Sciences and Center for Plant Cell Biology at University of California-Riverside for helpful suggestion and comments. The author thanks Mr. Akihito Yagi of Faculty of Agriculture at Shizuoka University for measuring the NMR and mass spectra, Mr. Takuya Muto of Graduate School of Agriculture at Shizuoka University for synthesis of AS_n , and Toray Industries Inc., Tokyo, Japan for the gift of (+)-ABA. Acknowledgments are made to all of the members of the Laboratory of Natural Products Organic Chemistry at Shizuoka University.

Finally, the author owes special thanks to his parents and family for their warm encouragement and financial support.

References

1. Davies, P. J. in *Plant Hormones: Physiology, Biochemistry and Molecular Biology* (ed. Davies, P. J.) 1-12 (Kluwer Academic, 1995).
2. Santner, A. & Estelle, M. Recent advances and emerging trends in plant hormone signalling. *Nature* **459**, 1071-1078 (2009).
3. Bleeker, A., Estelle, M., Somerville, C. & Kende, H. Insensitivity to ethylene conferred by a dominant mutation in *Arabidopsis thaliana*. *Science* **241**, 1086-1089 (1988).
4. Joachim, H., Dieckmann, M., Grantz, A. A. & Kim, S. H. The structure of the signal receiver domain of the *Arabidopsis thaliana* ethylene receptor ETR1. *Structure* **7**, 1547-1556 (1999).
5. Schaller, G. E., Ladd, A. N., Landhan, M. M. Spanbauer, J. M. & Bleeker, A. B. The ethylene response mediator ETR1 from *Arabidopsis* forms a disulfide linked dimer. *J. Biol. Chem.* **270**, 12525-12530 (1995).
6. Rodriguez, F. I. et al. A copper cofactor for the ethylene receptor ETR1 from *Arabidopsis*. *Science* **283**, 996-998 (1999).
7. Li, J. & Chory, J. A putative leucine-rich repeat receptor kinase involved in brassinosteroid signal transduction. *Cell* **90**, 929-938 (1997).
8. She, J. et al. Structural insight into brassinosteroid perception by BRI1. *Nature* **474**, 472-476 (2011).
9. Hothorn, M. et al. Structural basis of steroid hormone perception by the receptor kinase BRI1. *Nature* **474**, 476-471 (2011).
10. Gruszka, D. The brassinosteroid signaling pathway-new key players and interconnections with other signaling networks crucial for plant development and stress tolerance. *Int. J. Mol. Sci.* **14**, 8740-8774 (2013).
11. Clay, N. K. & Nelson, T. VH1, a provascular cell-specific receptor kinase that influences leaf cell patterns in *Arabidopsis*. *Plant Cell* **14**, 2707-2722 (2002).
12. Cano-Delgado, A. et al. BRL1 and BRL3 are novel brassinosteroid receptors that function in vascular differentiation in *Arabidopsis*. *Development* **131**, 5341-5351 (2004).
13. The *Arabidopsis* genome initiative. Analysis of the genome sequence of the flowering

- plant *Arabidopsis thaliana*. *Nature* **408**, 796-815 (2000).
14. Inoue, T. *et al.* Identification of CRE1 as a cytokinin receptor from *Arabidopsis*. *Nature* **409**, 1060-1063 (2001).
 15. Suzuki, T. *et al.* The *Arabidopsis* sensor His-kinase, AHk4, can respond to cytokinis. *Plant Cell Physiol.* **42**, 107-113 (2001).
 16. Yamada, H. *et al.* The *Arabidopsis* AHK4 histidine kinase is a cytokinin binding receptor that transduces cytokinin signals across the membrane. *Plant Cell Physiol.* **42**, 1017-1023 (2001).
 17. Ueguchi-Tanaka, M. *et al.* GIBBERELLIN INSENSITIVE DWARF1 encodes a soluble receptor for gibberellin. *Nature* **437**, 693-698 (2005).
 18. Griffiths, J. *et al.* Genetic characterization and functional analysis of the GID1 gibberellin receptor in *Arabidopsis*. *Plant Cell* **18**, 3399-3414 (2006).
 19. Nakajima, M. *et al.* Identification and characterization of *Arabidopsis* gibberellin receptor. *Plant J.* **46**, 880-889 (2006).
 20. Willige, B. C. *et al.* The DELLA domain of GA INSENSITIVE mediates the interaction with the GA INSENSITIVE DWARF1A gibberellin receptor of *Arabidopsis*. *Plant Cell* **19**, 1209-1220 (2007).
 21. McGinnis, K. *et al.* The *Arabidopsis* SLEEPY1 gene encodes a putative F-box subunit of an SCF E3 ubiquitin ligase. *Plant Cell* **15**, 1120-1130 (2003).
 22. Sakai, A. *et al.* Accumulation of phosphorylated repressor for gibberellin signaling in an F-box mutant *Science* **299**, 1896-1898 (2003).
 23. Dharmasiri, N., Dharmasiri, S. & Estelle, M. The F-box protein TIR1 is an auxin receptor. *Nature* **435**, 441-446 (2005).
 24. Kepinski, S. & Leyser, O. The *Arabidopsis* F-box protein TIR1 is an auxin receptor. *Nature* **435**, 446-451 (2005).
 25. Tan, X. *et al.* Mechanism of auxin perception by the TIR1 ubiquitin ligase. *Nature* **446**, 640-645 (2007).
 26. Reed, J. W. Roles and activities of Aux/IAA proteins in *Arabidopsis*. *Trends Plant Sci.* **6**, 420-425 (2001).
 27. Gagne, J. M., Downes, B. P., Shiu, S. H., Durski, A. M. & Vierstra, R. D. The F-box subunit of the SCF E3 complex is encoded by a diverse superfamily of genes in *Arabidopsis*. *Proc. Natl. Acad. Sci. USA* **99**, 11519-11524 (2002).

28. Feys, B., Benedetti, C. E., Penfold, C. N. & Turner, J. G. *Arabidopsis* mutants selected for resistance to the phytotoxin coronatine are males sterile, insensitive to methyl jasmonate, and resistant to a bacterial pathogen. *Plant Cell* **6**, 751-759 (1994).
29. Thines, B. *et al.* JAZ repressor proteins are targets of the SCFCOII complex during jasmonate signalling. *Nature* **448**, 661-665 (2007).
30. Chini, A. *et al.* The JAZ family of repressors is the missing link in jasmonate signalling. *Nature* **448**, 666-671 (2007).
31. Sheard, L. B. *et al.* Jasmonate perception by inositol-phosphate-potentiated COI1-JAZ co-receptor. *Nature* **468**, 400-405 (2010).
32. Fu, Z. Q. *et al.* NPR3 and NPR4 are receptors for the immune signal salicylic acid in plants. *Nature* **486**, 228-232 (2012).
33. Malamy, J., Carr, J. P., Klessig, D. F. & Raskin, I. Salicylic acid: a likely endogenous signal in the resistance response of tobacco to viral infection. *Science* **250**, 1002-1004 (1990).
34. Hamiaux, C. *et al.* DAD2 is an α/β hydrolase likely to be involved in the perception of the plant branching hormone, strigolactone. *Curr. Biol.* **22**, 2032-2036 (2012).
35. Jiang, L. *et al.* DWARF 53 acts as a repressor of strigolactone signalling in rice. *Nature* **504**, 401-405 (2013).
36. Zhou, F. *et al.* D14-SCFD3-dependent degradation of D53 regulate strigolactone signalling. *Nature* **504**, 406-410 (2013).
37. Chow, B. & McCourt, P. Plant hormone receptors: perception is everything. *Genes Dev.* **20**, 1998-2008 (2006),.
38. Finkelstein, R., Reeves, W., Ariizumi, T. & Steber, C. Molecular aspects of seed dormancy. *Plant Boil.* **59**, 387-415 (2008).
39. Hayashi, K. & Kinoshita, T. Abscisic acid receptor hole-in-one. *Nat. Chem. Biol.* **10**, 414-415 (2014).
40. Ohkuma, K., Lyon, J. L., Addicott, F. T. & Smith, O. E. Abscisin II, an abscission-accelerating substance from young cotton fruit. *Science* **142**, 1592-1593 (1963).
41. Wareing, P. F., Eagles, C. F. & Robinson, P. M. Natural inhibitors as dormancy agents. In: Nitsch JP (ed), *Regulateurs Naturels de la Croissance Vegetable. Cent. Nat. Rech. Sci. Paris* , pp. 377-386 (1964).

42. Addicott, F. T. et al. Abscisic acid : a new name for abscisin II (dormin). *Science*, **159**, 1493 (1968).
43. Ohkuma, K., Addicott, F. T., Smith, O. E. & Thiessen, W. E. The structure of abscising II. *Tetrahedron Letter* **6**, 2529-2535 (1965).
44. Lin, B. L. et al. Abscisic acid regulation of heterophylly in *Marsilea quadrifolia* L.: effects of *R*-(-)- and *S*-(+)-isomers. *J. Exp. Bot.* **56**, 2935-2948 (2005).
45. Cutler, S. R., Rodriguez, P. L., Finkelstein, R. R., Abrams, S. R. Abscisic acid : emergence of a core signaling network. *Ann. Rev. Plant Biol.* **61**, 651-679. (2010).
46. Zhang, X. et al. Structural insights into the abscisic acid stereospecificity by the ABA receptors PYR/PYL/RCAR. *PLOA ONE*, **8**, e67477 (2013).
47. Nishimura, N. et al. Structural mechanism of abscisic acid binding and signaling by dimeric PYR1. *Science* **326**, 1373-1379 (2009).
48. Cremer, D. & Szabo, K. J. In conformational behavior of six-membered ring; Juaristi, E., VCH: New York, 1995, pp. 59-135.
49. Milborrow, B. V. The conformation of abscisic acid by n. m. r. and a revision of the proposed mechanism for cyclization during its biosynthesis. *Biochem. J.* **220**, 325-332 (1984).
50. Willows, R. D. & Milborrow, B. V. Configurations and conformations of abscisic acid. *Phytochemistry* **34**, 233-237 (1993).
51. Todoroki, Y. & Hirai, N. Abscisic acid analogs for probing the mechanism of abscisic acid reception and inactivation. *Stud. Nat. Prod. Chem.* **27**, 321-360 (2002).
52. Komatsu, K. et al. Group A PP2Cs evolved in land plants as key regulators of intrinsic desiccation tolerance. *Nature communications* **4**, DOI: 10.1038/ncomms3219.
53. Degivry, L. P., Barthe, P. & Garello, G. Involvement of endogenous abscisic acid in onset and release of *Helianthus annuus* embryo dormancy. *Plant Physiol.* **92**, 1164-1168 (1990).
54. Karssen, C. M., Brinkhorst-van der Swan, D. L. C., Breekland, A. E. & Koornnef, M. Induction of dormancy during seed development by endogenous abscisic acid: studies on abscisic acid deficient genotypes of *Arabidopsis thaliana* (L.) heynh. *Planta* **157**, 158-165 (1983).
55. Koornnef, M., Leon-Kloosterziel, K. M., Schwartz, S. H. & Zeevaart, J. A. D. The genetic and molecular dissection of abscisic acid biosynthesis and signal transduction in

- Arabidopsis*. *Plant Physiol. Biochem.* **36**, 83-89 (1998).
56. Cutler, S., Ghassemian, M., Bonetta, D., Cooney, S. & McCourt, P. A protein farnesyl transferase involved in abscisic acid signal transduction in *Arabidopsis*. *Science* **273**, 1239-1241 (1996).
57. Finkelstein, R. Abscisic acid synthesis and response. *The Arabidopsis book* (2013).
58. Lee, S. J. *et al.* DREB2C interacts with ABF2, a bZIP protein regulating abscisic acid-responsive gene expression, and its overexpression affects abscisic acid sensitivity. *Plant Physiol.* **153**, 716-727 (2010).
59. Okamoto, M. *et al.* *CYP707A1* and *CYP707A2*, which encode abscisic acid 8'-hydroxylases, are indispensable for proper control of seed dormancy and germination in *Arabidopsis*. *Plant Physiol.* **141**, 97-107 (2009).
60. Seo, M., Nambara, E., Choi, G. & Yamaguchi, S. Interaction of light and hormone signals in germinating seeds. *Plant Mol. Biol.* **69**, 463-472 (2009).
61. Yamaguchi-Shinozaki, K. & Shinozaki, K. Transcriptional regulatory networks in cellular responses and tolerance to dehydration and cold stresses. *Ann. Rev. Plant. Biol.* **57**, 781-803 (2006).
62. Qin, F., Shinozaki, K. & Yamaguchi-Shinozaki, K. Achievements and challenges in understanding plant abiotic stress responses and tolerance. *Plant Cell Physiol.* **52**, 1569-1582 (2011).
63. Hong, G. J., Xue, X. Y., Mao, Y. B., Wang, L. J. & Chen, X. Y. *Arabidopsis* MYC2 interacts with DELLA proteins in regulating sesquiterpene synthase gene expression. *Plant Cell* **24**, 2635-2648 (2012).
64. Kwak, J. M., Maser, P. & Schroeder, J. I. The clickable guard cell, version II: Interactive model of guard cell signal transduction mechanisms and pathways. *The Arabidopsis Book* 6: e0114.doi: 10. 1199/tab. 0144.
65. Kim, T. H., Bohmer, M., Hu, H., Nishimura, N. & Schroeder, J. I. Guard cell signal transduction network: Advances in understanding abscisic acid, CO₂ and Ga²⁺ signaling. *Ann. Rev. Plant Biology* **61**, 561-591 (2010).
66. Ingram, J. & Bartels, D. The molecular basis of dehydration tolerance in plants. *Ann. Rev. Plant Physiol. Mol. Biol.* **47**, 377-403 (1996).
67. Hirai, N., Yoshida, R., Todoroki, Y. & Ohigashi, H. Biosynthesis of abscisic acid by the non-mevalonate pathway in plants, and by the mevalonate pathway in fungi. *Biosci.*

Biotechnol. Biochem. **64**, 1448-1458 (2000).

68. Taylor, H. F. & Smith, T. A. Production of plant growth inhibitors from xanthophylls: a possible source of dormin. *Nature* **215**, 1513-1514 (1967).

69. Schwartz, S. H., Qin, X. & zeevaart, J. A. D. Elucidation of the indirect pathway of abscisic acid biosynthesis by mutants, genes, and enzymes. *Plant Physiol.* **131**, 1591-1601 (2003).

70. Ruiz-Sola, M. A. & Rodriguez-Concepcion, M. Carotenoid biosynthesis in Arabidopsis: A colorful pathway. The Arabidopsis Book 10: e0158. doi: 10. 1199/tab. 0158.

71. North, H. M. *et al.* The Arabidopsis ABA-deficient mutant *aba4* demonstrates that the major route for stress-induced ABA accumulation is via neoxanthin isomers. *Plant J.* **50**, 810-824 (2007).

72. Endo, A. *et al.*, Drought induction of Arabidopsis 9-cis-epoxycarotenoid dioxygenase occurs in vascular parenchyma cells. *Plant Physiol.* **147**, 1984-1993 (2008).

73. Koiwai, H., *et al.* Tissue-specific localization of abscisic acid biosynthetic enzyme, AAO3 in Arabidopsis. *Plant Physiol.* **134**, 1697-1707 (2004).

74. Seo, M., and Koshiha, T., Transport of ABA from the site of biosynthesis to the site of action. *J Plant Res.* **124**, 501-507 (2011).

75. Kaiser, W. M. & Hartung, W. Uptake and release of abscisic acid by isolated photoautotrophic mesophyll cells, depending on pH gradients. *Plant Physiol.* **68**, 202-206 (1981).

76. Kuromori, Y., *et al.* ABC transporter AtABCG25 is involved in abscisic acid transport and responses. *Proc. Natl. Acad. Sci. USA* **107**, 2361-2366 (2010).

77. Kang, J., *et al.* PDR-type ABC transporter mediates cellular uptake of the phytohormone abscisic acid. *Proc. Natl. Acad. Sci. USA* **107**, 2355-2360 (2010).

78. Kanno, Y., *et al.* Identification of an abscisic acid transporter by functional screening using the receptor complex as sensor. *Proc. Natl. Acad. Sci. USA* **109**, 9653-9658 (2012).

79. Kushiro, T. *et al.* The Arabidopsis cytochrome P450 CYP707A encodes ABA 8'-hydroxylases: key enzymes in ABA catabolism. *EMBO J.* **23**, 1647-1656 (2004).

80. Saito, S. *et al.* Arabidopsis CYP707As encode (+)-abscisic acid 8'-hydroxylase, a key enzyme in the oxidative catabolism of abscisic acid. *Plant Physiol.* **134**, 1439-1449

(2004).

81. Okamoto, M. *et al.* ABA 9'-hydroxylation is catalyzed by CYP707A in Arabidopsis. *Phytochemistry* **72**, 712-722 (2011).
82. Lim, E. K. *et al.* Resolution of (+)-abscisic acid using an Arabidopsis glycosyltransferase. *Tetrahedron: Asymmetry* **16**, 143-147 (2005).
83. Lee, K. H. *et al.* Activation of glucosidase via stress-induced polymerization rapidly increases active pools of abscisic acid. *Cell* **126**, 1109-1120 (2006).
84. Xu, Z. Y. *et al.* A vacuolar β -glucosidase homolog that possesses glucose-conjugated abscisic acid hydrolyzing activity plays an important role in osmotic stress responses in Arabidopsis. *Plant Cell* **24**, 2184-2199 (2012).
85. Hocking, T. J. Clapham, J. & Cattell, K. J. Abscisic acid binding to subcellular fractions from leaves of *Vicia faba*. *Planta* **138**, 303-304 (1978).
86. Hornberg, C. & Weiler, E. W. High-affinity binding sites for abscisic acid on the plasmalemma of *Vicia faba* guard cells. *Nature* **310**, 321-324 (1984).
87. Allan, A., Fricker, M. D., Ward, J. L., Beale, M. H. & Trewavas, A. J. Two transduction pathways mediate rapid effects of abscisic acid in *Commelina* guard cells. *Plant Cell* **6**, 1319-1328 (1994).
88. Schwartz, A., Wu, W-H., Tucker, E. B. & Assmann, S. M. Inhibition of inward K^+ channels and stomatal response by abscisic acid: an intracellular locus of phytohormone action. *Proc. Natl. Acad. Sci. USA* **91**, 4019-4023 (1994).
89. Jeannette, E. *et al.* Induction of *RABI8* gene expression and activation of K^+ outward rectifying channels depend on an extracellular perception of ABA in *Arabidopsis thaliana* suspension cells. *Plant. J.* **18**, 13-22 (1999).
90. Ritchie, S. & Gilroy, S. Abscisic acid stimulation of phospholipase D in the barley aleurone is G-protein mediated and localized to the plasma membrane. *Plant Physiol.* **124**, 693-702 (2000).
91. Razem, F.A. *et al.* The RNA-binding protein FCA is an abscisic acid receptor. *Nature*, **439**, 290-294 (2006).
92. Shen, Y. Y. *et al.* The Mg-chelatase H subunit is an abscisic acid receptor. *Nature* **443**, 823-826 (2006).
93. Du, S. Y. *et al.* Roles of the different components of magnesium chelatase in abscisic acid signal transduction. *Plant Mol. Biol.* **80**, 519-537 (2012).

94. Liu, X. *et al.* A G protein-coupled receptor is a plasma membrane receptor for the plant hormone abscisic acid. *Science* **315**, 1712-1716 (2007).
95. Risk, J. M.; Macknight, R. C.; Day, C. L.; FCA does not bind abscisic acid. *Nature* **456**, 290-294 (2008).
96. Pandey, S., Nelson, D. C., Assmann, S. M. Two novel GPCR-type G proteins are abscisic acid receptors in *Arabidopsis*. *Cell* **136**, 136-148 (2009).
97. Alvarez, S., Choudhury, S. R., Hicks, L. M.; Pandey, S. Quantitative proteomics-based analysis supports a significant role of GTG proteins in regulation of ABA response in *Arabidopsis* roots. *J. Proteome Res.* **12**, 1487-1501 (2013).
98. Ma, Y.*et al.* Regulators of PP2C Phosphatase activity function as abscisic acid sensors. *Science* **324**, 1064-1068 (2009).
99. Park. S. Y. *et al.* Abscisic acid inhibits type 2C protein phosphatases via the PYR/PYL family of START Proteins. *Science* **324**, 1068-1071 (2009).
100. Dupeux, F. *et al.* A thermodynamic switch modulates abscisic acid receptor sensitivity. *EMBO J.* **30**, 4171–4184 (2011).
101. Hao, Q. *et al.* The molecular basis of ABA-independent inhibition of PP2Cs by a subclass of PYL proteins. *Mol. Cell* **42**, 662–672 (2011).
102. Li, W. *et al.* Molecular basis for the selective and ABA-independent inhibition of PP2CA by PYL13. *Cell Res.* **23**, 1369-1379 (2013).
103. Zhao, Y. *et al.* The unique mode of action of a divergent member of the ABA-receptor protein family in ABA and stress signaling. *Cell Res.* **23**, 1380-1395 (2013).
104. Fuchs, S., Tischer, S. V., Wunschel., C., Christmann, A. & Grill, E. Abscisic acid sensor RCAR7/PYL13, specific regulator of protein phosphatase coreceptors. *Proc. Natl. Acad. Sci. USA* **115**, 5741-5746 (2014).
105. Melcher, K. *et al.* A gate-latch-lock mechanism for hormone signaling by abscisic acid receptors. *Nature* **462**, 602-610 (2009).
106. Miyazono, K. *et al.* Structural basis of abscisic acid signaling. *Nature* **462**, 609-615 (2009).
107. Yin, P. *et al.* Structural insight into the mechanism of abscisic acid signaling by PYL proteins. *Nat. Struct. Mol. Biol.* **16**, 1230-1236 (2009).
108. Zhang, X. *et al.* Complex structures of the abscisic acid receptor PYL3/RCAR13

- reveal a unique regulatory mechanism. *Structure* **20**, 780-790 (2012).
109. Soon, F. F. *et al.* Molecular mimicry regulates ABA signaling by SnRK2 kinases and PP2C phosphatases. *Science* **335**, 85-88 (2012).
110. Santiago, J. *et al.* Modulation of drought resistance by the abscisic acid receptor PYL5 through inhibition of clade A PP2Cs. *Plant J.* **60**, 575–588 (2009).
111. Yoshida, T. *et al.* ABA-hypersensitive germination3 encodes a protein phosphatase 2C (AtPP2CA) that strongly regulates abscisic acid signaling during germination among Arabidopsis protein phosphatase 2C. *Plant Physiol.* **140**, 115-126 (2006).
112. Nishimura, N. *et al.* ABA-hypersensitive germination1 encodes a protein phosphatase 2C, an essential component of abscisic acid signaling in *Arabidopsis* seed. *Plant J.* **50**, 935-949 (2007).
113. Fujita, Y. *et al.* Three SnRK2 protein kinases are the main positive regulators of abscisic acid signaling in response to water stress in Arabidopsis. *Plant Cell Physiol.* **50**, 2123-2132 (2009).
114. Fujii, H. *et al.* In vitro reconstitution of an abscisic acid signalling pathway. *Nature* **462**, 660-U138 (2009).
115. Ng, L. M. *et al.* Structural basis for basal activity and autoactivation of abscisic acid (ABA) signaling SnRK2 kinases. *Proc. Natl. Acad. Sci. USA* **108**, 21259-21264 (2011).
116. Brandt, B. *et al.* Reconstitution of abscisic acid activation of SLAC1 anion channel by CPK6 and OST1 kinases and branched ABI1 PP2C phosphatase action. *Proc. Natl. Acad. Sci. USA* **109**, 10593–10598 (2012).
117. Geiger, D. *et al.* Activity of guard cell anion channel SLAC1 is controlled by drought-stress signaling kinase-phosphatase pair. *Proc. Natl. Acad. Sci. USA* **106**, 21425–21430 (2009).
118. Xue, S. *et al.* Central functions of bicarbonate in S-type anion channel activation and OST1 protein kinase in CO₂ signal transduction in guard cell. *EMBO J.* **30**, 1645–1658 (2011).
119. Umezawa, T. *et al.* Type 2C protein phosphatases directly regulate abscisic acid-activated protein kinases in *Arabidopsis*. *Proc. Natl. Acad. Sci. USA* **106**, 17588–17593 (2009).
120. Fujii, H. & Zhu, J. K. Arabidopsis mutant deficient in 3 abscisic acid-activated

protein kinases reveals critical roles in growth, reproduction, and stress. *Proc. Natl. Acad. Sci. USA* **106**, 8380-8385 (2009)

121. Nakashima, K. *et al.* Three *Arabidopsis* SnRK2 protein kinases, SRK2D/SnRK2.2, SRK2E/SnRK2.6/OST1 and SRK2I/SnRK2.3, involved in ABA signaling are essential for the control of seed development and dormancy. *Plant and Cell Physiol.* **50**, 1345-1363 (2009).

122. Gonzalez-Guzman, M. *et al.* Arabidopsis PYR/PYL/RCAR receptors play a major role in quantitative regulation of stomatal aperture and transcriptional response to abscisic acid. *Plant Cell* **24**, 2483-2496 (2012).

123. Antoni, R. *et al.* PYRABACTIN RESISTANCE1-LIKE8 plays an important role for the regulation of abscisic acid signaling in root. *Plant Physiol.* **161**, 931-941 (2013).

124. Okamoto, M. *et al.* Activation of dimeric ABA receptors elicits guard cell closure, ABA-regulated gene expression, and drought tolerance. *Proc. Natl. Acad. Sci. USA* **110**, 12132–12137 (2013).

125. Ben-Ari, G. The ABA signal transduction mechanism in commercial crops: learning from *Arabidopsis*. *Plant Cell Rep.* **31**, 1357-1369 (2012).

126. He, Y. *et al.* Identification and characterization of ABA receptors in *Oryza sativa*. *Pro one* **9**, e95246 (2014).

127. Kim, H. *et al.* A rice orthologue of the ABA receptor, OsPYL/RCAR5, is a positive regulator of ABA signal transduction pathway in seed germination and early seedling growth. *J. Exp. Bot.* **63**, 1013-1024 (2012).

128. Kim, H. *et al.* Overexpression of *PYL5* in rice enhances drought tolerance, inhibits growth, and modulates gene expression. *J. Exp. Bot.* **65**, 453-464 (2014).

129. Bai, G. *et al.* Interactions between soybean ABA receptors and type 2C protein phosphatases. *Plant Mol. Biol.* **83**, 651-664 (2013).

130. Gonzalez-Guzman, M. *et al.* Tomato PYR/PYL/RCAR abscisic acid receptors show high expression in root, differential sensitivity to the abscisic acid agonist quinabactin, and the capability to enhance plant drought resistance. *J. Exp. Bot.* in press.

131. Sun, L. *et al.* Transcriptional regulation of SIPYL, SIPP2C, and SISnRK2 gene families encoding ABA signal core components during tomato fruit development and drought stress. *J. Exp. Bot.* **62**, 5659-5669 (2011).

132. Chai, *et al.* FaPYR1 is involved in strawberry fruit ripening. *J. Exp. Bot.* **62**,

5079-5089 (2011).

133. Boneh, U., Biton, I., Zheng, C., Schwartz, A. & Ben-Ari, G. Characterization of potential ABA receptors in *Vitis vinifera*. *Plant Cell Rep.* **31**, 311-321 (2012).

134. Kumari, S. & van der Hoorn, R.A.L. A structural biology perspective on bioactive small molecules and their plant targets. *Curr. Opin. Plant Biol.* **14**, 480–488 (2011)

135. Lumba, S., Cutler, S. & McCourt, P. Plant nuclear hormone receptors: a role for small molecules in protein-protein interactions. *Annu. Rev. Cell Dev. Biol.* **26**, 445–469 (2010).

136. Murase, K., Hirano, Y., Sun, T. P., & Hakoshima, T. Gibberellin-induced DELLA recognition by the gibberellin receptor GID1. *Nature* **456**, 459-463 (2008).

137. Shimada, A., *et al.* Structural basis for gibberellin recognition by its receptor GID1. *Nature* **456**, 520-523 (2008).

138. Santiago, J., Henzler, C. & Hothorn, M. Molecular mechanism for plant steroid receptor activation by somatic embryogenesis co-receptor kinases. *Science* **341**, 889–892 (2013).

139. Sun, Y. *et al.* Structure reveals that BAK1 as a co-receptor recognizes the BRI1-bound brassinolide. *Cell Res.* **23**, 1326–1329 (2013).

140. Wells, J.A. & McClendon, C.L. Reaching for high-hanging fruit in drug discovery at protein-protein interfaces. *Nature* **450**, 1001–1009 (2007).

141. Yoon, J.M. *et al.* Chemical screening of an inhibitory for gibberellin receptors based on a yeast two-hybrid system. *Bioorg. Med. Chem. Lett.* **23**, 1096–1098 (2013).

142. Hayashi, K. *et al.* Rational design of an auxin antagonist of the SCF^{TIR1} auxin receptor complex. *ACS Chem. Biol.* **7**, 590–598 (2012).

143. Hayashi, K. *et al.* Small-molecule agonists and antagonists of F-box protein-substrate interactions in auxin perception and signaling. *Proc. Natl. Acad. Sci. USA* **105**, 5632–5637 (2008).

144. Muto, T. & Todoroki, Y. Brassinolide-2,3-acetonide: a brassinolide-induced rice lamina joint inclination antagonist. *Bioorg. Med. Chem.* **21**, 4413–4419 (2013).

145. Melcher, K. *et al.* Identification and mechanism of ABA receptor antagonism. *Nat. Struct. Mol. Biol.* **17**, 1102-1109 (2010).

146. X. *et al.* Control of abscisic acid catabolism and abscisic acid homeostasis is important for reproductive stage stress tolerance in cereals. *Plant Physiol.* **156**, 647–662

(2011).

147. Santiago, J. *et al.* The abscisic acid receptor PYR1 in complex with abscisic acid. *Nature*, **462**, 665-668 (2009).

148. Hao, Q. *et al.* The Molecular Basis of ABA-Independent Inhibition of PP2Cs by a Subclass of PYL Proteins. *Mol. Cell* **42**, 662-672 (2011).

149. Sun, D. *et al.* Crystal structures of the Arabidopsis thaliana abscisic acid receptor PYL10 and its complex with abscisic acid. *Biochem. Biophys. Res. Commun.* **418**, 122-127 (2012).

150. Cao, M. *et al.* An ABA-mimicking ligand that reduces water loss and promotes drought resistance in plants. *Cell. Res.* **23**, 1043-1054 (2013).

151. Hao, Q. *et al.* Mechanism of the Abscisic Acid Agonist Pyrabactin. *J. Biol. Chem.*, **285**, 28946-28952 (2010).

152. Gao, M. *et al.* An ABA-mimicking ligand that reduces water loss and promotes drought resistance in plants. *Cell Res.* **23**, 1043-1054 (2013).

153. Walker-Simmons, M. K., Rose, P. A., Shaw, A. C. & Abrams, S. R. The 7'-methyl group of abscisic acid is critical for biological activity in wheat embryo germination. *Plant Physiol.* **106**, 1279-1284 (1994).

154. Walton, D. C. Structure-activity relationships of abscisic acid analogs and metabolites. In *Abscisic Acid* (Addicott, F. T. *et al.*). Praeger, New York, pp. 113-146.

155. Hornberg, C. & Weiler, E. W. High-affinity binding sites for abscisic acid on the plasmalemma of *Vicia faba* guard cells. *Nature* **310**, 321-324 (1984).

156. Todoroki, Y., Hirai, N. & Koshimizu, K. Synthesis and biological activity of 1'-deoxy-1'-fluoro-and-8'-fluoroabscisic acids. *Phytochemistry* **40**, 633-641 (1995).

157. Allan, A. C., Fricker, M. D., Ward, J. L., Beale, M. H. & Trewavas, A. J. Two transduction pathways mediate rapid effects of abscisic acid in commelica guard cells. *Plant Cell* **6**, 1319-1328 (1994).

158. Asami, T. *et al.* Synthesis and biological activity of 4'-methoxy derivatives of abscisic acid. *Boorg. Med. Chem. Lett.* **10**, 1571-1574 (2000).

159. Todoroki, Y. & Ueno, K. Development of specific inhibitors of CYP707A, a key enzyme in the catabolism of abscisic acid. *Curr. Med. Chem.* **17**, 3230-3244 (2010).

160. Pettersen, E. F. *et al.* UCSF Chimera-A visualization system for exploratory research and analysis. *J. Comput. Chem.* **25**, 1605-1612 (2004).

161. Todoroki, Y., Hirai, N. & Ohigashi, H. Synthesis, biological activity and metabolism of (S)-(+)-3'-fluoroabscisic acid. *Tetrahedron* **51**, 6911-6926 (1995).
162. Balsevich, J., Bishop, G. & Banowitz, G. Activity and utility of abscisic acid having a 3' thioether linker arm. *Phytochemistry* **44**, 215-220 (1997).
163. Ueno, K. *et al.* Differences between the structural requirements for ABA 8'-hydroxylase inhibition and for ABA activity. *Bioorg. Med. Chem.* **13**, 3359–3370 (2005).
164. Fjeld, C. C. & Denu, M.J. Kinetic analysis of human serine/threonine protein Phosphatase 2C α . *J. Biol. Chem.* **274**, 20336–20343 (1999).
165. Pizzio, G. A. *et al.* The PYL4194T mutant uncovers a key role of PYR1-LIKE4/PROTEIN PHOSPHATASE 2C α interaction for abscisic acid signaling and plant drought resistance. *Plant Physiol.* **163**, 441–455 (2013).
166. GaussView. Version 5, (Dennington, R., Keith, T. & Millam, J., Semichem Inc., Shawnee Mission, Kansas, USA, 2009)
167. Gaussian 09, Revision A.02, (Frisch, M. J. *et al.*, Gaussian, Inc., Wallingford, Connecticut, USA, 2009)
168. Vanquenef, E. *et al.* R.E.D. Server: a web service for deriving RESP and ESP charges and building force field libraries for new molecules and molecular fragments. *Nucleic Acids Res.* **39**, W511–W517 (2011) <http://q4md-forcefieldtools.org/REDS/>.
169. TINKER. Ver. 6.0. (Ponder, J.W., Washington University School of Medicine, St. Louis, Missouri, USA, 2011).
170. Okazaki, M. *et al.* Abscinazole-E2B, a practical and selective inhibitor of ABA 8'-hydroxylase CYP707A. *Bioorg. Med. Chem.* **20**, 3162–3172 (2012).
171. Otwinowski, Z. & Minor, W. Processing of X-ray diffraction data collected in oscillation mode. *Methods Enzymol.* **276**, 307–326 (1997).
172. Evans, P. Scaling and assessment of data quality. *Acta Crystallogr. D Biol. Crystallogr.* **62**, 72–82 (2006).
173. Vagin, A. & Teplyakov, A. *MOLREP*: an automated program for molecular replacement. *J. Appl. Crystallogr.* **30**, 1022–1025 (1997).
174. Winn, M. D. *et al.* Overview of the *CCP4* suite and current developments. *Acta Crystallogr. D Biol. Crystallogr.* **67**, 235–242 (2011).
175. Murshudov, G. N., Vagin, A. & Dodson, E. J. Refinement of macromolecular

- structures by the maximum-likelihood method. *Acta Crystallogr. D Biol. Crystallogr.* **53**, 240–255 (1997).
176. Schüttelkopf, A.W. & van Aalten, D.M.F. *PRODRG*: a tool for high-throughput crystallography of protein-ligand complexes. *Acta Crystallogr. D Biol. Crystallogr.* **60**, 1355–1363 (2004).
177. Emsley, P., Lohkamp, B., Scott, W.G. & Cowtan, K. Features and development of *Coot*. *Acta Crystallogr. D Biol. Crystallogr.* **66**, 486–501 (2010).
178. Saito, S. *et al.* A plant growth retardant, uniconazole, is a potent inhibitor of ABA catabolism in *Arabidopsis*. *Biosci. Biotechnol. Biochem.* **70**, 1731–1739 (2006).
179. Kondo, S., Ponrod, W., Kanlayanarat, S. & Hirai, N. Abscisic acid metabolism during fruit development and maturation of mangosteens. *J. Am. Soc. Hortic. Sci.* **127**, 737–741 (2002).

List of Publications

Takeuchi, J., Okamoto, M., Akiyama, T., Muto, T., Yajima, S., Sue, M., Seo, M., Kanno, Y., Kamo, T., Endo, A., Nambara, E., Hirai, N., Ohnishi, T., Cutler, S. R., Todoroki, Y. Designed abscisic acid analogs as antagonists of PYL-PP2C receptor interactions. *Nat. Chem. Biol.* **10**, 477-482 (2014).